LAPPEENRANTA UNIVERSITY OF TECHNOLOGY
LUT School of Technology
LUT Chemtech

Tuomas Melanen

MIXING IN ROTATING DRUMS

Examiners: Professor Tuomas Koiranen
M. Sc. (Tech.) Nina Venäläinen

TIIVISTELMÄ

Lappeenrannan teknillinen yliopisto

Teknillinen tiedekunta

LUT Kemiantekniikka

Tuomas Melanen

Sekoittuminen rumpu-uuneissa

Diplomityö

2014

118 sivua, 62 kuvaa, 29 taulukkoa ja 12 liitettä

Tarkastajat: Professori Tuomas Koiranen

DI Nina Venäläinen

Hakusanat: Meesauuni, rumpu-uunit, sekoitus, lämmönsiirto, nostimet

Tämän diplomityön tarkoitus on parantaa meesauunin toiminnallista tehokkuutta tehostamalla lämmönsiirtoa. Lämmönsiirron parantamiseksi kehitetään erilaisia nostinratkaisuja. Kokeita suoritetaan käyttäen eri sekoitinratkaisuja ja erilaisia prosessiparametreja.

Työn kirjallisuusosassa esitetään meesauuni sekä rumpumaisten uunien toiminta. Työssä selvitetään myös sekoituksen analysointiin käytettäviä tapoja ja laskukaavoja. Kirjallisuusosassa keskitytään myös rummussa tapahtuviin fysikaalisiin ilmiöihin sekä erilaisten fluidien reologiaan.

Työn kokeellisessa osassa käytettiin LUT Kemiantekniikalla suunniteltua pilot -kokoluokan rumpu-uunia, jolla kokeitaan suoritettiin, käyttäen erilaisia sekoitinratkaisuja ja sekoitusprosessiparametreja. Kokeissa käytettiin myös eri viskositeetin omaavia materiaaleja. Valitut materiaalit olivat vesi, CMC (karboksimetyyliselluloosa) ja kiinteä meesa.

Kokeiden tuloksena löydettiin nostinratkaisuja, joilla sekoittumista ja lämmönsiirtoa pystytään parantamaan sekä pidentämään viipymäaikaa.

ABSTRACT

Lappeenranta University of Technology
LUT School of Technology
LUT Chemtech

Tuomas Melanen

Mixing in rotating drums

Master's thesis

2014

118 pages, 62 figures, 29 tables and 12 appendices

Examiners: Professor Tuomas Koiranen
M. Sc. (Tech.) Nina Venäläinen

Keywords: Lime kiln, rotating drums, mixing, heat transfer, lifters

The purpose of this master's thesis is to improve the operating efficiency of a lime kiln by intensifying the heat transfer. In order to find the best heat transfer solutions different lifter geometries are designed and tested. Different mixing process parameters and mixing configurations are used in the experiments.

The literature part of the thesis presents the lime kiln and different drum mixers. Different ways to observe mixing including formulas are also presented. Physical phenomena in rotating drums and rheology of different fluids are also presented in the literature part.

In the experimental part a pilot drum was designed. Experiments were carried out by using different lifter geometries and process parameters. Different materials with different viscosities were chosen for the experiments. The chosen materials were water, CMC (Carboxymethyl cellulose) and solid lime mud.

As a result, it was found lifter designs to improve mixing, to improve heat transfer and to increase the residence time.

FOREWORDS

This thesis was conducted for Andritz Oy at the Lappeenranta University of Technology during the year 2014.

To begin with I would like to thank Professor Tuomas Koiranen for all the help he gave to me during my work. I would also like to thank Andritz Oy and especially Nina Venäläinen, Mika Kottila and Casimir Svensson for giving their advices during the work. I would also like to thank all the other people who helped me during my thesis in Lappeenranta including Anna-Riina Haverinen, Jesse Tikka, Jyri Nyman and Markku Maijanen. Special thanks also to Jarmo Ilonen for all the help.

And last I would like to thank my family and friends. Thank you for being there when I needed you and thank you for all your love and support. "Who knows where life will take you. The road is long and in the end, the journey is the destination."

Lappeenranta, 27th of November, 2014

Tuomas Melanen

CONTENTS

APPENDICES

SYMBOLS

A	Constant
a	The angle of the repose, °
B	Constant depending on material, -
b	The included angle, °
C_c	Compressibility,-
C_i	Concentration difference, mol/dm^3
$\bar{C}$	Average of concentration difference, mol/dm^3
D	Dispersion coefficient, m^2/s
$\frac{D}{uL}$	Dimensionless dispersion coefficient, -
D_i	Diffusion constant, m^2/s
D_p	Diameter of the pipe, m
d	Constant
e	Constant
F	Feed rate, lb/hr/ft^2
Fr	Froude number, -
f	Constant
G	Freeboard gas velocity, lb/hr/ft^2
g	Acceleration due to gravity, m/s^2
h	Distance of plates, m
j	Constant
k_B	Bolzmann's constant, J/K
K	Consistency factor, -
L	Length of pipe, m
M	Mixing index, -
N	Kiln rotational speed, rpm
Nu	Nusselt number, -
m	Flow behavior index, -
n	Number of measurements, -
Pr	Prandtl number, -
R	Kiln internal radius, m
Re	Reynolds' number, -

R_0	Solute radius, m
S	Source term, -
s	The slope, degree/radians/ ft/ft
T	Temperature, K
$TIPS_{ind}$	TIP speed of the industrial lime kiln, m/s
$TIPS_p$	TIP speed of the pilot scale drum, m/s
t	Time, s
$\bar{t}$	Mean time of passage, s
U	Velocity, m/s
u	Flow rate, m/s
V_{ind}	Linearized flow rate of the industrial lime kiln, m/s
V_p	Linearized flow rate of the pilot scale drum, m/s
x_i	position, m
X	Mixing variable (Concentration, temperature etc.), -
X_0	Mixing variable at time 0, -
X_1	Mixing variable at the end of experiment, -
y	Distance variable in radial direction, m
σ	Standard deviation, -
σ^2	Variance, -
σ^2_0	Upper limit of mixture variance
σ^2_R	Lower limit of mixture variance
ρ	Fluid density, kg/m^3
ρ_A	Aerated bulk density, kg/m^3
ρ_p	Packed bulk density, kg/m^3
ρ_w	Working bulk density, kg/m^3
μ	Fluid viscosity, Pa s
μ_w	Viscosity at the tube wall, Pa s
ω	Angular velocity, 1/s
τ	shear stress, kg/s^2 m
γ	Shear rate, s^{-1}

ABBREVIATIONS

$CaCO_3$	Lime mud
CaO	Quicklime
CMC	Carboxymethyl cellulose
CNCG	Concentrated non-condensable gas
CO_2	Carbon dioxide
CoV	Coefficient of Variation, -
H_2	Hydrogen gas
HSV	Hue, Saturation, Value
M	Modified
NOX	Mono-nitrogen oxides
NMR	Nuclear magnetic resonance
PEPT	Positron emission particle tracking
TiO_2	Titanium oxide
TRS	Total Reduced Sulfur
ΔH	Enthalpy change, kJ/kg

LITERATURE PART

1 INTRODUCTION

1.1 Background

This master's thesis is done for Andritz Oy, Finland. The ANDRITZ Group is a global world market leader in most business areas with more than 220 production and service sites worldwide and it employees approximately 23 800 people. It produces services and products like plants and services for hydropower stations, the pulp and paper industry, the metalworking and steel industries and the solid/liquid separation in the municipal and industrial sectors. (Andritz Oy, 2014.)

Mankind could not survive without air and water but there are also other materials without which the modern industry could not exist. Among these materials are limestone and lime which are among the oldest materials used by mankind. Limestone and lime are directly or indirectly use in manufacturing almost every object that exists in everyday life. The abundance of is evidenced by the fact that an estimated 2 % of the elements in earth's crust contain magnesium and 3.5–4 % calcium. Calcium is ranked fifth in abundance of all elements. (Boynton, 1980.)

Limestone is a general term describing fossils or carbonate rocks. It is composed primarily of calcium carbonate or the composition of magnesium and calcium carbonate with impurities like silica and alumina. In turn *Lime* is always a calcined or burned form of limestone. Lime is also known as quicklime (calcium oxide) or hydrated lime (calcium hydroxide). The calcination process removes the carbon dioxide from the stone, forming quicklime and after water is added the product is hydrated lime. (Boynton, 1980.)

In pulp and paper processes, cooking liquors are formed on site by mixing quicklime, sodium carbonate and sodium sulfite together. Lime mud is a by-product of this process. Lime mud is produced in the causticizing plant of the kraft process and it is a mixture of calcium carbonate, inorganic sulfur components, a small quantity of sodium hydroxide and water. In order to improve the economics of the

process this by-product is recovered to quicklime on site in a calcining rotary kiln. (Boyden, 1991.)

Regeneration of the lime mud in a lime kiln is one of the principal unit operations of the kraft recovery process. The kraft recovery process does not produce pulp or paper but it is essential for pulp and paper processes because it for example recovers and reuses the inorganic pulping chemicals and removes the organic by-product chemicals. Other principal unit operations are evaporation of black liquor, combustion of black liquor in a recovery furnace to form sodium sulfide and sodium carbonate. Finally sodium carbonate is causticized to sodium hydroxide. There are also other minor operations to ensure the continuous operation of the recovery cycle such as removal soap in the black liquor to produce tall oil. (Vakkilainen, 1999.)

The purpose of the evaporation is to produce black liquor to high concentration with minimum chemical losses. After washing, pulp and black liquor are separated. The weak black liquor contains 12–20 % organic and inorganic solids. Burning this weak black liquor requires more heat that it can produce. It must therefore undergo concentration for efficient energy recovery. The concentration must be increased to 65–80 % before the recovery boiler stage. Electricity and low pressure steam for the process are generated in the recovery boiler. The main unit operation is combustion of organic material in black liquor to generate steam. In a lime kiln the lime mud is calcined to reactive lime by drying and later heating. Rotating furnaces or fluidized bed reactors can be used in the calcinating process. The main unit operations are drying of the lime mud and calcining of calcium carbonate. In the causticizing stage the sodium carbonate in green liquor is converted to caustic soda. The unit operations in causticizing include dissolving of molten smelt to weak white liquor to produce green liquor, green liquor clarification or filtration, mixing lime and green liquor in a slaker to form sodium hydroxide and lime mud with subsequent completion of the causticification reaction in reaction tanks, white liquor clarification and filtration for lime mud separation and lime mud washing. (Vakkilainen, 1999.)

1.2 Objectives and Restrictions

The aim of this master's thesis is to increase the operating efficiency of lime kiln and in this way to improve the efficiency of current pulp and paper mills. The purpose of the studies is to intensify the heat transfer. In order to find best heat transfer solutions different mixing applications are studied. Different mixing applications are studied by the literature search and pilot tests. By improving the mixing the dust accumulation increases so the gas flow in the optimum mixing region is also studied.

In this master's thesis the lime kiln process is presented. Thesis also includes the literature search for different drum mixers with different mixing, lifting and geometry opportunities. Physical phenomena in drums are described. Also the mixing as unit operation, the properties and rheology of fluid are presented.

In pilot tests the mixing in lime kiln is studied with tracers. Some pH and pulsed tests are performed by using different geometries and lifters. Residence time experiments are done and those residence time distributions are studied to find best conditions for lime kiln process. Also the gas flow is studied to find optimal conditions for dust accumulation.

The restrictions of this master's thesis are in experimental part. A pilot scale system is built but due to the high operating temperature the lime mud is replaced by the substance with the same viscous properties in lower temperatures.

2 LIME KILN

The rotary lime kiln is used in the calcination process where the solid $CaCO_3$, lime mud, is burned into CaO, quicklime. In a lime kiln the lime mud is calcined to lime by heating according the following reaction:

$$CaCO_3 + Heat \rightleftarrows CaO + CO_2,\ \Delta H = -3180\ \frac{kJ}{kg_{CaO}} \quad (1)$$

The kiln is heated around 900–1 300 °C, but the dissociation of $CaCO_3$ to CaO and CO_2 begins at the temperature 820 °C (Arpalahti *et al*., 1999; Seppälä *et al*., 2001*)*. When the temperature increases the reaction accelerates. The lime mud entering in the lime kiln contains also unreacted lime, a small amount of alkali, some impurities and occasionally water. The amount of impurities is usually about 7–10 % of total lime mud dry solids. (Arpalahti *et al*., 1999; Kottila, 2014) Conventional lime kiln and treatment zones are shown in Figure 1. In flash drier kiln lime mud is dried out side of the kiln. In this case dry lime mud is fed to kiln and therefore, drying section is part of the heating section.

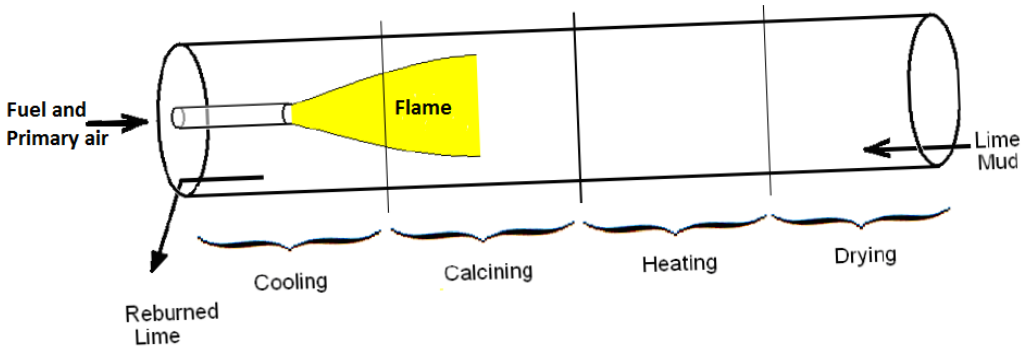

Figure 1 Conventional lime kiln and treatment zones (Malahat, 2010).

2.1 Lime Reburning

Lime reburning is a part of the chemical circuit in a kraft pulp mill. It is called the lime cycle. Purpose of the lime cycle is to convert calcium carbonate from causticizing back to calcium oxide. Calcium oxide is a recirculating chemical used to convert green liquor to white liquor in the causticizing plant. In lime generation the lime mud is treated at high temperatures so the regeneration is called

reburning. Makeup lime or limestone are used to compensate lime losses in the lime cycle. The kraft recovery process is presented in Figure 2. (Arpalahti *et al.*, 1999.) The recovery process involves two loops which are sodium loop (white liquor loop) and the calcium loop. A simplified representation of the kraft pulping and chemical recovery system with reaction equations is presented in Figure 3. (Miner *et al.*, 2001).

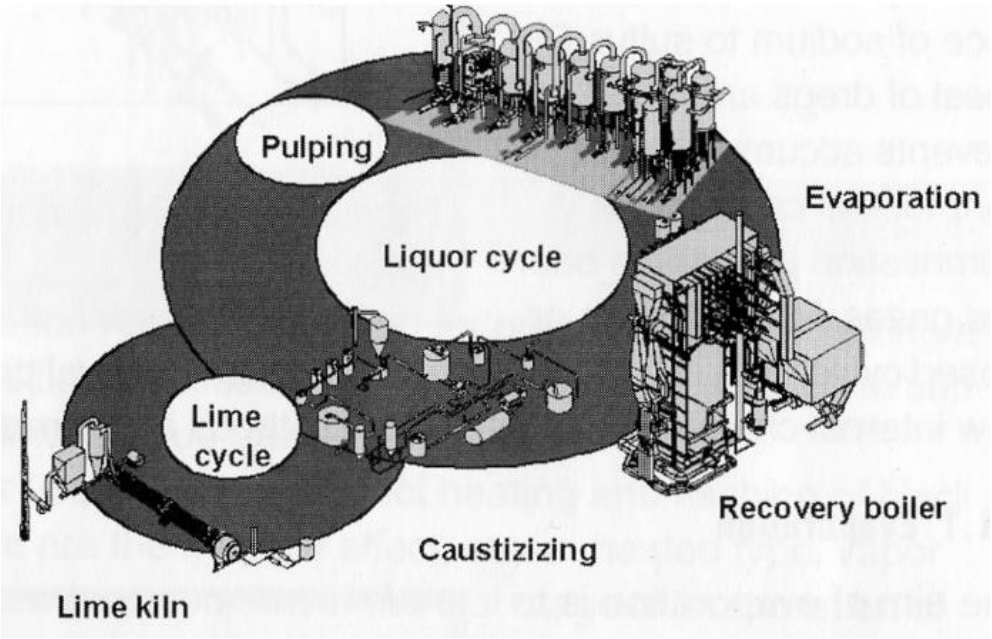

Figure 2 Kraft recovery process (Vakkilainen, 1999).

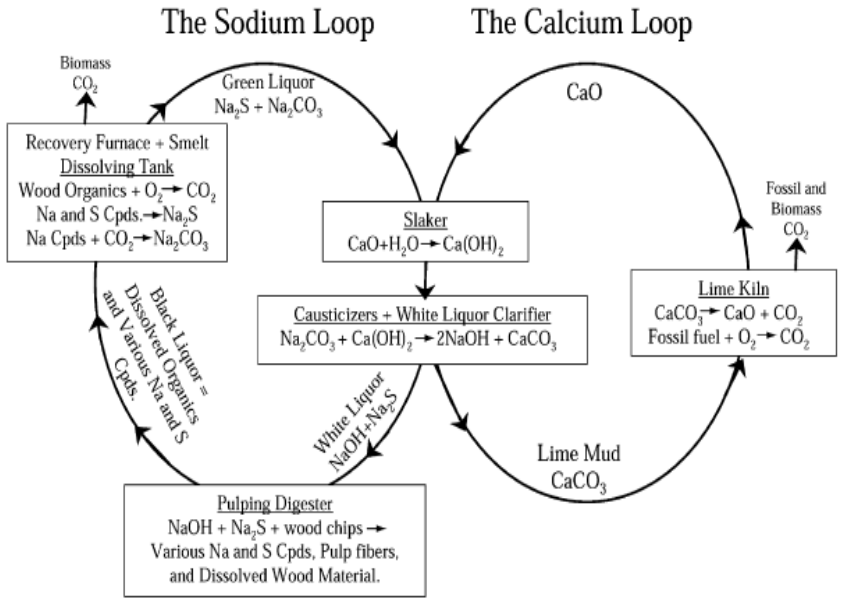

Figure 3 A simplified representation of the kraft pulping and chemical recovery system (Miner *et al.*, 2001).

The process uses a counter-currently operating, heat exchanging reactor where heat transfers from combustion gas to lime by direct contact. Typically natural gas or heavy oil are used as a heat source. Today also other fuels such as gasified bio fuel and wood powder can be used as main fuel of the lime kiln. (Kottila, 2014.) Kilns can be classified in vertical, rotary and miscellaneous kilns (Boynton, 1980). A rotary kiln with typically diameter 4–4.5 m in diameter and 100–140 m in length with capacity of approximately 530 t reburned lime/day are built nowadays depending on the feed and construction. Kilns are getting bigger due to increasing capacity demand so the diameter and the length of the kilns are getting bigger. The kiln is usually supported by three or four piers. Slope of the kiln is usually between 1.5–3.0 °. Rotary kilns can accept a wide range of feed stone sizes from 60 mm down to dust but with modern rotary kilns fitted with preheaters the accepted size may be 10 mm or less. (Arpalahti *et al.*, 1999; Seppälä *et al.*, 2001; The McIlvaine Company.)

A rotary kiln slopes slightly towards the firing end and typically the rotation speed is 0.5–1.5 rpm while lime kiln travels downhill toward the firing end. The lime retention time in the kiln is normally 2.5–4 hours and it depends on kiln dimensions like rotation speed and lime mud properties. Too short retention time leads to uncooked, high residual $CaCO_3$. Too long retention time leads to dead burned lime with low lime availability. The retention time can be controlled by using damns at the discharge end of the kiln. The conventional kiln has four treatment zones which are drying, heating, calcination and final treatment. In flash drier kiln there are only three zones because the drying zone is part of the heating zone. First three kiln zones require external heat so the kiln therefore burns fuel oil or natural gas. After moisture evaporates in the drying zone and the lime mud heats to the reaction temperature (820 °C) at heating zone, the calcination reaction occurs in the burning zone where the temperature increases to 1 100 °C. Heat transfer depends mainly on radiation and convection dominates only in the drying phase where the flue gas temperature has decreased considerably. The lime kiln heating profile is presented in Figure 4. (Arpalahti *et al.*, 1999; Seppälä *et al.*, 2001.)

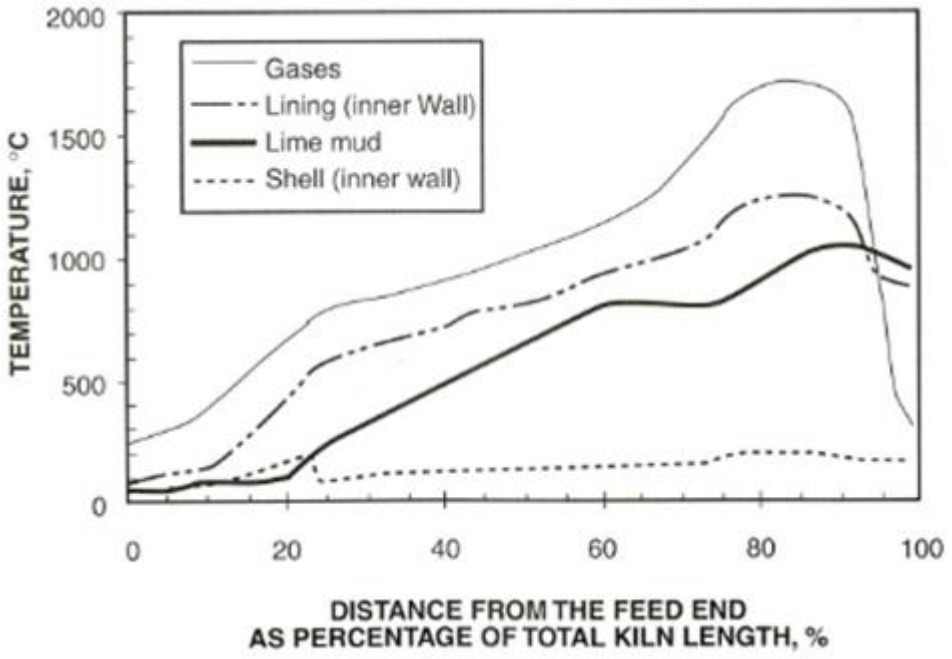

Figure 4 The temperature profile of lime kiln (Arpalahti *et al.*, 1999).

Kiln temperature effects on the quality of CaO produced. Very small particle sizes with large specific surfaces are the most wanted end product from CaO, The impact of kiln temperature on particle size, thus surface area, of hydrated particles of Cao is presented in Figure 5.

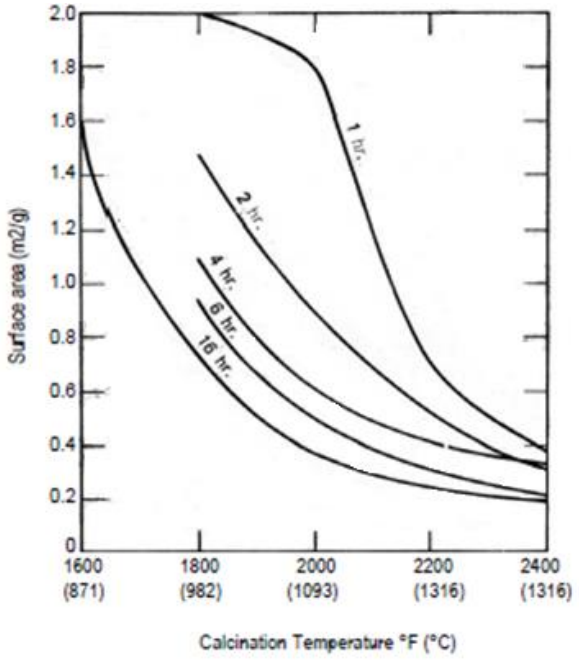

Figure 5 Relation of surface area to calcination temperature (Hassibi, 1999).

2.1.1 Unit Operations in the Lime Reburning Process

The lime reburning process consists of unit operations such as mechanical dewatering of lime mud, thermal drying, heating and calcining, cooling of the product, screening and crushing. The lime kiln process also needs firing equipment to raise the temperature in the kiln and dust handling to separate the lime dust escaping from the kiln with flue gases. All lime kilns have a refractory lining with or without insulation bricks to protect the kiln shell from overheating and to limit the heat losses. Unit operations in lime reburning are shown in Figure 6. (Arpalahti *et al.*, 1999.)

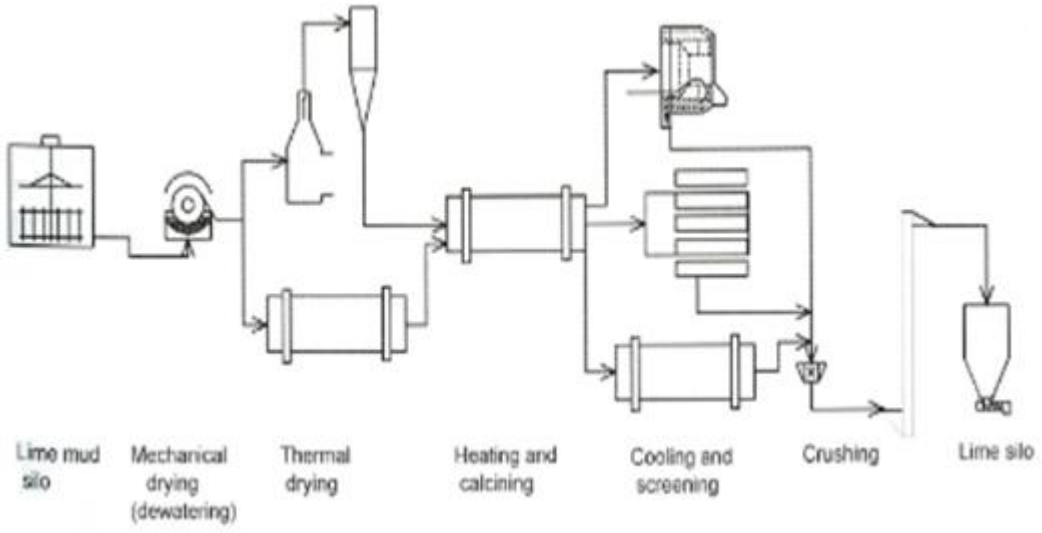

Figure 6 Unit operations in lime reburning (Arpalahti et al., 1999).

Before entering into the kiln the lime mud is treated in the vacuum filter used for dewatering to give a uniform flow and moisture for lime mud. Lime mud dry solids have an effect on the heat consumption of a lime kiln. With low lime mud dry solids content the heat consumption is high due to excess evaporation of moisture. High dry solids content increases the flue gas outlet temperature when the excess heat energy in the flue gases cannot be fully used in the lime mud drying. From the filter the lime mud is moved into the kiln via belt conveyor or a screw feeder. Thermal drying can be done in two alternative ways. Traditional method for drying is to use kiln feed and drying section with or without chain section were several patterns exist for hanging the chains. With the chain section

the heat transfer from flue gas to the lime mud is increased. The most typical chains are the garland and curtain type. Pneumatic dryer can be used as an alternative way for thermal drying. First lime mud is fed to flue gas stream where the lime mud is dried. Finally cyclone separates the dry lime mud and feeds it into the kiln. (Arpalahti *et al.*, 1999.)

The lime mud is heated to the calcining temperature in the rotary part of the kiln. Different lifters, bars, cam lining or baffles can be used to improve the heat transfer in the heating zone. The purpose of the heating is to obtain homogeneous and porous lime that will slake easily and produce the lime mud that can be separated easily from the liquor. Lime activity reaches maximum value at certain calcination temperature and then decreases. The crystal structure of the lime can change if the temperature in the kiln gets too high. This leads to poorly slaking, hard-burnt lime. Burned lime exits the kiln via the cooler. Product cooler is used for heat recovery which is attached to kiln itself. Secondary combustion air recovers heat from the hot lime and flows then into the kiln. Separated cooling drums are also used. Finally lime needs to be crushed because the burned lime has a wide size distribution. Cooling systems have the screen devices so the lump and hammer mills will handle only oversized material. (Arpalahti *et al.*, 1999.) The need of makeup lime comes from purchasing burnt lime or limestone which is then burned with lime mud in the lime kiln (Seppälä *et al.*, 2001).

2.1.2 Firing Equipment

The kiln needs a firing equipment to raise the temperature in the kiln. A firing hood covers the discharge end of the kiln. The main burner can be supported from the hood or attached to a trolley. The design can approve one or many fuels. Heat transfer inside the kiln happens primarily by the radiation which needs a high fuel combustion temperature. Almost all lime kilns use natural gas or heavy oil because the combustion temperature of both is high. (Arpalahti *et al.*, 1999.) Also biofuels such as wood residues (gasification gas and wood dust), tall oil or pet coke and additional fuels like methanol, CNCG (concentrated non-condensible gas) and H_2 can be also used partially to replace the heavy oil (Kottila, 2014). The

flame length has an effect on the process. Shorter flames are too hot and may cause overburned lime or refractory damages. Also NOX gases have tendency to increase. Longer flames cause loss in production capacity and efficiency. Desirable compact medium flame length is about three times kiln diameter in length. (Honghi, 2008.)

Nowadays the emissions are the main concern in the lime kiln process. Limitations in formation of NO_x, SO_2, CO and TRS (Total Reduced Sulfur) regulate the process because achieving emission limits without reducing the capacity and flame temperature is often difficult. (Arpalahti *et al.*, 1999.) The CO_2 from the kraft mill lime kilns is from three sources: CO_2 released from $CaCO_3$ in the calcining process, CO_2 from fossil fuel burned in the kiln and CO_2 from pulp mill-derived gases burned in the kiln (Miner *et al.*, 2001).

2.1.3 Heat Exchanger Cross Section Design

As the drum rotates, the bed of particles in the drum is moved upwardly by friction a distance along the interior periphery of the drum wall. When the weight of the particle bed overcomes the friction, the particles slide downwardly to the bottom of the drum. This phenomenon continues as the drum rotates. As a result there is little or no mixing of the particles and the particles in the interior of the bed may never be exposed to the environment in the drum while the particles on the surface of the bed can be overexposed to the environment in the drum. Due to this the particle bed is non-homogenous with respect to the particle size and temperature. (Sunnergren *et al.*, 1979.)

Heat exchanger cross section design increases the interior surface area of the kiln as to affect a greater heat transfer of hot exhaust gases to the kiln feed, increase throughput and reduce radiation losses. These kiln adjuncts are composed of either refractory brick or special heat-resistant metal alloys. Dams are superimposed onto the kiln refractory linings of about 20–25 cm which induces a gentle tumbling action so that all the particles are turned over number of times and exposed to hot gases for uniform calcination. (Boynton, 1980.) Otherwise the

finest particles sizes would remain at the bottom in contact with hot firebrick and the coarser particles form an upper layer of the bed (deBeus, 1987). Lifters offer a similar purpose except that they produce greater mixing action. The lifters are designed to lift the particles along the interior of the drum wall and drop the particles to the bottom of the drum. This leads to more homogenous product but also increases the dust formation and operation costs. It is preferred to use a lifter which is at least one-third the depth of the particles but does not exceed 90 % of the depth. The leading surface is the first of the lifter to contact the particles as the drum rotates. The included angle formed by the intersection of the leading surface and the base surface should be about same angle as the angle of repose of the material in the drum. The included angle, **b**, can be within plus 10 ° and minus 10 °of the angle of the repose of the material in the drum. The angle of the repose, **a**, or rest angle of a material is the maximum angle with a horizontal plane at which loose material will stand on a horizontal base without sliding and is often between 30 ° and 35 °. In case of limestone angle is about 38 °. (Sunnergren *et al.*, 1979.) Lifters are usually installed parallel to the kiln length as metal angle irons with a lip that enlarges about 15 cm from the refractory lining. Lifters can be installed in a series for 6.1–18.3 m or more in length. The lifter oversizing in the kiln is possible so that excessive attrition loss occurs as a result of turbulent tumbling and collision of the lime mud feed. The positioning of lifters is critical in lessening attrition loss. (Boynton, 1980.) There are many patents of different lifter designs but only few of those are in commercial use. The main problem is the optimization between lifter design and dusting. Because the drum is rotating, the material slowly rotates up to the side wall of the drum and in some point gravity and other forces cause the material to fall in a downward direction from sidewall of the drum. When material falls, it occasionally passes through the flame. This leads to dusting and forming of the unwanted residue. (Dillman. 2008.) Examples of lifter designs are shown in Figures 7 and 8.

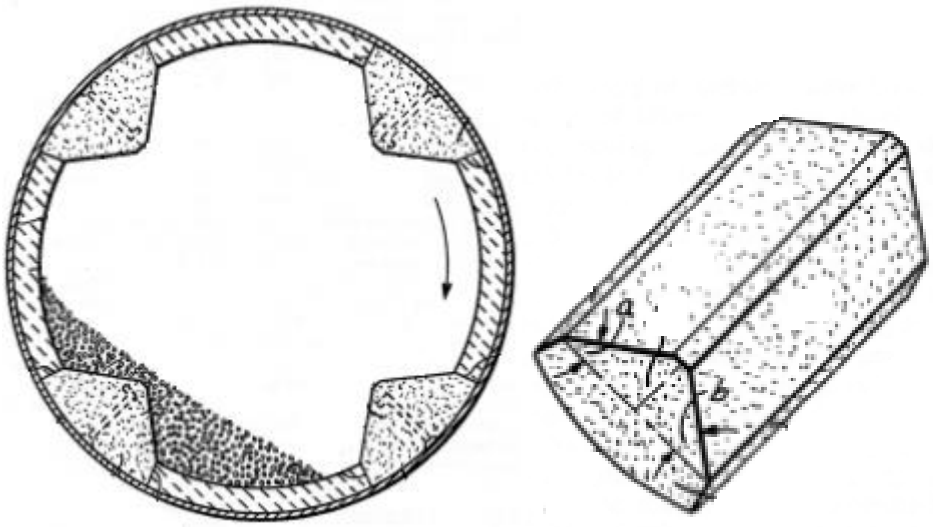

Figure 7 Typical lifter (Sunnergren *et al.*, 1979).

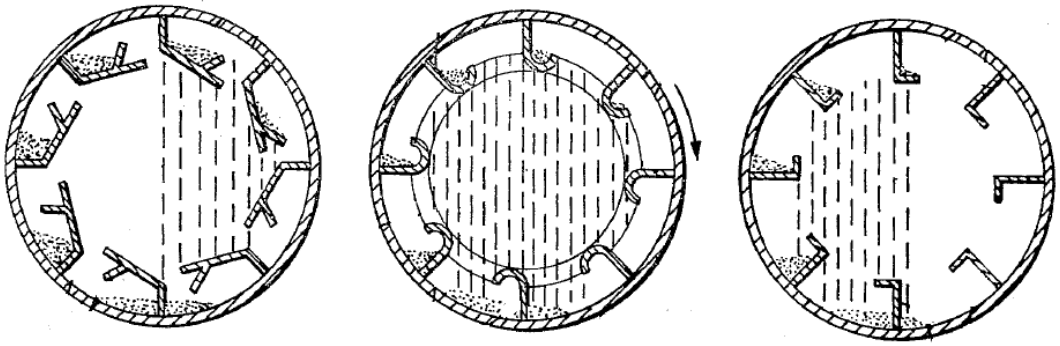

Figure 8 Different lifter designs (Flemming, 1970).

2.1.4 Ring Formation

Excess ring formation in lime kilns is a problem in some kraft pulp mills. Sodium is one of the impurities in lime mud. Small amount of sodium is good because it promotes lime nodulation and lows dusting. Too high sodium content may lead to ring formation, high TRS, dead burned lime or refractory damage. Temperature variation in the kiln has also effect on excess ring formation. Lime kiln ring formation occurs at many mills. It causes process disturbances and reduces cost effectiveness at many mills. It may also cause the reduction in production because of unscheduled shut-down may occur. In the middle of the kiln, melting of sodium compounds near 800 °C can create a sticky kiln surface that picks up lime particles and begins ring formation. These deposits are relatively weak but become harder via recarbonation reaction with carbon dioxide. Recarbonation

typically occurs when the deposit temperature drops below 800 °C, as calcined CaO particles react with CO_2 to form $CaCO_3$. Kiln rings may also occur soon after the chain section of the kiln. This can occur if mud moisture content is too high and can be promoted by high lime content in precipitator catch recycle. (Honghi, 2008.) *Björk* (2002) has studied ring formation in side of front-end temperature. The release of sodium increases drastically at temperature above 900 °C. The released sodium is transported with flue gases and plays an active role in ring formation earlier in the kiln. Björk also claims that high O_2 content in flue gases and the sulphur content of fuel have an active role in ring formation.

2.1.5 Dusting

Dusting is an essential phenomenon because dust loss out of the feed end of a kiln is typically between 5–20 % of the dry mud feed rate (Ellis, 1989). Dusting occurs during the kiln operation when dried lime particles are picked up, entrained and dispersed in the turbulent kiln gas while lime mud moves along the kiln from the feed end towards the discharge end. Lime particles on the surface of the bed are dried by the heat produced by the flame and the kiln gas picks up the small lime particles and entrains those into the turbulent kiln gas to form dust suspension. (Honghi, 2008.)

Dusting is one of major source of energy losses among the evaporation of water, heat losses by radiation thought the kiln shell and reburned lime product heat losses. Most of the entrained lime particles are captured and returned to the kiln by scrubbers and precipitators. Without recycling there would be a significant raw material loss. However, raw material loss occurs because dust leaks from the kiln shields, firing hood and gas ducts. For kilns with scrubbers, dust is recycled via pre-coat filters by adding water to the filtered dust material and then fed back to the kiln. This however causes energy losses due to additional moisture that comes from the recycled dust. (Honghi, 2008.)

Dusting occurs because of different material properties and operation variables. Particle size, local gas velocity, mud feed rate, angle of repose, moisture content

and rotation speed of the kiln affect dusting. Particle size is an important factor. Dusting depends greatly on the degree of agglomeration of lime mud at the feed end and nodulization of lime of the calcination zone. If the moisture content of lime is low at fully dried feed, it is easier for particles to become powdery and be entrained in the kiln gas. Nodulization occurs in the calcination zone. Lime forms and nodulizes due to the melting guarded sodium and water soluble sodium compound in the mud. While particles move towards firing end the nodules grow larger. However the mud which is slightly water soluble and guarded sodium contents, reburned lime cannot nodulize easily. Dusting in general may be minimized by decreasing mud solids content and by increasing the sodium content. However, this is not the desired way of operation. (Honghi, 2008.) Local gas velocity and rotational speeds of the kilns need to be optimized. Too fast gas velocity picks up the small lime particles more easily and with higher rotational speed more material is displaced and dropped on the bed of the kiln so that gas velocity can entrain those the turbulent kiln gas to form dust suspension. *Malahat* (2010) has studied the minimum gas velocities required to pick up the particles from the bed. Results are shown in Figure 9.

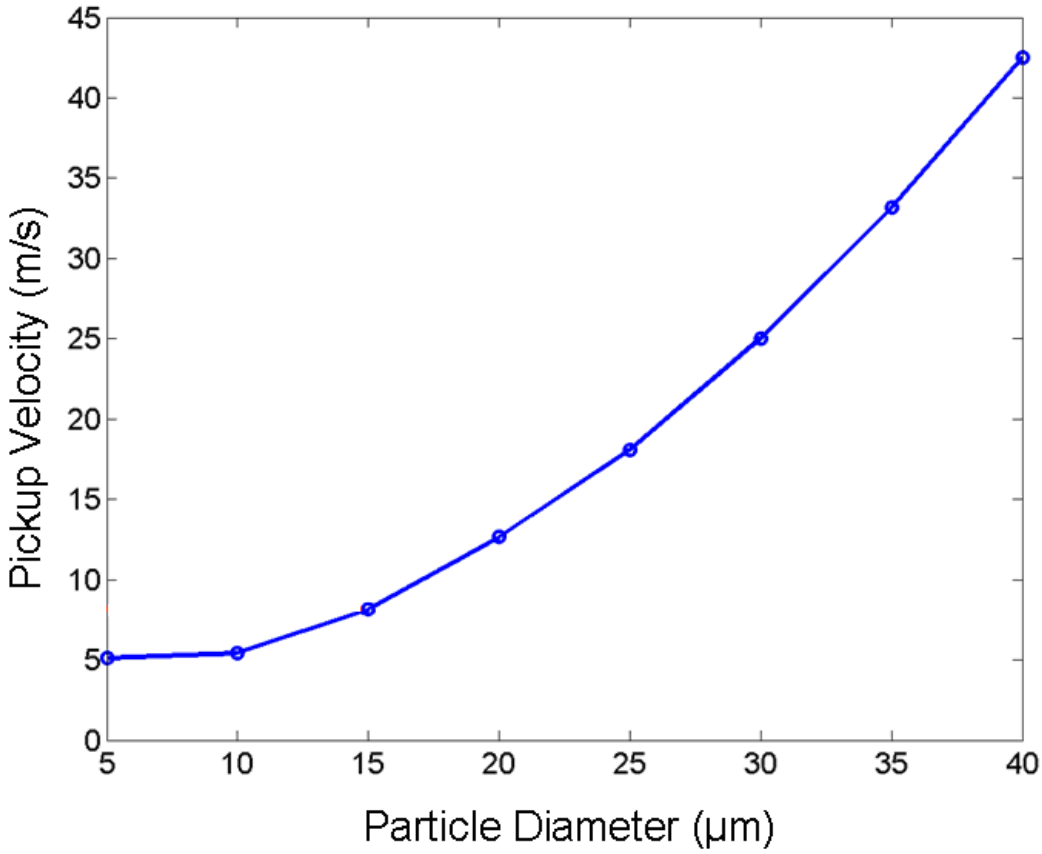

Figure 9 Minimum gas velocity required to pick up a particle from the bed. Mean gas temperature in the dusting zone was approximately 810 K. (Malahat, 2010).

According to Malahat (2010) smaller particles have a higher pick up probability, but they contribute little to the mass flow rate because of their small mass. Particles that are smaller than 10 µm in size are the most easily picked up when gas velocity is greater than 6 m/s. However, their maximum dust generation rate is relatively low comparing to larger particles that are less likely to be picked up. When the gas velocity is high enough to pick up larger particles in the air, a relatively high mass flow rate of dust occurs. Gas velocity and dust production rate with different particle sizes is demonstrated in Figure 10.

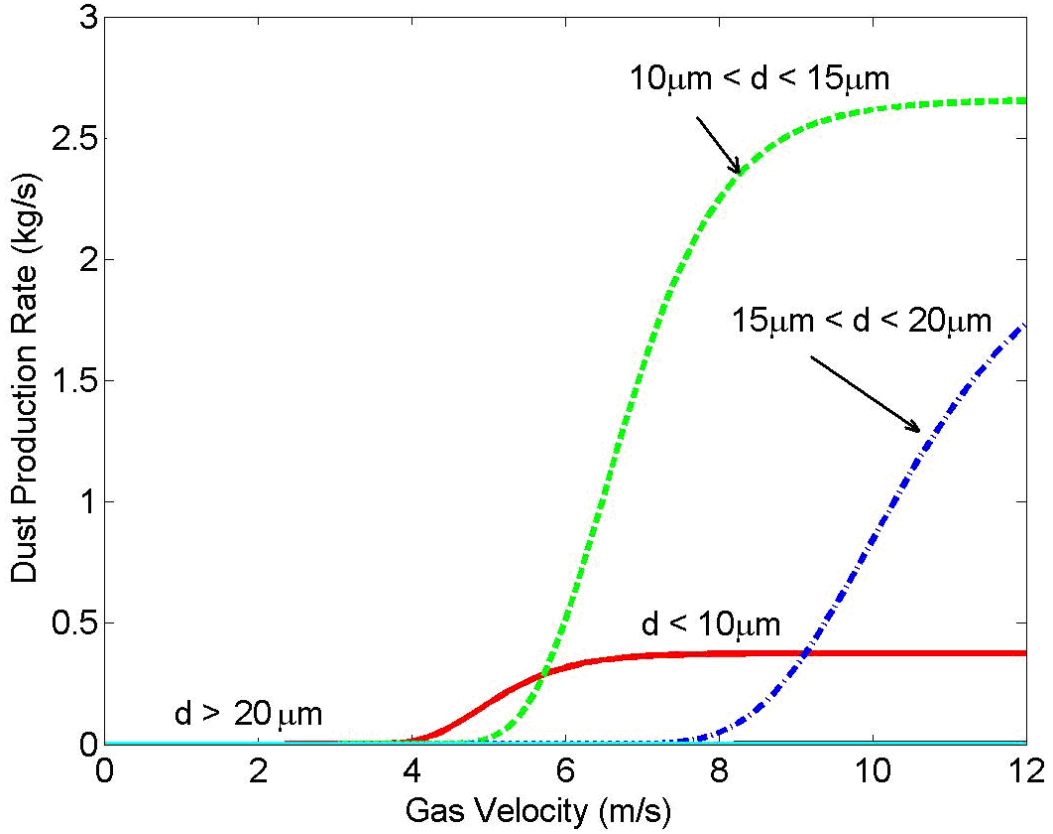

Figure 10 Gas velocity and dust production rate with different particle sizes. Mean gas temperature in the dusting zone was approximately 810 K. (Malahat, 2010).

3 MIXING

Solid mixing is the key step in almost all particulate processing applications. It is used to reduce the non-uniformity in the composition of the bulk. Thorough mixing of particles in the transverse plane of a rotary kiln is fundamental to uniform heating or cooling of the charge and for generating a homogenous product. Differences in particle density and size result in a de-mixing process according to which the smaller or denser particles segregate to form an inner core which may never reach the bed surface to be exposed to freeboard temperature. The rheological properties of the bed material can be expected to change from the feed end to the discharge end. Several changes can lead to alterations to material properties, including particle size, shape and surface character, and change the bed behavior. One of these behavioral phenomena is segregation which has influence on heat transfer within the bed. Segregation may also influence the rate at which particles are elutriated from the exposed bed surface when large amounts of gas are being released from the bed. The effect of segregation on heat transfer is very

important because it significantly influences the degree of product homogeneity. Most rotary kiln segregation issues arise from differences in particle size but also differences in density, shape, roughness and resilience causes segregation. The mechanisms by which size segregation occurs might be classified as percolation or trajectory segregation. Trajectory segregation happens due to fact that particles being discharged from the plug flow region into the active layer may be projected horizontally from the apex onto the exposed bed surface. This can happen in the rolling, slumping and cataracting modes when different sized particles are emptied onto surface during material turnout. Percolation happens when a bed of particles is disturbed so that the rearrangement takes place. (Boateng, 2008.)

In tumbling applications, dilation and flow principally play out near the unconstrained upper surface of granular bed, and except for solid-body rotation, the bulk grains beneath are thought to remain nearly motionless during the rotation of the drum. Flow in rotary drums with increasing tumbling speed can be characterized in term of regimes such as slipping, avalanching, rolling, cascading, cataracting and centrifuging. (Muzzio *et al.*, 2004.)

Slipping regime occurs when the granular bed undergoes solid body rotation and then slides against the rotating drum walls. This phenomenon is typical in simple drums that are only partially filled. *Avalanching,* also referred to as slumping, is a second regime seen at slow tumbling speeds. In avalanching regime, flow consists of discrete avalanches that occur as a grouping of grains travel down the free surface and come to rest before a new grouping is released from above. At higher tumbling speeds, discrete avalanches give way to continuous flow at the surface of a blend so the grains beneath this surface flowing layer rotate nearly as a solid body with the blender until they reach the surface. This phenomenon is known as *rolling*. Even higher rotation speeds the flow is termed as *cascading*. It differs from rolling so that the flowing layer is thin and has been modeled as depth-averaged plug like flow. As the rotation speed is increased, the surface becomes increasingly sigmoidal until grains become airborne, and with higher rotation speeds, the grains centrifuge against the drum wall. These phenomena are termed *centrifuging* and *cataracting*. Different regimes are shown in Figure 16 on page 45 with Froude numbers. (Muzzio *et al.*, 2004.)

3.1 Experimental Observations

Early workers estimated mixing by using tracer particles to observe and characterize mixing. The residence time distribution is typically studied by tracers introduced into rotating drum with a subsequent measurement of the concentration of the tracer at the discharge end or some other suitable point of the drum. If the tracer is chosen it is expected to behave like the normal material in the drum. If it is inserted in the form of a perfect impulse, a normalized version of the measured concentration is the distribution function of the residence time in corresponding part of the kiln. (Nyström, 1978.) Nowadays nonintrusive techniques like nuclear magnetic resonance (NMR) and positron emission particle tracking (PEPT) are used but these techniques have limitations. Fiber-optic probes have been used for bulk processing in the past to establish bulk velocity profiles that have allowed estimates of the parameters necessary for bulk convection heat transport. (Boateng, 2008.)

3.1.1 Coefficient of Variation (CoV)

The degree of homogeneity in mixing can be studied with the coefficient of variation (CoV). For example temporal CoV can be studied with concentration difference as shown with equation

$$CoV = \frac{\sigma}{\bar{C}} = \frac{\sqrt{\frac{\sum_{i=1}^{n}(C_i - \bar{C})^2}{n-1}}}{\bar{C}} \qquad (2)$$

where
- $\bar{C}$ Average of concentration difference, mol/dm^3
- C_i Concentration, mol/dm^3
- n Number of measurements made in measurement point
- σ Standard deviation of the concentration difference values, -

When CoV number decreases the mixing quality improves so that zero value is for perfect mixing. (Aubin *et al.*, 2003.)

3.1.2 Other Mixing Indexes

Homogeneity must be considered when determining the quality of product. The mixing index is directly proportional to the standard deviation. The most known mixing index is presented by *Lacey* (1954)

$$M = \frac{\sigma_0^2 - \sigma^2}{\sigma_0^2 - \sigma_R^2} \quad (3)$$

Where σ^2 Mixture variance, -

σ^2_0 Upper limit of mixture variance, -

σ^2_R Lower limit of mixture variance, -

Mixing quality can also be presented by logarithmic scale according to equation

$$M^2 = \frac{log\sigma_0^2 - log\sigma^2}{log\sigma_0^2 - log\sigma_r^2} \quad (4)$$

Degree of homogeneity can also be calculated by using some mixing variables such as concentration, temperature etc. to present quality of mixing

$$M(t) = \frac{X_o - X(t)}{X_o - X_1} \quad (5)$$

Where X Mixing variable (Concentration, temperature etc.), -

X_0 Mixing variable at time 0, -

X_1 Mixing variable at the end of experiment, -

3.1.3 Simulant Materials

Some common simulant materials used in mixing are:

- Water
- Glucose Syrup and Corn Syrup
- Glycerol
- Silicone Oils
- Sodium carboxymethylcellulose (CMC)
- Carbopol
- Natrosol
- Versicol

Water is an ideal simulant fluid for Newtonian mixing in the turbulent regime because it is cheap and readily available. Also its density and conductivity can readily be modified by the addition of various salts. The dynamic viscosity of water at 20 °C is 1.002 mPa·s so it is very low viscous material. Due to this diffusion coefficients in water are relatively high compared to other simulant materials mentioned above. *Glucose Syrup* is extremely viscous transparent Newtonian material with viscosity of about 150 Pa s at room temperature. Due to high viscous property it can be noted that diffusion coefficients are negligible because each element of fluid slides past next element with almost no interaction by molecular diffusion. 99.9 % *glycerol* viscosity is about 1.6 Pa s at room temperature and it is even more transparent than glucose syrup. It is good for transitional and laminar flow Newtonian LDA (Laser Doppler Anemometry) work. *Silicone oils* are clear Newtonian fluids available in a large range of viscosities. Due to this also the diffusion coefficients in silicones are varying. With lower viscosity the coefficients are higher and with higher viscosity the coefficient are negligible. *CMC* solutions need to be made up from appropriate grade of powdered CMC. With different concentrations and large range of viscosities the diffusion coefficients are also varying. Even though specialist equipment can be obtained to perform mixing, a laboratory mixing vessel can also be used for this process. CMC solutions are especially useful for performing

mixing experiments because they are inexpensive and the viscosity is relatively intensive to small changes in temperature and dilution. Also great quantities of salt can be dissolved in a CMC solution without greatly affected its rheological properties. (Brown *et al.*, 2004; Levenspiel, 1999; CPKelco, 2014.)

3.1.4 Plug Flow Reactor

Assume an ideal pulse of tracer is introduced into the fluid that flows in a vessel. The pulse spreads as it flows through the vessel and the spreading a diffusion-like process superimposed on plug flow is assumed. This is called dispersion or longitudinal dispersion to distinguish it from molecular diffusion. The dispersion coefficient ,**D**, represents the spreading of the pulse so that large D coefficient means rapid spreading, small D means slow spreading and if the D is 0 it means that there is no spreading. The $\frac{D}{uL}$ is the dimensionless group characterizing the spread in the whole vessel. (Levenspiel, 1999.)

Tubular reactor is one of the most common reactor types in an industrial scale. In a turbulent reactor the fluid phases flow though a fixed bed of catalyst. The plug flow reactor model can be divided into dynamic and steady state models. Dynamic models reveal more information about the reactor performance and can also be used for simulating steady-state operation. Dynamic models are used typically in process start-ups, shutdowns, transients during process disturbances and in safety studies. (Lou *et al.*, 2006.) A dynamic tubular reactor model consists of partial differential equations. Usually, the solution is to reduce them into a set of ordinary differential equations by spatial discretization and to use well-known algorithms for ordinary differential equations to solve the time-depended model. (Alopaeus *et al.*, 2008.)

Plug flow reactor can be observed with the species transport equation

$$\frac{\partial \mathrm{C}}{\partial \mathrm{t}} + \frac{\partial}{\partial \mathrm{x}_i}(u_i C) = \frac{\partial}{\partial \mathrm{x}_i}\left(\boldsymbol{D}\frac{\partial \mathrm{C}}{\partial \mathrm{x}_i}\right) + S \qquad (6)$$

Where D Dispersion coefficient, m^2/s

S Source term, -

t time, s

x_i position, m

And by eliminating the source term, S the transport equation can be given as

$$\frac{\partial \mathrm{C}}{\partial \mathrm{t}} + u\frac{\partial \mathrm{C}}{\partial \mathrm{x}_i} = \boldsymbol{D}\frac{\partial^2 \mathrm{C}}{\partial {\mathrm{x}_i}^2} \qquad (7)$$

The spreading of tracer according to the dispersion model is presented in Figure 11.

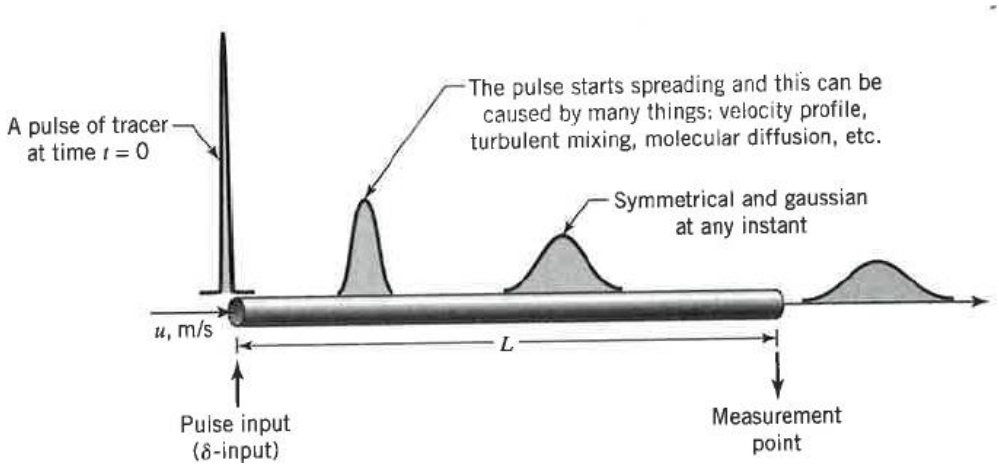

Figure 11 The spreading of tracer or impulse response test according to the dispersion model (Levenspiel, 1999).

Dispersion can be related to diffusion. The relation exists on two different levels. Dispersion is a form of mixing and because of this on a molecular level it involves diffusion of molecules. Diffusion and dispersion are also described with similar mathematics, meaning that analyses developed for diffusion can be also correlate results for dispersion. (Cussler, 2009.) Diffusion constant D_i can be presented with Stokes Einstein equation

$$D_i = \frac{k_B T}{6\pi\mu R_0} \quad (8)$$

Where k_B Bolzmann's constant, J/K

T Temperature, K

R_0 Solute radius, m

As noted above the mathematical analyses developed for diffusion can be also correlate results for dispersion. Thus equation 7 can also be presented in the form of

$$\frac{\partial \mathrm{C}}{\partial \mathrm{t}} + u\frac{\partial \mathrm{C}}{\partial \mathrm{x}_i} = D_i \frac{\partial^2 \mathrm{C}}{\partial {\mathrm{x}_i}^2} \quad (9)$$

3.1.5 Axial Dispersion

To evaluate D or $\frac{D}{uL}$by the shape of the tracer curve the mean time of passage, $\bar{t}$ and variance of the spread of the curve, σ^2, which are directly linked to theory of D or $\frac{D}{uL}$. The mean, $\bar{t}$, for continuous or discrete data can be defined by equation

$$\bar{t} = \frac{\int_0^\infty t\ C\ dt}{\int_0^\infty C\ dt} = \frac{\sum t_i C_i \Delta t_i}{\sum C_i \Delta t_i} \quad (10)$$

The variance is defined by equation

$$\sigma^2 = \frac{\int_0^\infty (t-\bar{t})^2 C\ dt}{\int_0^\infty C\ dt} = \frac{\int_0^\infty t^2\ C\ dT}{\int_0^\infty C\ dT} - \bar{t}^2 \quad (11)$$

Or in discrete form

$$\sigma^2 = \frac{\sum (t-\bar{t})^2 C_i \Delta t_i}{\sum C_i \Delta t_i} = \frac{\sum {t_i}^2 C_i \Delta t_i}{\sum C_i \Delta t_i} - \bar{t}^2 \quad (12)$$

The variance represents the square of the spread of the distribution as it travels the vessel exit and has units of (time) ^{2}. Different distributions are presented in Figure 12.

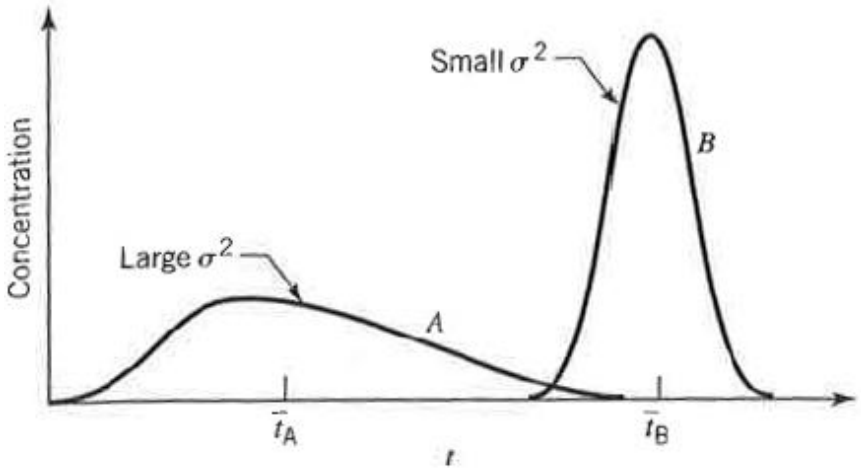

Figure 12 Large and small spreading of variances (Levenspiel, 1999).

Correlation variance, mean and the dimensionless group, $\frac{D}{uL}$, can be studied with equation

$$\sigma^2{}_\theta = \frac{\sigma^2}{\bar{t}} = 2\frac{D}{uL} \tag{13}$$

Where L Length of pipe, m

u Flow rate, m/s

If the $\frac{\boldsymbol{D}}{uL}$ is closer the 0 the dispersion is negligible. When $\frac{\boldsymbol{D}}{uL}$ grows it means larger dispersion hence mixed flow. (Levenspiel, 1999.)

However, this model is not suitable for high viscosity fluids and non-mixed systems. For high viscous fluids it is assumed that each element of fluid slides past its neighbor with no interaction by molecular diffusion. Thus, the spread in residence times is caused only by the velocity variations. (Levenspiel, 1999.)

3.1.6 Bulk Density

The bulk density is defined as the weight per unit volume of a large group of particles. Measurement of bulk density should not be a problem but the difficulty is in interpreting the results from such measurements, since the several definitions of bulk solids exist including aerated, packed, tapped, fluid, average and the working bulk density. Working bulk density can be defined by equation

$$\rho_w = (\rho_p - \rho_A) \cdot C_c + \rho_A \quad (14)$$

Where	C_c	Compressibility	,-
	ρ_A	Aerated bulk density	,kg/m^3
	ρ_p	Packed bulk density	,kg/m^3

Compressibility can be expressed as a fraction of packed bulk density and aerated bulk density

$$C_c = \frac{\rho_p - \rho_A}{\rho_p} \quad (15)$$

With the present state knowledge, it is hard if not impossible to establish any relationship between the bulk density of a material and its flow behavior because bulk material with widely different bulk densities can have similar flow characteristics. (Shamlou, 1988).

The bulk density of fine-grained or cohesive bulk solids is strongly dependent on consolidation stress while free-flowing, coarse materials are typically almost incompressible. While the consolidation stress increases the bulk density increases. For example the limestone has a solid density of around 2 700 kg/m3. With a shear tester a bulk density of 1 050 kg/m3 has been determined for a fine-grained limestone powder at a certain stress level. When studying the flow properties of bulk solids it is seen that the larger the difference between the principal stresses in x- and y-directions and between the corresponding strains the

better the particles can move and thus rearrange to a denser packing. (Schulze, 2008.)

4 DRUM MIXERS

Direct-fired rotary kiln is one of the most important of the high-temperature process furnaces. Due to high-temperatures rotary kiln shells are lined in part or for their entire length with a refractory brick to prevent overheating of the steel with resulting weakening. Usually insulating brick is also used. (Porter *et al.,* 1973.) Rotary kilns are widely in industry including calcination of limestone, reduction of oxide ore, reclamation of hydrated lime, calcination of petroleum coke and waste incineration (Yin *et al.,* 2014). Rotary kilns are commonly used in mineral processing industry to thermally process granular materials. While kiln rotation promotes particle mixing and heat transfer it leads to mixing through segregation of finer and denser particles. (Dhanjal *et al.,* 2004.) Pilot and industrial kiln trials have shown that poor mixing can lead to poor energy utilization, poor product quality and lower productivity. Kiln mixing performance can be improved by adding lifters but the direct effect of these devices on mixing, heat transfer and breakage have not been optimized. Radial segregation is affected by difference in size, density, kiln diameter and kiln rotation speed. (Henein, 1991.)

Direct rotary kiln is a metal cylinder lined on the interior with insulating block and refractory brick due to high temperature operations. The feed is fed into the upper end of the kiln by various methods including inclined chutes, overhung screw conveyors and slurry pipes. Ring dams or chokes of a refractory material are installed within the kiln to build a deeper bed at one point to change the flow pattern. The product discharged from the lower end of the kiln onto conveyors or into tanks or cooling devices which may recover the heat content. (Porter *et al.,* 1973) Schematic diagram of counter-current flow rotary kiln configuration is shown in Figure 13.

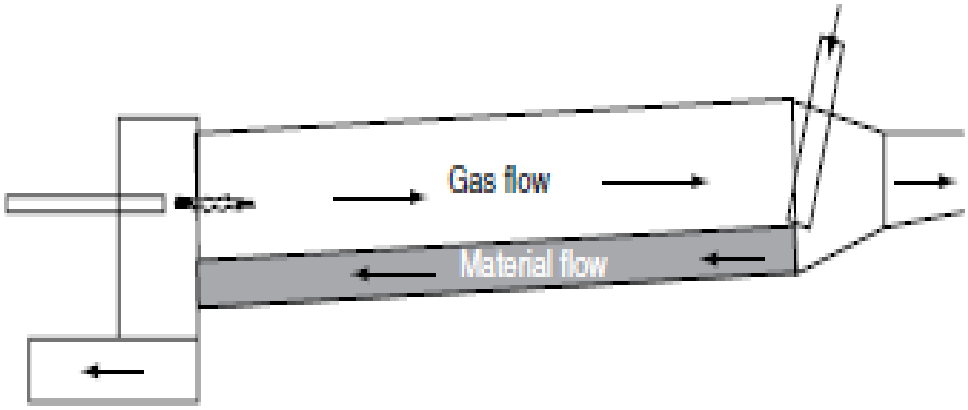

Figure 13 Schematic diagram of counter-current flow rotary kiln configuration (Boateng, 2008).

A typical kiln comprises a cylinder up to 6 m in diameter with length/diameter ratio between 10 and 40 depending on residence time which is typically 2 to 5 hours. Some kilns may have two or three different diameters. It is claimed that this arrangement improves product quality, increases kiln capacity and decreases fuel consumption. The percent fill of the kilns is usually between 8–15 % while the rotation speed ranges from 1 rpm to 5 rpm. Granular material is fed from a raised end and a rotary kiln slopes slightly (few degrees) towards the firing end where the material is removed. The gas flow is counter-current to bed movement and the gas is heated to supply the needed energy for processing the material. The heat can be transferred by conduction, convection and radiation from gas to wall, gas to bed and wall to bed. The heat transfer is important when studying size segregation of the kiln. The finest particles remain at the bottom in contact with hot brick while the coarser particles form the upper layer of the agitated mass. Mixing of the particles and heat transfer can be intensified by adding lifters which raise the particles up and at the certain point drop the particles to the bottom of the kiln. (Yin *et al.*, 2014; Dhanjal *et al.*, 2004; Davies *et al.*, 2010; Porter *et al.*, 1973) Inclination of the kiln depends on process and varies usually from 2 to 6 cm/m. Rotation speed is usually very slow and also depends on process for example 0.15 m/s is typical to TiO_2 pigment kiln process, 0.22 m/s for cement kiln and 0.64 m/s for calcining phosphate materials. (Porter *et al.*, 1973)

Some special features are getting popular including the discharge end designed for air cooling or kilns that operate in high temperatures such as cement, magnesia

and dead-burned dolomite. As fuel prices are increasing the heat transfer must be intensified. This can be done by adding internal heat recuperators of numerous different designs. Also thermocouple collectors can be installed at various points on to shell for indicating and recording internal temperatures. Scoops are provided for introducing collected dust or feed component through the shell at some intermediate point or points. Ports are installed in the shell for admitting combustion air at points beyond the hot zone. These are used in kilns for reducing volatiles from materials being processed and for burning carbon monoxide. (Porter *et al.,* 1973)

Firing can be accomplished at either end, depending on whether concurrent or countercurrent flow of charge and gases is desired. Sometimes a solid fuel is mixed with the charge and moves down the kiln while burning. The burner can be attached directly at the end of the kiln with combustion occurring inside. Then the discharge-end is a housing that usually consists of a fixed or movable kiln hood through which the fuel pipe enters the kiln. The exhaust gases are usually discharged into dust and fume knockdown equipment to avoid contamination of the atmosphere. Cyclones, settling chambers, scrubbing towers and electrical precipitators are used as gas-cleaning equipment. Waste-heat boilers, grates, coil systems and chains can be used as heat recovery devices used in both ends of the kiln. Fuel consumption can be decreased and kiln capacity increased with heat recovery devices. Chains are attached at the feed end of the rotary kiln for accelerated drying of slurries. Thus slurry is heated by direct transfer from chains after suspension in hot gases, by lifting material into the path of hot gases and by directing the flow of hot gas over the slurry bed in the space formed under the suspended chains. (Porter *et al.,* 1973)

During the operation it may encounter the dilemma of how to operate the kiln at an optimal air excess ratio. High temperatures in the combustion chamber cause damage to the kiln lining, contamination of the surface of the stone which can fuse one lump to another and cause the formation of clay lumps. The flame must be cooled with a great amount of relatively cold secondary air due to high temperatures in the combustion chambers at optimal air excess ratio. This results in greater heat loss with the exhaust kiln gas, lower kiln efficiency and bigger fuel

consumption. Air excess ratio can be reduced to its optimal level by recirculation of recuperator waste gas and its injection into the combustion chambers. Stack losses also reduce while the temperature in the combustion chamber remains within the permissible range. This leads to reduced specific energy consumption. (Senegacnik *et al*, 2008.)

The capacity of the existing kiln can be increased with the following changes:

- Increase charge volume held in kiln.
- Increase temperature and quantity of combustion gases.
- Decrease quantity of air in excess of combustion gases.
- Increase speed of rotation of kiln.
- Install ring dams at intermediate and discharge mechanisms.
- Decrease moisture content of feed material.
- Increase temperature of feed material.
- Install chains in the feed end.
- Preheat all combustion air.
- Reduce leakage of cold air into kiln at hot end.
- Increase of stack draft by increasing height or by use of jets.
- Install instrumentation to control the kiln at maximum-capacity condition.

When determining thermal efficiency the kiln length is a major factor. The kilns with high ratio of length to diameter have a greater thermal efficiency than those with a low ratio. By using chains inside the kiln and by using heat-recovery equipment on the gases and product leaving the kiln the thermal efficiency of the kiln installation is increased significantly. Efficiencies are varying from 45 % to more than 80 %. (Porter *et al.,* 1973)

4.1 Different Drum Mixers

A kiln consists of four heating zones which are *drying zone* at feed end where the moisture is removed, *heating zone* where the charge is heated to the reaction temperature, *reaction zone* in which the charge is burned, decomposed, reduced,

oxidized etc. and *the soaking zone* where the reacted charge is superheated or soaked at the temperature of cooled before being removed from the kiln. Some of the major uses of direct rotary kiln are: (Porter *et al.*, 1973)

- Cement kiln, where the maximum charge temperature is 1400 °C to 1500 °C.
- Lime kiln, where the maximum charge temperature is 900 °C to 1300 °C.
- Roasting: Rotary kilns are used for oxidizing and driving off sulfur and arsenic from various ores in the temperature varying from 500 °C to 1300 °C.
- Chloridizing. Silver ore are chloridized in rotary kiln at temperature between 755 °C and 815 °C.
- Black ash. Barium sulfide is produced by calcining a mixture of barite and carbon at a temperature of 1075 °C.
- Titanium oxide. Titanium oxide is produced from ilmenite ore by mixing ore with carbon and heating in a rotary kiln. The rotary kiln is also used in the process of recovery of titanium oxide from hydrated titanium precipitate at about 975 °C.
- Spodumene. A mixture of quartz, feldspar and spodumene is being calcined in rotary kiln to produce lithium aluminum silicate at temperature of 1200 °C.
- Vermiculite. A miscaceous mineral is roasted to cause exfoliation for use as an insulation material.
- Zinc. Oxidized ores are calcined to drive off water of hydration and carbon dioxide. The sulfide ores are roasted before smelting.
- Roofing granules. Crushed sand or quartz of definite size is treated with various minerals, soda ash, borax etc. and calcined at temperatures from 975 °C to 1325 °C.
- Alumina. Alumina is produced by calcining either aluminum hydroxide or bauxite in rotary kilns at temperatures from 975 °C to 1325 °C.
- Potassium salts. Potassium chloride is fed to rotary kiln at a fineness of minus 100 mesh and containing 9 % percent water. The salt is brought to the fusion temperature of 775 °C.

- Phosphate rock. The rotary kiln is used to nodulize the fines in the ore and prepare them for electric-furnace operation. Ore nodulizes at approximately 1200 to 1225 °C.
- Mercury. Cinnarbar ore is fed to rotary kiln where it is calcined to over 525 °C. Because the mercury exists as mercuric sulfide, the sulfur is oxidized to SO_2 and the mercury vaporized. The gases are passed though cooling chambers when the mercury condenses and is collected.
- Gypsum. The rotary kiln is replacing the kettle in producing plaster of paris. Temperatures for reaction are low and within narrow limits from 109 °C to 130 °C.
- Clay. Clay is calcined in rotary kilns to produce lightweight aggregate for concentrate. Temperatures vary from 1080 to 1330 °C.
- Iron ores. Iron ores are partially reduced in rotary kiln to obtain nodules which are used in blast-furnace charges.
- Manganese. Manganese ore, rhodochrosite or manganese carbonate is calcined at about 1250 °C to produce the oxide.
- Petroleum coke. To eliminate excess volatile matter, petroleum coke is calcined at temperatures varying from 1200 °C to 1250 °C.

Modern day rotary kilns can also be divided in wet kilns, long dry kilns, short dry kilns, indirect fired kilns and coolers and dryers. *Wet kilns* usually operate slurry material. The length of the wet kiln is usually long and varies between 150 m and 180 m. The feed end is usually equipment with chains to help the feed to be dried and to break the feed lumps. Lime mud kilns are used as wet kilns in pulp and paper industry. (Boateng, 2008.)

Long dry kilns are shorter than wet kilns. Typical length is 90–120 m. The main reason for shorten length is that feed is dry with a moisture content the same as granular solids rather than dry. Drying, preheating and calcination all occur in the same vessel in the same way as in wet kiln. *Short dry kilns* are connected by an external preheater or pre-calciner in which the feed is dried, preheated or even partially calcined prior to entering the main kiln. Because of pre-heater the main kiln is short usually 15–75 m depending of process. If the feed is almost calcined

the kiln can be shorter. Applications include cement industry and some lime kilns. Due to large feed particle size encountered in limestone calcination modern lime kilns are equipment with preheaters function as packed bed of stone with counter-current flow of the kiln exhaust gases rather than the typical cyclone preheaters in cement kiln system. (Boateng, 2008.)

Indirect fired kilns are heated externally. They are designed for cases where direct contact between material and gas is undesirable. Due to low thermal efficiency these kilns are usually small typically up to 1.3 m in diameter and are used for niche applications such as calcining of specialty materials. Typical applications include calcination, controlled oxidation, reduction, solid-state reactions, carburization and purification including waste remediation on a small scale. Extremely high temperatures and control are needed and these are achieved by heating electrically. Materials processed in indirectly fired kilns include materials like titanates, phosphors, zinc oxide and quartz ferrites. (Boateng, 2008.)

5 PHYSICAL PHENOMENA

The energy needed to raise the bed temperature to the level required for the intended reactions originates with the combustion of hydrocarbon fuels in the gas phase near the heat source or burner. This energy is transferred by the heat exchange between the gas phase and the bed. Heat transfer between bed and gas phase is complex and occurs by all paths established by the geometric view factors in radiation exchange as shown in Figure 14. (Boateng, 2008.) Many descriptions of the rotary kiln bed phenomenon have been proposed and all of these assume that at each axial position the bed is well mixed in the transverse plane while the bed is isothermal over any transverse section of the kiln (Brimacombe *et al*., 1978, Gorog *et al*, 1981). The industrial problems are that many processes produce a uniform product where large particles may be dead-burned and while finer particles are fully calcined. Evidence like this suggests that substantial transverse temperature gradients are generated within the bed. (Boateng, 2008.)

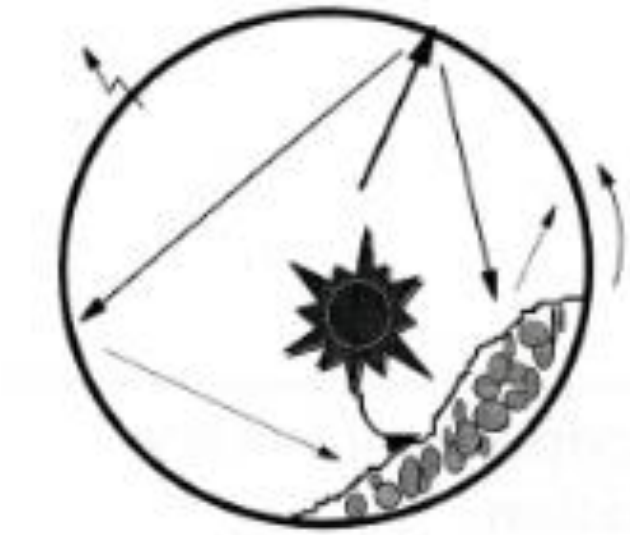

Figure 14 Heat flow paths in a rotary kiln. Radiation heat exchange in the cross section (Boateng, 2008).

5.1 Heat Transfer

Heat transfer in the freeboard is more than just to sustain combustion at the combustion zone. It involves the exchange of energy from the freeboard to the bed to carry out the operated process. Most of the energy needs to be transferred into the material and later exhaust the rest for process to be efficient. Heat transfer in rotating kiln includes the modes of conduction, convection and radiation. Radiation and conduction are fundamental physical transfer mechanism and convection is really conduction as effected by fluid flow. Radiation is believed to be the dominated mode of heat transfer in the freeboard constituting over 90 % primarily due to the large flame and curvature of the combustion chamber. Convection in the freeboard occurs as a function of the turbulent flow of gases and participates in the heat transfer to the free surface of the bed and the refractory wall in a manner alike to flow over heated plates. Heat is conducted from the freeboard to outside environment through the refractory wall. In the bed the heat transfers by interparticle conduction. (Barr *et al*., 1989; Boateng, 1993.)

5.1.1 Turbulent Flow Heat Transfer in Pipes

The relations for heat transfer to or from the fluid and the wall are well known and are the basis of many heat transfer designs in turbulent flows in pipes. The overall heat transfer consists of a resistance on the cooling or heating side, a fluid resistance inside the pipe and a wall resistance. The fluid resistance inside the pipe depends on the nature of the fluid and the flow regime. Static mixers and other pipe inserts are not usually justified in turbulent flow, since the cost and added pressure drop are high relative to the benefit achieved. Heat transfer coefficient for predicting inside or process heat transfer is studied according to Nusselt number

$$Nu = A \cdot Re^{d} \cdot Pr^{e} \cdot \left(\frac{\mu}{\mu_w}\right)^{f} \quad (16)$$

Where	A	Constant, typically 1 to 2
	d	Constant, typically 0.66
	e	Constant, typically 0.33
	f	Constant, typically 0.14
	Re	Reynolds' number, -
	Pr	Prandtl number, -
	μ	Fluid viscosity, Pa s
	μ_w	The viscosity at the tube wall, Pa s

However, even though the flow is turbulent, there is a significant viscosity effect meaning that the addition of the viscosity ratio is empirical. Based on the observation that the heat transfer coefficients are lower in case of cooling than in case of heating. The heat transfer takes place in a wall film and the conditions of the film are better characterized by the local properties at the local temperature. (Etchells III, 2004.)

5.1.2 Laminar Flow Heat Transfer in Pipes

In laminar flow the heat transfer rates are significantly reduced. There is not radial flow and temperature gradients build up, reducing the heat transfer rate. Besides, the parabolic velocity distribution causes the center to spend little time in the heating zone and the fluid near the walls to spend more time. The overall effect is that the local heat exchange coefficient becomes a function of the length and can even approach zero at long lengths. As result, heat transfer in laminar flow is very poor and uniform. Heat transfer coefficients for laminar flow in empty pipe are correlated by according the equation (Etchells III, 2004.)

$$Nu = A \cdot Re^{d} \cdot Pr^{e} \cdot \left(\frac{\mu}{\mu_w}\right)^{f} \left(\frac{D_p}{L}\right)^{j} \quad (17)$$

Where

A	Constant, typically 1.62
d	Constant, typically 0.33
e	Constant, typically 0.33
f	Constant, typically 0 to 0.14
j	Constant, typically 0.33
D_p	Diameter of the pipe, m

Because the static and motionless mixer promotes radial flow of both momentum and heat, it will significantly enhance the heat transfer rate and the heat transfer coefficients are correlated by according the equation (Etchells III, 2004.)

$$Nu = A \cdot (Re \cdot Pr)^{a} \cdot \left(\frac{\mu}{\mu_w}\right)^{b} \left(\frac{D}{L}\right)^{c} \quad (18)$$

Where

A	Constant, Depends on vendor correlation
a	Constant, Depends on vendor correlation
b	Constant, typically 0.14
c	Constant, Depends on vendor correlation

5.2 Bed Phenomenon

During the thermal processing of granular materials, heat transfer within bed material occurs by the same mechanism as in any packed bed. Heat transfer occurs particle-to-particle by conduction, radiation and gas-to-particle convection as shown in Figure 15. The movement of the particles themselves superimposes an advective component for energy transport which has a potential to determinate heat transfer. The motion in the transverse plane is the key feature of a rotary granular bed. It sets the axial flow in motion. It depends upon the rotation rate, rheological properties of the particulate material and degree of fill. Because the kiln is typically cylindrical and partially filled it possesses two dispersion mechanisms. They are *the axial direction* that is characterized by an axial mixing coefficient and in *the transverse direction* characterized with a radial mixing coefficient. The axial mixing component is caused by the mechanism that results in an overall convection and causes the bulk of the material to move to outlet of the kiln with an average velocity equal to plug flow velocity. The radial mixing component involves mechanisms at the smaller scale that causes local constraints on individual particles. It results in velocity components both in the transverse direction and the axial direction. When the rotation speed of the kiln increases both transverse and axial mixing coefficients are increasing. (Boateng, 2008.)

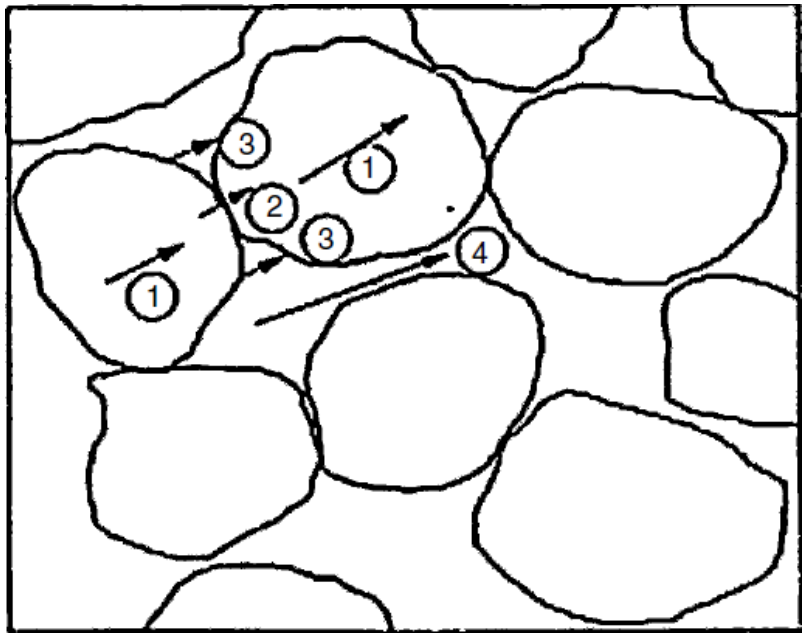

Figure 15 Bed heat transfer paths. 1. Internal conduction. 2. Particle-to-particle conduction. 3. Particle-to-particle radiation. 4. Interparticle convection. (Boateng, 1993.)

5.3 Axial Motion

Transverse dispersion is depended on axial dispersion. For each transition within the cross section a particle on the free surface transporting on the chord length makes an axial move either forward or backward. This occurs because of the random nature of flow within the active layer. The forward advance is based on the apparent forward angle resulting from the transverse flow pattern as well as the cylinder slope in the axial direction. (Boateng, 2008.)

Vessel size is the key geometrical feature. Diameter and length of the cylinder plays an important role with length-to-diameter ratio (L/D). Also the slope of the kiln is a key geometrical feature. Other relevant features include the internals such as constriction dams and lifters that have an effect on residence time. The sizing of the rotary kiln depends on the application, the feed rate and related transport properties like temperature, gas flow rate and material flow rate that will determine the residence time. The empirical relationship relating the residence time and the kiln geometry is presented with equation (Perry, 1984.)

$$\bar{\tau} = \frac{0.23L}{sN^{0.9}D_p} \pm 0.6\frac{BLG}{F} \quad (19)$$

Where

B	Constant depending on material, -
D_p	Diameter, ft
F	Feed rate, lb/hr/ft^2
G	Freeboard gas velocity, lb/hr/ft^2
L	Kiln length, ft
N	Kiln rotational speed, rpm
s	The slope, degree/radians/ ft/ft

5.4 Transverse Bed Motion

At critical and high rotational speed of a kiln the bed motion in the transverse plane can be characterized as centrifuging. This is an extreme condition in which all the bed particles rotate with the drum wall. Cascading occurs at relatively high rotation speeds in which the height of the leading edge of the powder rises above the bed surface and particles shower or cascade down on the free surface. However operating kiln in these conditions is rare because of the dusting and attrition problems. If the drum behavior and the type of transverse bed motion occurs during the powder processing the dynamic similarity depends on the rotational Froude number, Fr, which is presented with equation

$$Fr = \frac{\omega^2 R}{g} \quad (20)$$

Where

g	Acceleration due to gravity, m/s^2
R	Kiln internal radius, m
ω	Angular velocity, 1/s

The ranges of Froude numbers for the different modes are shown in Figure 16.

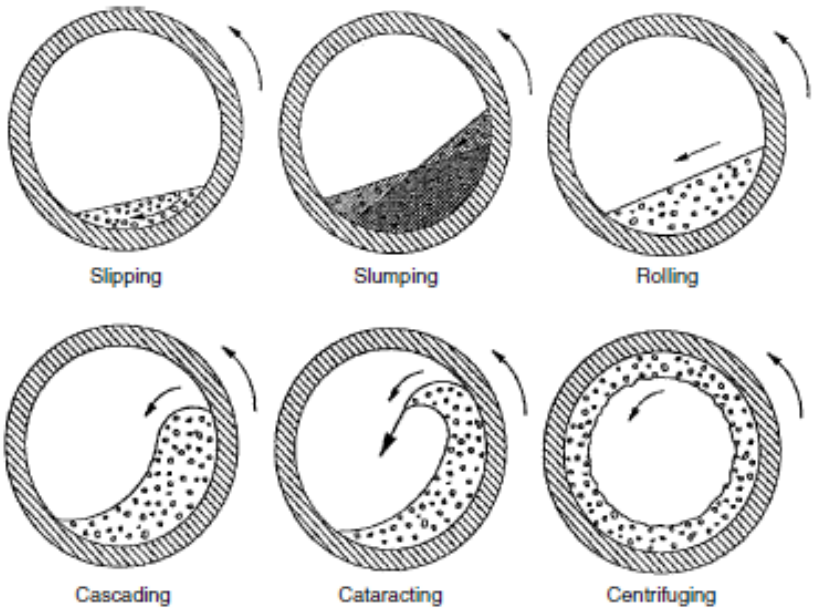

Mode	$Fr(=\omega^2 R/g)$ at $\phi = 35°$
1. Slipping	$Fr < 1.0 \times 10^{-5}$
2. Slumping	$1.0 \times 10^{-5} < Fr < 0.3 \times 10^{-3}$
3. Rolling	$0.5 \times 10^{-3} < Fr < 0.2 \times 10^{-1}$
4. Cascading	$0.4 \times 10^{-1} < Fr < 0.8 \times 10^{-1}$
5. Cataracting	$0.9 \times 10^{1} < Fr < 1$
6. Centrifuging	$Fr > 1.0$

Figure 16 Bed motion in cross sectional plane. Froude numbers are given for each of the different modes. (Henein, 1980.)

Two regions of the transverse plane can be observed which are *the active region* near the top of the bed where surface renewal occurs and *the passive region* beneath the active region. Particles in the active region are not restricted and they move faster. The active region is usually thinner than the passive region. Because the bed is constrained within the cylinder's geometrical domain the laws of conservation of mass requires that the depth of the active region must be less than that of the passive region. Most of the mixing in drum cross section takes place in the active region and the mixing is always better in active layers if the active region is deeper. The active layer depth can be increased by increasing the rotation speed of the kiln. Tracer studies (Ferron *et al.*, 1991) show that particles move forward along the kiln only through the active region. Because the longitudinal slope of the kiln is small and far less than the material angle of repose the forward motion cannot be sustained by the gravitational component of the stresses alone indicating that the longitudinal slope assists this forward motion but does not drive it. So, for every kiln revolution the bed particles make several excursions in the cross section resulting in an axial advance. When rotation speed

is increased the mixing improves but the residence time of the material decreases. That is why it is important to know the needed residence time to achieve the wanted product quality. (Barr *et al*., 1997; Boateng, 2008.)

5.5 Freeboard Aerodynamic Phenomena

Fluid flow through the kiln freeboard is generated from number of sources such as combustion products, combustion air and the air infiltrated into the vessel. In direct-fired kilns the fuel is introduced from a pipe. Because the chamber is much larger than the burner pipe the fuel emerges as a jet. The freeboard flow phenomenon near the combustion zone therefore exhibits the properties of jets. Because of this the gross pattern of the flow in the region near the burner is determined by the geometry or the physical boundaries surrounding the burner typically involving a jet confined in a cylindrical vessel and by the manner in which the fuel is discharged. To prevent pulverized fuel from settling the primary combustion air is introduced at high velocity greater than 30 m/s. The secondary air into which the primary air is discharged is introduced at lower velocity in the range 5–15 m/s. The primary air usually comprises about 25 % of the combustion air requirements in a direct-fired rotary kiln and the secondary air makes up for the remaining 75 % of the combustion air. The secondary air can be introduced through the inlet surrounding the primary air or from discharge coolers that recuperate some of the energy in the discharge product and return it into the kiln to improve combustion and fuel efficiencies. In the region further away from the combustion zone the flow field is made up of combustion gases and other gases released due to the bed reactions. In the feed end the high turbulent kinetic energy can lead to increased dust generation and discharge through the exhaust. (Boateng, 2008.)

6 RHEOLOGY OF FLUID

Rheology is a science of flow and deformation of materials. The definition of fluid refers to either a liquid or gas. The principal theoretical concepts are kinematics, dealing with geometrical aspects of flow and deformation, forces, stress, conservation laws and energy interchanges.

The nature of viscosity can be described by the velocity distribution between two plates. The fluid motion is supported by applying a radial force to the upper plate. Fluid velocity is proportional to the distance between plates illustrated by the equation

$$u(y) = \frac{y}{h}U \tag{21}$$

Where h Distance of plates, m

U Velocity, m/s

y Distance variable in radial direction, m

The frictional force per unit area or the frictional shear stress, τ, is directly proportional to velocity and inversely proportional to the spacing, h, yielding according to equation

$$\tau = \mu\frac{du}{dy} \tag{22}$$

Kinematic viscosity, v, is defined between the dynamic viscosity and fluid density according to equation

$$v = \frac{\mu}{\rho} \tag{23}$$

Where ρ Fluid density, kg/m^3

6.1 Rheology Types

There are the Newtonian and non-Newtonian fluids based on the constitutive relations, namely, the relationship between stress, strain and time. The dynamic viscosity can be defined with equation

$$\mu = \frac{\tau}{\gamma} \tag{24}$$

Where τ Shear stress, Pa

γ Shear rate, s^{-1}

The dynamic viscosity of pure substances is mainly influenced by temperature, pressure, time and shear rate. With mixtures of substances, factors like solids content in the case of suspensions have an impact. In case of Newtonian media, the viscosity is typically highly temperature dependent. (Marte, 2000.) The flow characteristics of a substance can be presented in the form of flow curves or viscosity curves. While the viscosity of Newtonian media exhibits no dependency on shear rate, most non-Newtonian media are highly dependent on it.

6.1.1 Time-dependent Fluids

In the case of Newtonian fluids, the viscosity is constant but for non-Newtonian fluids the viscosity varies which means that the shear stress varies with the rate of shear strain. Most of semi-solids such as mineral slurries are non-Newtonian fluids. The time-dependent non-Newtonian fluids are characterized by a change in viscosity with time under conditions of constant shear rate meaning that fluids can be characterized as thixotropic or rheopectic fluids. A rheopectic fluid undergoes an increase in viscosity with the time when it is subjected to constant shearing, whereas a thixotropic fluid essentially exhibits the opposite of rheopectic behavior, thus the thixotropic fluid's viscosity decreases with time as it is sheared at a constant rate as presented in Figure 17. (He, 2005.)

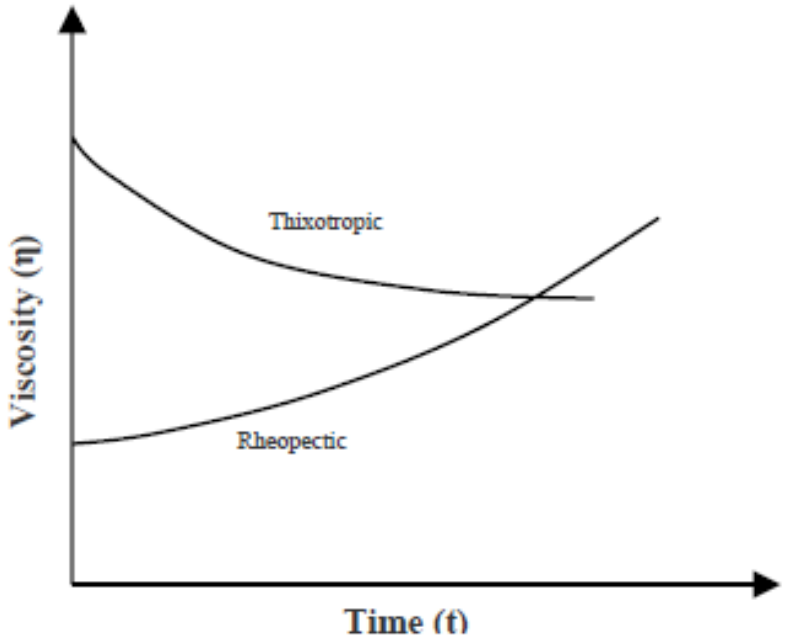

Figure 17 Viscosity versus time curves at a given shear rate for time-dependent non-Newtonian suspensions (He, 2005).

When time-dependent fluid is subjected to a varying shear rate which is increased to a specific value first and then decreased to the starting point, the "up" and "down" rheological curves do not coincide but cause a hysteresis loop presented in Figure 18 (He, 2005).

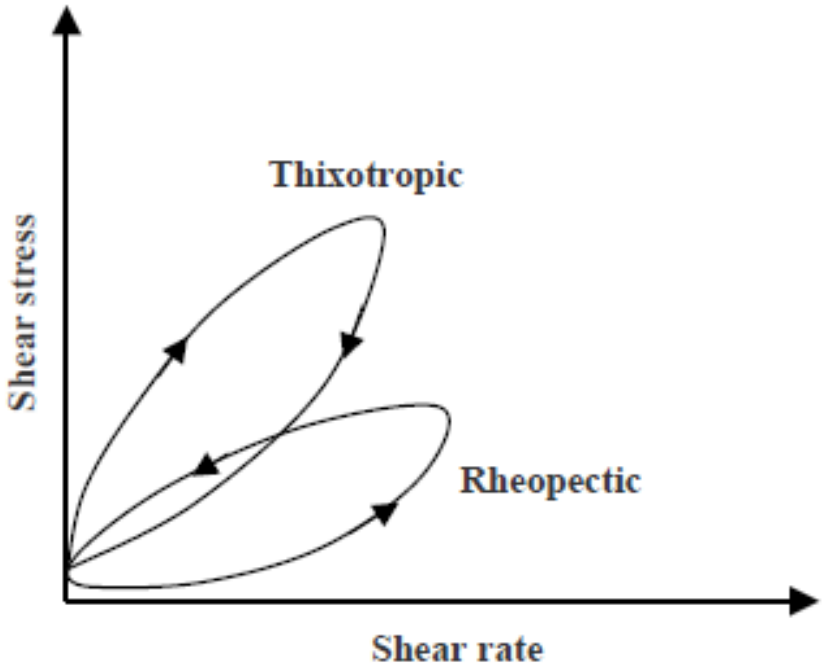

Figure 18 Shear stress versus shear rate curves of time-dependent fluids subjected to varying shear rates (He, 2005).

These effects may or may not be reversible. Rheopexy and thixotrophy may both occur in combination with any of the time-dependent flow behaviors or only at specific shear rate. The time element is highly variable meaning that some fluids will reach their final viscosity values in a few seconds while others may take up to several days. (He, 2005.)

6.1.2 Time-independent Fluids

For time-independent fluids the shear stress at any point is dependent only on the instantaneous shear rate at that point. The most frequently encountered flow anomaly is known as structural viscosity in which the viscosity decreases with increasing shear rate. The rate of increase in shear rate then decreases with increasing shear rate. In many cases non-Newtonian fluids can be described with equation by the Ostwald-de Waele

$$\tau = K\gamma^{m} \tag{25}$$

Where K Consistency factor

m Flow behavior index

This equation can be combined with Newton's viscosity equation (24) to give equation

$$\mu = K\gamma^{m-1} \tag{26}$$

If the shear gradient, flow behavior index and consistency factor are known the corresponding viscosity can be calculated at different shear rates. Typical viscosity curves for several structurally viscous media are shown in Figure 19. (Marte, 2000.)

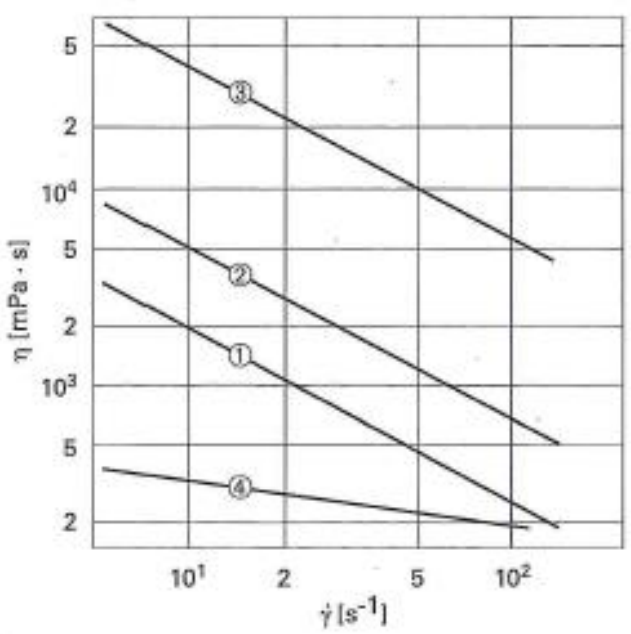

Ostwald-de Waele: $\eta = K \cdot \dot{\gamma}^{m-1}$

Conc. [c_g %]	K [Pa · s^m]	m [—]
Xanthan		
① 1	13.5	0.12
② 3	40	0.12
③ 5	300	0.12
CMC		
④ 0.5	0.6	0.78

Figure 19 Viscosity curves for CMC and xanthan solutions (Marte, 2000).

Non-Newtonian can also be divided into viscoelastic fluids. These fluids have both viscous fluid and elastic solid characteristics. They exhibit partial elastic recovery after a deforming shear stress is removed. (Marte, 2000.)

6.2 Viscosity Effect in Pipes

Gas flow downstream from the entry region in kilns follows principles similar to the generalized pipe flow laws. Though, it is more complex in the near field involving entrained jets. Principles are based the ideal gas laws that demand that PV/T is constant for a nonreacting gas. So changes in any variables P, V or T results changes in others. Most theoretical considerations in fluid dynamics are based on the concept of perfect fluids thus requiring that the fluid is incompressible and frictionless. The no-slip condition in an incompressible fluid means that two contacting layers acting on each other exert only normal or pressure forces but not shear stresses or tangential forces. This assumption falls

shortly in real fluids since they offer internal resistance to a change in shape. This results in the concept of viscosity according to which the existence of intermolecular interactions causes the fluid to adhere to the solid walls containing them. (Boateng, 2008.)

The viscosity can be applied to flow conditions in cylinder pipes similar to conditions in rotary kilns. Fluid flow in conduits was first presented by Reynolds' early experiments that identified the regimes as laminar and turbulent. For rotary kilns these are characterized by the relationships between flow rate and pressure drop. First Reynolds' principle characterizes the laminar flows stating that the pressure drop of a flowing fluid is proportional to the flow rate at low velocities. At high velocities, turbulent flow, the pressure drop of flowing fluid is proportional to roughly the square of the flow rate. The transition regime between laminar and turbulent is defined by Reynolds-' number

$$Re = \frac{\rho U D_p}{\mu} = \frac{Ud}{v} \tag{27}$$

EXPERIMENTAL PART

7 TEST EQUIPMENT AND MATERIALS

Sizing of the pilot-scale rotating drum and lifter design are described in this chapter. Also the used materials are presented. The main parameters such as diameter, length and rotation speed of some Andritz Oy's limekilns are shown in Table 1.

Table 1 Diameter, length and rotation speed of some Andritz Oy's limekilns (Venäläinen, 2014).

Diameter, m	Length, m	Rotation speed, rpm
2.5	45	1.75
3.0	80	1.60
4.0	105	1.50
5.0	145	1.40
5.5	155	1.30

Due to the high operating temperature the lime mud is replaced by the substance with the same rheological properties in lower temperatures. The simulant material to simulate the lime mud was chosen by the rheological studies. To examine the mixing difference between high viscous and less viscous material water was also used. Experiments were also carried out with solid lime mud dust. With this large range of different viscous materials it is more accurate to study the mixing in the kiln due to its challenging and changing operation conditions which have an effect on viscosity inside the kiln.

7.1 Rotary Drum Sizing

Pilot-scale rotating drum was designed mainly based on Andritz Oy's limekiln with diameter 3 m, inner diameter 2.56 m, length 80 m and rotation speed 1.6 rpm. Pilot-scale drum was built up on a small roller so the main structure parameters were set to be 1.15 m in length with diameter 0.3 m. The inner diameter of the drum was 0.29 m. The kiln was supported by two piers and the slope of the drum was 2.5°. Material used for tube construction was acrylic.

Lifter zone and stabilization zones for fluid were designed by the information given by Andritz Oy. The cross section design was planned so that there are four circumferences and 0–8 lifters can be installed on one circumference. It is possible to perform tests with empty pipe or fill all four circumferences with different lifter geometries. The maximum amount of lifters inside the drum is 32.

Mixing zone of lifters is 580 mm in length. The distance of the lifter circumferences from each other is 20 mm. The length 580 mm corresponds to the length of 10 200 mm of a commercial drum. The rest 570 mm of total length of pilot-scale drum are designed as stabilization zones for a fluid. At the feed end the length of stabilization zone is 215 mm and after the lifter zone there is a stabilization zone for 355 mm in length. The total length 1 150 mm of pilot-scale drum corresponds to the length of 20 240 mm of a commercial drum. Basic information of a pilot drum is presented in Table 2. Pilot drum and peripherals are shown in Figures 20 and 21.

Table 2 The basic information of a pilot-scale drum.

Length, m	1.15
Diameter, m	0.3
Inner diameter, m	0.29
Slope, °	2.5
Degree of filling, %	~10
Amount of lifter circumferences, -	4
Amount of lifters on one circumference, -	0–8
Length of lifter zone, m	0.58

Figure 20 The rotating drum used in the experiments. Feed end on the left of the drum and discharge end on the right.

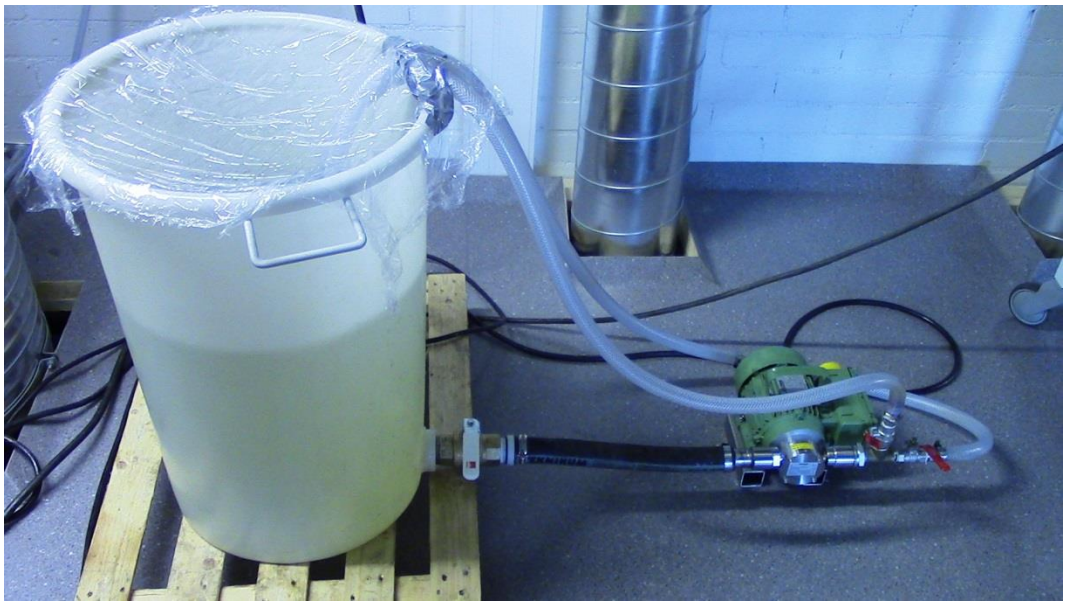

Figure 21 Pump and the feed tank.

7.1.1 Lifter Design

Lifters were designed based the knowledge given by *Venäläinen* (2014) and also based on *Sunnergren et al.* (1979) where it is preferred to use a lifter which is at least one-third the depth of the particle bed but does not exceed 90 % of the depth. With this knowledge three different lifters were designed and the height of the one lifter was determined to be 10 mm.

Different straight lifter geometries were used and lifters were installed horizontally to x-direction of the drum. The length of the horizontal lifter was designed to be 130 mm. Lifter is shown in figure 22.

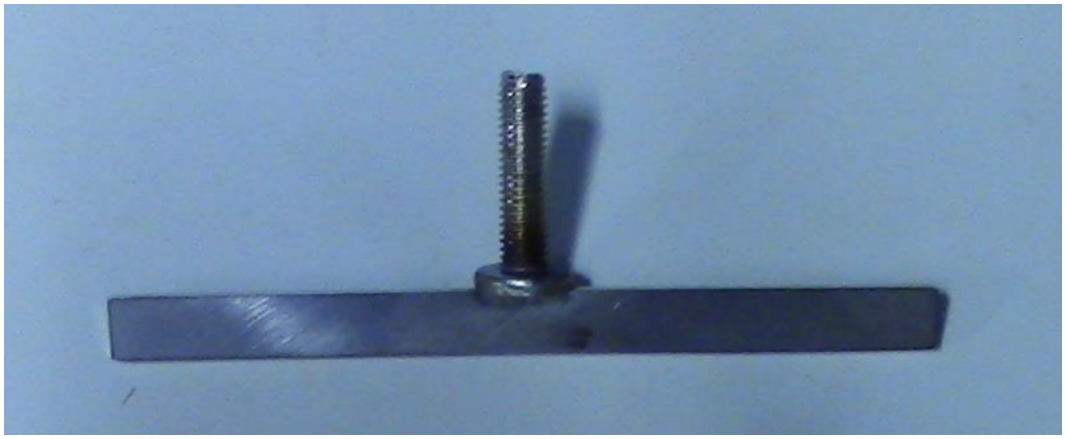

Figure 22 Lifter used in the experiments.

7.2 Rheology of Lime Mud

The temperature in the lime kiln's lifter network varies from 300 °C to 500 °C. Due to the high operating temperature the lime mud is replaced in measurements by the substance with the same viscous properties at lower temperatures.

Finnfix 50 000 (CMC) with mass concentration 1 % was chosen as high viscous material. Rheology studies of lime mud and comparison between different CMC materials are shown in Appendix II. Particle size of lime mud was measured with Malvern Mastersizer 3000. The cumulative particle size distribution was: D_{10} = 5.11 µm; D_{50} = 15.75 µm; D_{90} = 32.90 µm. Mixing was also studied with solid material and less viscosity material. Lime mud dust was chosen as a solid material to give information about solid mixing (highest viscosity). Water was chosen as a low viscosity material due to following reasons:

- It is easily available. (Free and unlimited availability)
- It allows more measurements with different lifter variations. (Measurements are performed faster)
- It provides basic information about mixing.

8 SCALE DOWN FOR PROCESS PARAMETERS

In this chapter the scale down from industrial rotating drums into pilot-scale equipment is presented. The main process parameters for this study were the rotation speed of the drum and the volumetric flow rate. Process parameters for pilot-scale rotating drum were determined based on information by *Venäläinen* (2014) (see Table 1).

As a result of scale up the rotation speeds 2.0 rpm and 4.0 were chosen for measurements. The basis for the determination of the rotating speed in the pilot scale equipment was based on linearly extrapolated results from industrial rotary kilns and based on Froude number (Eq. 20).

The basis for determination of the volumetric flow rates was based on TIP speeds. With TIP speeds the linearized flow rates for pilot scale drum with rotational speeds 2 rpm and 4 rpm were determined according to equations

$$\frac{TIPS_{ind}}{V_{ind}} = \frac{TIPS_p}{V_p} \tag{28}$$

$$V_p = \frac{TIPS_p}{\frac{TIPS_{ind}}{V_{ind}}} \tag{29}$$

Where $TIPS_{ind}$ TIP speed of the industrial lime kiln, m/s

$TIPS_p$ TIP speed of the pilot scale drum, m/s

V_{ind} Linearized flow rate of the industrial lime kiln, m/s

V_p Linearized flow rate of the pilot scale drum, m/s

As a result of scale down the linearized flow rate 0.001 m/s was chosen for measurements with rotational speed 2 rpm. For rotational speed 4 rpm the linearized flow rate 0.002 m/s was chosen. More detailed scale down for process parameters is shown in Appendix I.

9 MEASUREMENTS

For the mixing studies in the drum different materials, process parameters and methods for analyzing the results were used. Water was chosen as a low viscosity material and Finnfix 50 000 (CMC) with mass concentration 1 % was chosen as a high viscosity material to characterize lime mud dust. Some measurements were also done with solid lime mud dust.

Rotation speed of the drum and the linearized flow rate used were based on the down scaling from industrial scale operational parameters:

- Rotation speed 2 rpm; Linearized flow rate 0.001 m/s
- Rotation speed 4 rpm; Linearized flow rate 0.001 m/s
- Rotation speed 4 rpm; Linearized flow rate 0.002 m/s

With these parameters it was also possibly to study the effect of rotation speed and flow rate on mixing alongside the lifters.

Different methods were used for analyzing the mixing results. With a low viscosity water CoV and dispersion coefficient were used. Also the effect of axial dispersion was studied with the species transport equation. CoV was used in case of a high viscous CMC material. Dispersion coefficient is unsuitable for high viscous material and the effect of diffusion can be assumed to be insignificant in case of high viscous material (Levenspiel, 1999). Mixing was also studied by machine vision techniques when CMC and water were used. This was done by adding a colored tracer in the feed. In the case of solid lime mud machine vision technique was also used.

9.1 Water Experiments

For the water experiments the mass flow rates were determined for linearized flow rates 0.001 m/s and 0.002 m/s. The rotameter was installed and calibrated for the determination of mass flow rates. Results of calibration are shown in Figure 64 in

Appendix I 3(3). Results for rotameter value to achieve flow rates 0.001 m/s and 0.002 m/s are shown in Tables 3 and 4.

Table 3 Mass flow, volumetric flow rate and flow rate of the drum to achieve linearized flow rate 0.001 m/s. Density of water was 998 kg/m^3.

Flow in rotameter, %	10
Volume inside the drum, m^3	0.01
Mass flow rate, kg/s	0.009
Volumetric flow, m^3/s	8.8E-06
Length of the drum, m	1.15
Residence time, s	1128
Linearized flow rate, m/s	0.001

Table 4 Mass flow, volumetric flow rate and flow rate of the drum to achieve linearized flow rate 0.001 m/s. Density of water was 998 kg/m^3.

Flow in rotameter, %	20
Volume inside the drum, m^3	0.01
Mass flow rate, kg/s	0.017
Volumetric flow, m^3/s	1.7E-05
Length of the drum, m	1.15
Residence time, s	583
Linearized flow rate, m/s	0.002

9.1.1 Measurement Procedure for Mixing

Water measurements were carried out by using acid pulse as tracer. 150 ml of HNO_3 with pH 1 was chosen as acid impulse. Drum was first filled with water and the water flow was let to stabilize before starting the measurements. Acid was fed at the feed end and the pH of water solution was measured with pH-meter (Schott CG840). Meter was installed 0.85 m from the drum feed. The duration of one experiment was limited to 30 minutes and the values from the pH-meter were collected in 15 second intervals.

All of the operating parameters described on page 58 were used in water acid experiments. 38 different measurements were carried out with different lifter geometries and operating parameters. For every measurement a repetition experiment was performed so the total number of experiments was 76.

Experiments were started without lifters with drum rotational speeds 2 rpm and 4 rpm with linearized flow rates 0.001 m/s and 0.002 m/s. In next experiments the straight lifters were used. First 2 lifters were installed on one circumference so the total amount of lifters in the drum was 8 when 4 circumferences were used. This lifter geometry was follow by 4 lifters in one circumference (total 16 lifters) and finally 8 lifters on one circumference so that the drum was fully loaded with lifters (total 32 lifters). These measurements with straight lifters were also carried out by 2 rotational speeds and 2 linearized flow rates. Experiments were also carried out with 4 lifters on one circumference organized in overlapping structure and by using only three circumferences with eight straight lifters on one circumference. These experiments were carried out using rotational speed 2 rpm with linearized flow rate 0.001 m/s. After these experiments lifters were organized in random lifter geometries to find out the best mixing structures. Measurement configuration has been presented in Table 32 in Appendix III. Lifter geometries are presented in Appendix XII.

Water measurements were also performed by using colored blue water as tracer. Water was colored with Oy Roberts Ab's food additive product nr. 202805. For color impulse 9 ml of strong color was first diluted to 400 ml of water. 5 ml of this solution was used as an impulse in every experiment. Duration of one experiment was limited to 24 minutes and mixing was recorded with video camera. Video material was analyzed by Machine Vision and Pattern Recognition laboratory in Lappeenranta University of Technology. Some changes in lifter design were made after water acid impulse response test before the machine vision experiments. The angle of the straight lifter was changed so that the material falls earlier on the top of the bed. Change is illustrated in Figure 23.

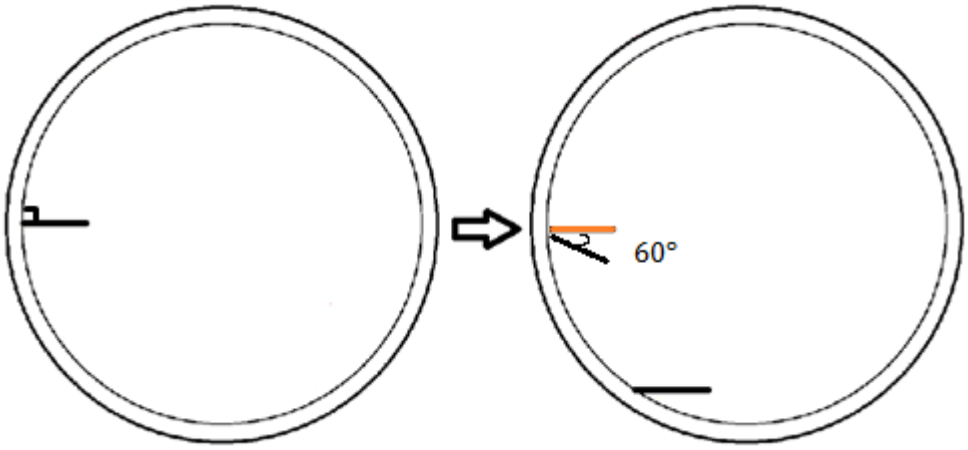

Figure 23 Change in straight lifter position.

23 experiments were performed and those were mainly carried out with rotational speed 2 rpm with flow rate 0.001 m/s. Two experiments were performed with rotational speed 4 rpm with flow rate 0.001 m/s and one experiment with rotational speed 4 rpm with flow rate 0.002 m/s. Also two new lifter geometries (Lifter 24 and Lifter 25) were tested. All the performed experiments are shown in Appendix IV in Table 33.

9.2 CMC Experiments

For the high viscous CMC experiments the mass flow rates were determined for linearized flow rates 0.001 m/s and 0.002 m/s. The rotameter could not be used due to a high viscosity of CMC so the mass flow rate was determined with bucket and scale to the determination of flow rates 0.001 m/s and 0.002 m/s (Tables 5 and 6).

Table 5 Mass flow, volumetric flow rate and flow rate of the drum to achieve linearized flow rate 0.001 m/s. Density of CMC was 1000 kg/m^3.

Volume inside the drum, m^3	0.01
Mass flow rate, kg/s	0.009
Volumetric flow, m^3/s	9.2E-06
Length of the drum, m	1.15
Residence time, s	1156
Linearized flow rate, m/s	0.001

Table 6 Mass flow, volumetric flow rate and flow rate of the drum to achieve linearized flow rate 0.002 m/s. Density of CMC was 1000 kg/m^3.

Volume inside the drum, m^3	0.01
Mass flow rate, kg/s	0.018
Volumetric flow, m^3/s	1.8E-05
Length of the drum, m	1.15
Residence time, s	578
Linearized flow rate, m/s	0.002

9.2.1 Measurement Procedure for Mixing

CMC measurements were started by using HNO_3 pulse as tracer. Some pre-experiments were done to find optimal conditions for acid impulse. First the pH of CMC was dropped to 1. It was seen that the structure of CMC was changed to lumpy and the rheological properties were changed when comparing to normal CMC. Then the pH of CMC was then dropped to 3 according the knowledge that the rheological properties remain the same in pH region from 3 to 9. It was seen that CMC did not get lumpy anymore. Finally 200 ml of HNO_3 with pH ~3 was chosen as acid impulse. Otherwise the measurement procedure was same as with water described in the beginning of chapter 9.1.1 on page 59.

The experiments were started using all operating parameters. Used lifter geometries were: no lifters, straight 8 lifters and lifter 12. During the experiments it was noted that there was a lot of noise in the results. Repetition measurement did not correlate. Due to noisy data it was seen that the results with this method are not reliable and some changes to procedure has to be done.

Due to problems with acid impulse the measurement technique of mixing was changed to machine vision. Measurements were carried out by using a colored blue CMC as tracer. CMC was colored with Oy Roberts Ab's food additive product nr. 202805. For color impulse 10 ml of strong color was first diluted to 20 ml of water. 3 ml of this solution was then mixed with 600 ml of CMC. Finally 60 ml of colored CMC was used as an impulse in every experiment.

The chosen geometries were based on results from water experiments. 36 different measurements were carried out with different lifter geometries. Both original and modified straight lifters were used. With the modified lifters the angle was changed according to Figure 23. Repetitions were not done in these experiments. In experiments rotation speed 2 rpm with flow rate 0.001 m/s was used. Rotation speed 4 rpm with linearized flow rates 0.001 m/s and 0.002 m/s were also tested without lifters. All the experiments performed are shown in Appendix V in Table 34.

9.3 Solid Experiments

For the solid lime mud dust mixing experiments the mass flow rate was determined for linearized flow rate 0.001 m/s The optimal mass flow rate was measured by feeding lime mud dust in the rotating drum and at same time keeping a record how much dust was fed in the drum. Feed was stopped when the lime mud started to fall off from the discharge end. Result to achieve linearized flow rate 0.001 m/s is shown in Table 7. Feed of the lime mud dust was arranged with screw conveyor. The pilot drum and screw conveyor are shown in Figure 24.

Table 7 Mass flow, volumetric flow rate and flow rate of the drum to achieve linearized flow rate 0.001 m/s. Density of lime mud dust was 700 kg/m^3.

Volume inside the drum, m^3	0.013
Mass flow rate, kg/s	0.008
Volumetric flow, m^3/s	1.2E-05
Length of the drum, m	1.15
Residence time, s	1080
Linearized flow rate, m/s	0.001

Figure 24 Pilot drum with screw conveyor.

9.3.1 Measurement Procedure for Mixing

Solid mixing measurements were carried out by using blue Kiilto "SAUMAUSLAASTI 94" joint mortar as tracer. Feed was calculated to be approximately 500 g/min and was organized so that in every 10 seconds approximately 80 g of lime mud was fed to screw conveyor. Some pre-experiments were done to find optimal conditions for impulse. First 300 g of joint mortar was fed in the drum via screw conveyor. However, it was noticed that the joint mortar mixes rapidly with feed material even before the lifter zone. Next 300 g of joint mortar was placed to the second lifter circumference to see the effect of first and third lifter zone. Fourth lifter zone was not used in these experiments. In addition the joint mortar was placed on the top of the white lime mud. In these pre-tests it was seen that with straight lifters the mixing is so intensive that the blue tracer was once again rapidly mixed with white material. Finally 800 g of only blue joint mortar was placed onto the second lifter circumference. This option was seen to be suitable for the rest of the experiments. Machine vision was

used as a technique to observe the mixing. Mixing time was limited to 15 minutes. Mixing and transverse bed motion were also examined visually.

Rotation speed 2 rpm with linearized flow rate 0.001 m/s was used in experiments. 8 different measurements with 8 lifters on one circumference were carried out with different lifter geometries. Repetitions were not done in these experiments. All the experiments performed are shown in Table 8.

Table 8 The lifter geometries used in solid experiments with different tracer placing. Tracer was placed on the second lifter circumference in every experiment.

Lifter design	**Amount of tracer, g**	**Placing**
No lifters	300	On the top of the white lime dust bed
No lifters	600	Only blue tracer in the second lifter zone
Straight	300	On the top of the white lime dust bed
Straight	800	Only blue tracer in the second lifter zone
Lifter 9	800	Only blue tracer in the second lifter zone
Lifter 12	800	Only blue tracer in the second lifter zone
Lifter 16	800	Only blue tracer in the second lifter zone
Lifter 17	800	Only blue tracer in the second lifter zone

9.4 Results Analysis Methods

Different methods were used to analyze to results. CoV was mainly used to analyze the mixing but also the dispersion coefficient was used in water experiments. CoV was also calculated from the video analysis simulated by machine vision. Species transport equation was used to examine the effect of diffusion on mixing. A closer look to results analysis methods is given in Appendix VII.

10 RESULTS

Results from water, CMC and solid lime dust experiments are shown in this chapter. Results are based on results analysis methods described in Appendix VII. More detailed analyses and conclusions about the results are given in chapter 11 starting on page 111.

10.1 Water Experiments

Water experiments were carried out by using HNO_3 as an acid impulse. Mixing was measured based on concentration values which were collected using pH meter and analyzed with CoV number and dimensionless $\frac{D}{uL}$ value. Water experiments were also performed using colored water as impulse. In this case degree of mixing was analyzed using CoV number using saturation based on machine vision.

10.1.1 Coefficient of Variation

CoV numbers were calculated according to Equation 2. Concentration curves and and CoV numbers for no lifter geometry are shown in Figures 25 and 26. It is noted that calculated CoV numbers between repetition runs are almost similar despite the differences in impulse response curves.

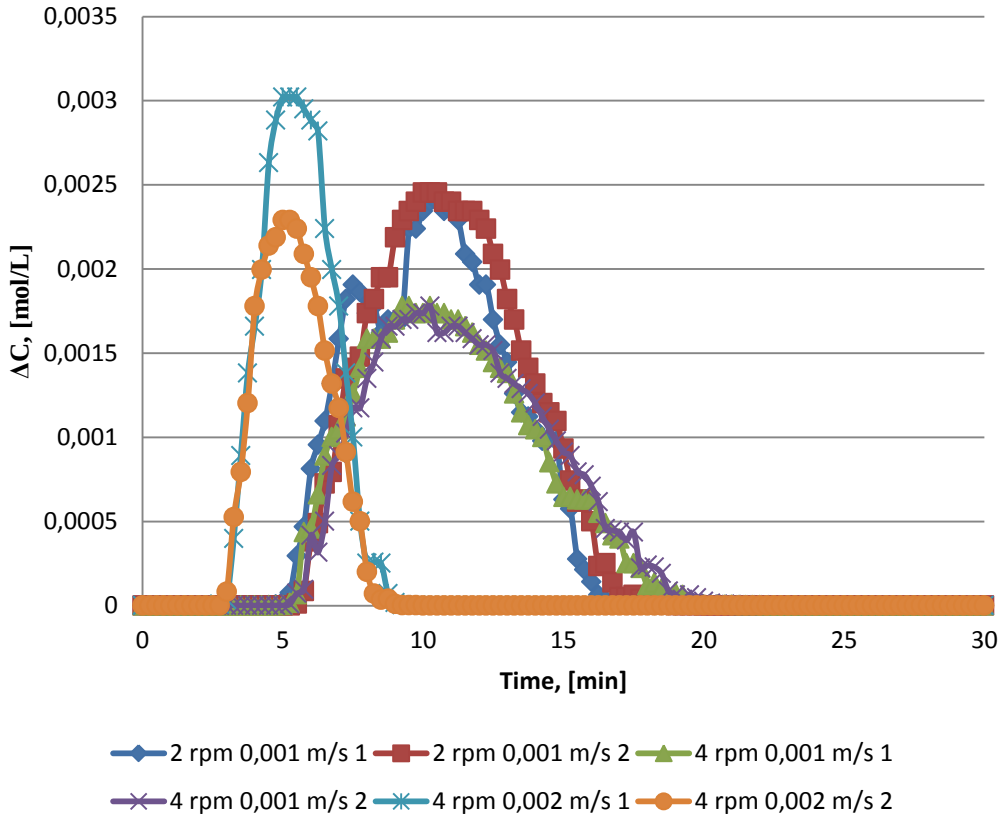

Figure 25 Concentration curves without lifters including repetion runs.

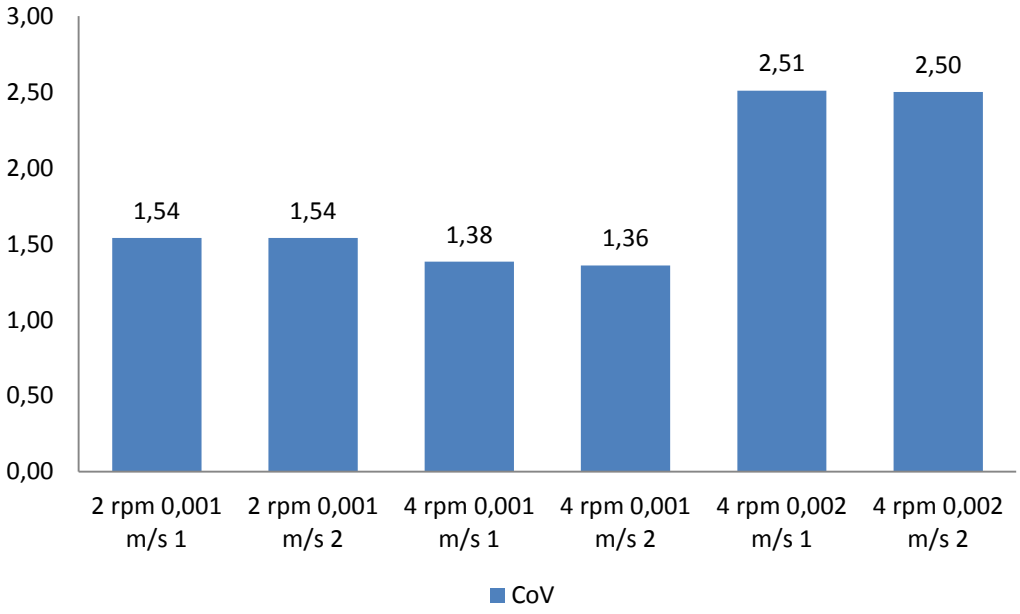

Figure 26 CoV numbers without lifters including repetitions runs.

Concentration curves and CoV numbers using rotation speed 2 rpm and axial flow velocity 0.001 m/s for straight lifters designs with different amount of lifters on one circumference are presented in Figures 27 and 28.

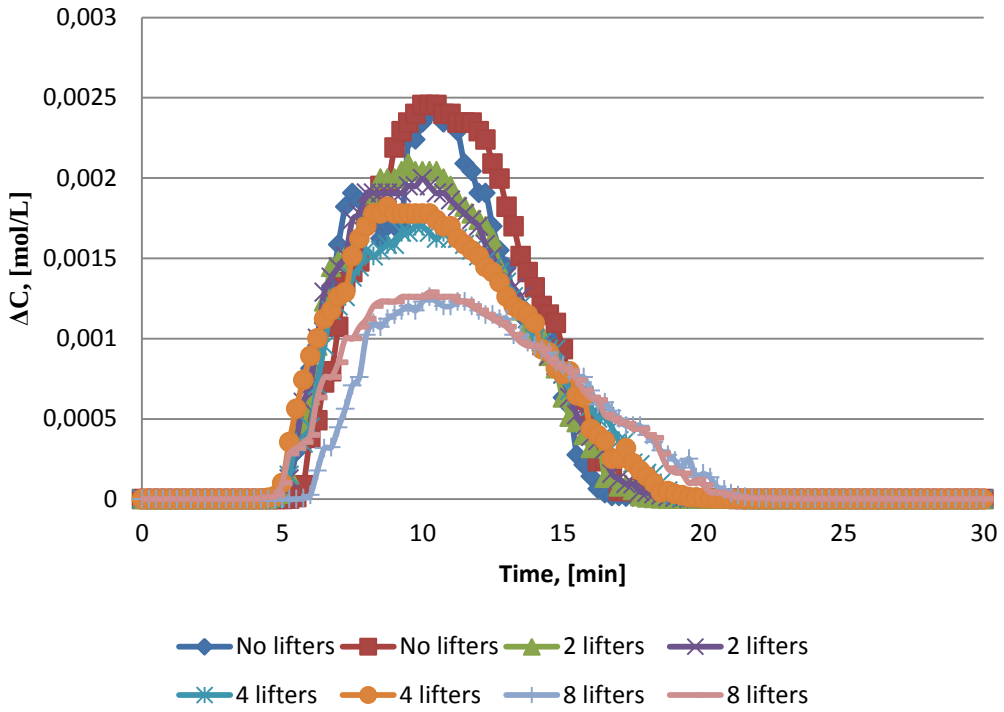

Figure 27 Concentration curves for straight lifter geometries using rotation speed 2 rpm and axial flow velocity 0.001 m/s including repetion runs.

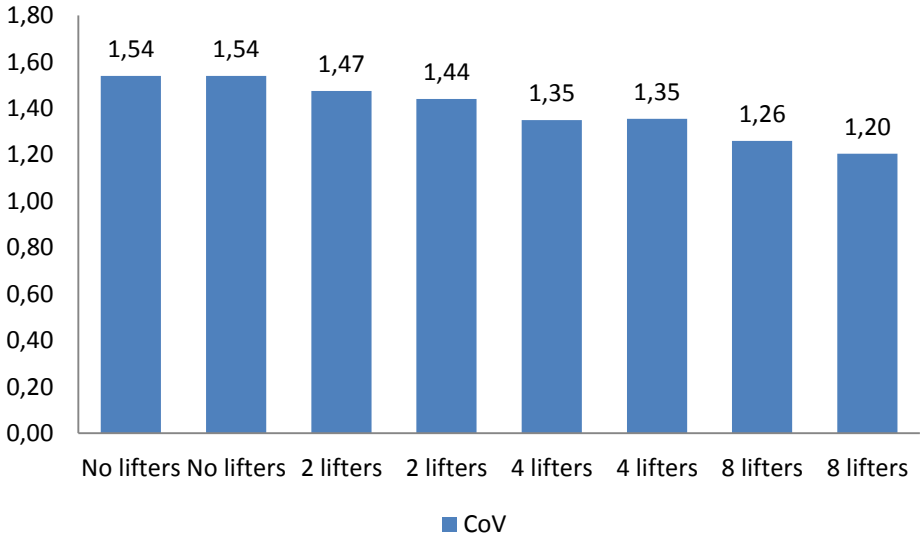

Figure 28 CoV numbers for straight lifter geometries using rotation speed 2 rpm and axial flow velocity 0.001 m/s including repetion runs.

Concentration curves and CoV numbers using at 4 rpm and 0.001 m/s axial flow velocity for straight lifters designs with different amount of lifters on one circumference are presented in Figures 29 and 30.

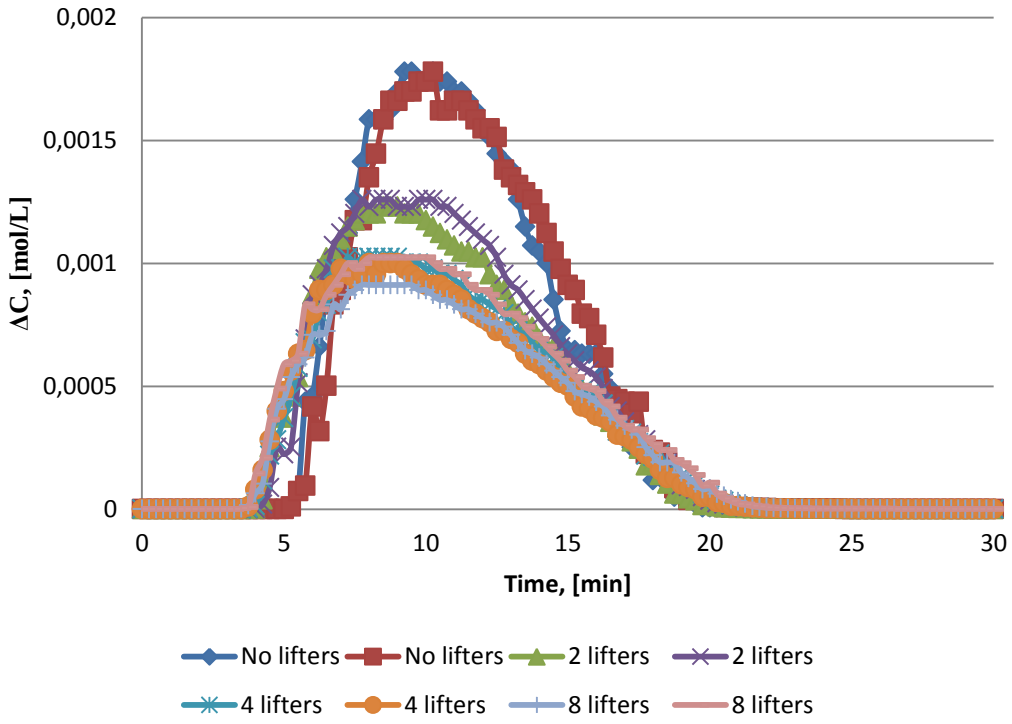

Figure 29 Concentration curves for straight lifter geometries using rotation speed 4 rpm and axial flow velocity 0.001 m/s including repetion runs.

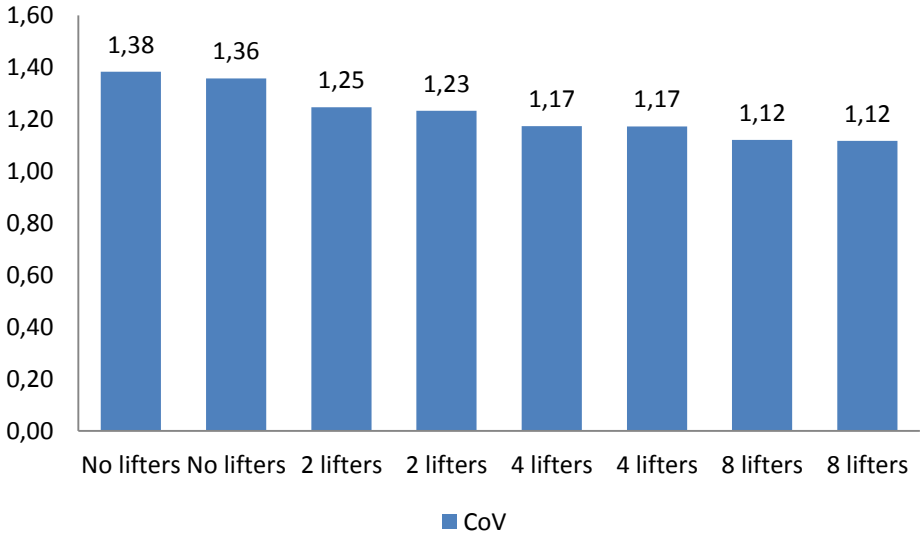

Figure 30 CoV numbers for straight lifter geometries using rotation speed 4 rpm and axial flow velocity 0.001 m/s including repetion runs.

Concentration curves and CoV numbers at 4 rpm and 0.002 m/s axial flow velocity for straight lifters designs with different amount of lifters on one circumference are presented in Figures 31 and 32.

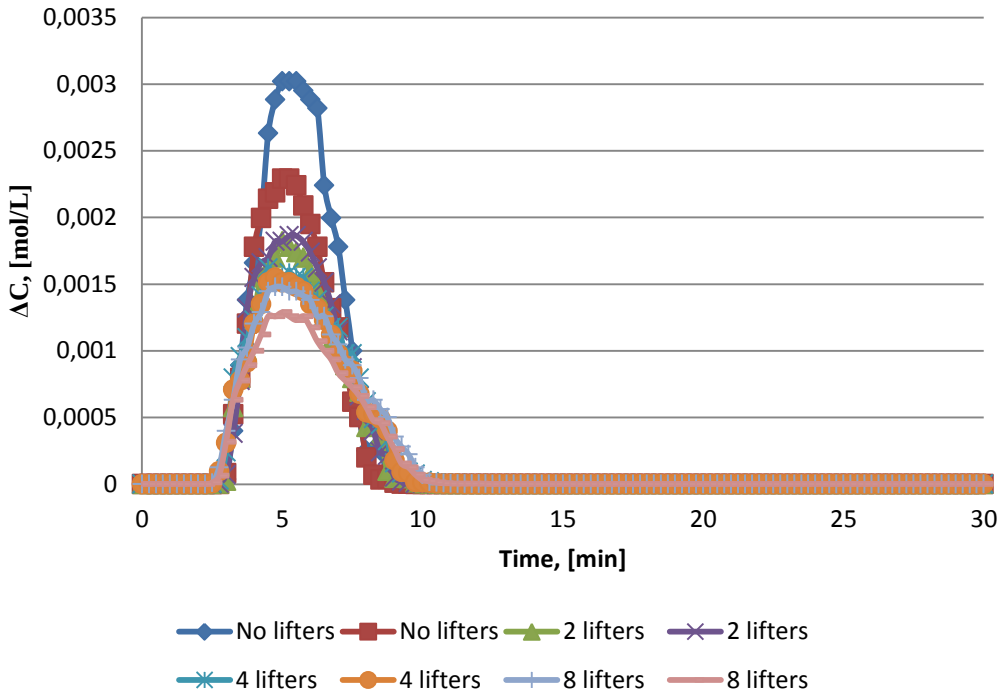

Figure 31 Concentration curves for straight lifter geometries at 4 rpm and 0.002 m/s axial flow velocity including repetion runs.

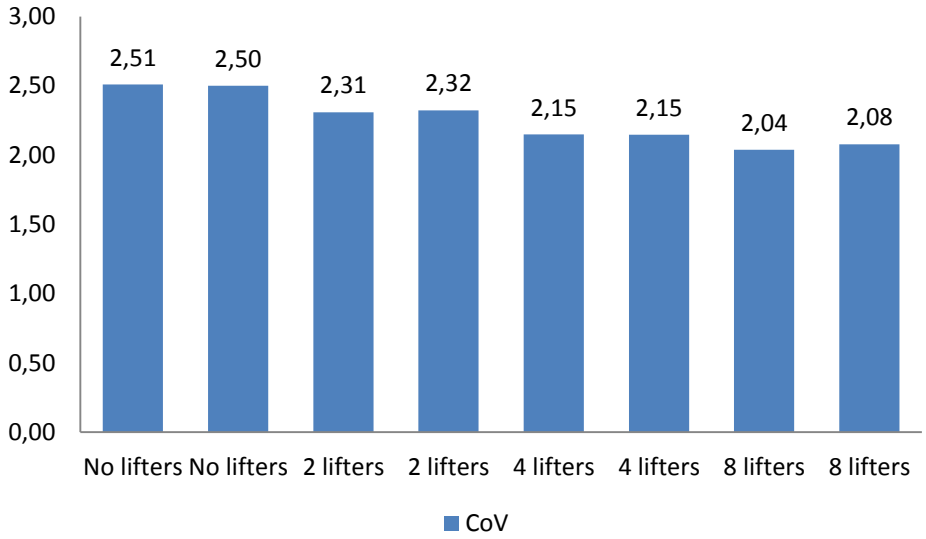

Figure 32 CoV numbers for straight lifter geometries at 2 rpm and 0.002 m/s axial flow velocity including repetion runs.

It is noted that the tracer impulse has the most plug flow -type character at 4 rpm and 0.002 m/s axial flow velocity. The peak also travels faster than with the other operational parameters. In case of flow rate 0.001 m/s it is noted that concentration peak is lower with rotational speed of 4 rpm than with 2 rpm. The concentration peak is also wider with rotational speed 4 rpm than with 2 rpm. Concentration peaks are getting lower and wider when adding lifters on the circumferences. Average of CoV numbers (included repetitions) using straight lifters and different process parameters are shown in Table 9.

Table 9 CoV numbers for straight lifter designs using different process parameters.

	CoV, -		
Lifters on one circumference, -	**2 rpm 0.001 m/s**	**4 rpm 0.001 m/s**	**4 rpm 0.002 m/s**
0	1.54	1.37	2.50
2	1.46	1.24	2.32
4	1.35	1.17	2.15
8	1.23	1.12	2.06

It is noted that CoV number decreases when the amount of lifters increases. This is shown in Figure 33 using different process parameters.

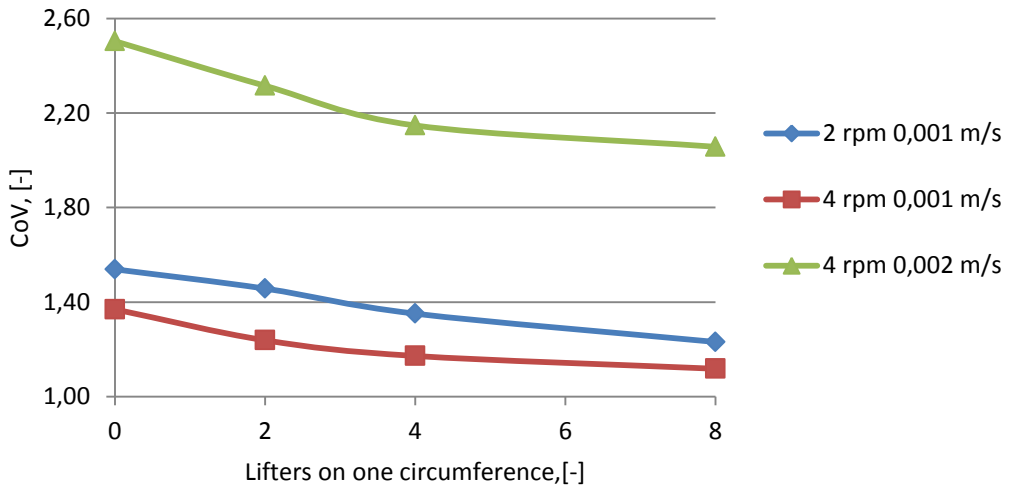

Figure 33 The effect of amount of lifters on CoV number using different process parameters. CoV number decreases when the amount of lifters on one circumference increases. Experiments were carried out using straight lifters.

Concentration curves at 2 rpm and 0.001 m/s axial flow velocity with different lifter designs are presented in Figure 34. In these experiments 8 lifters on one circumference were used.

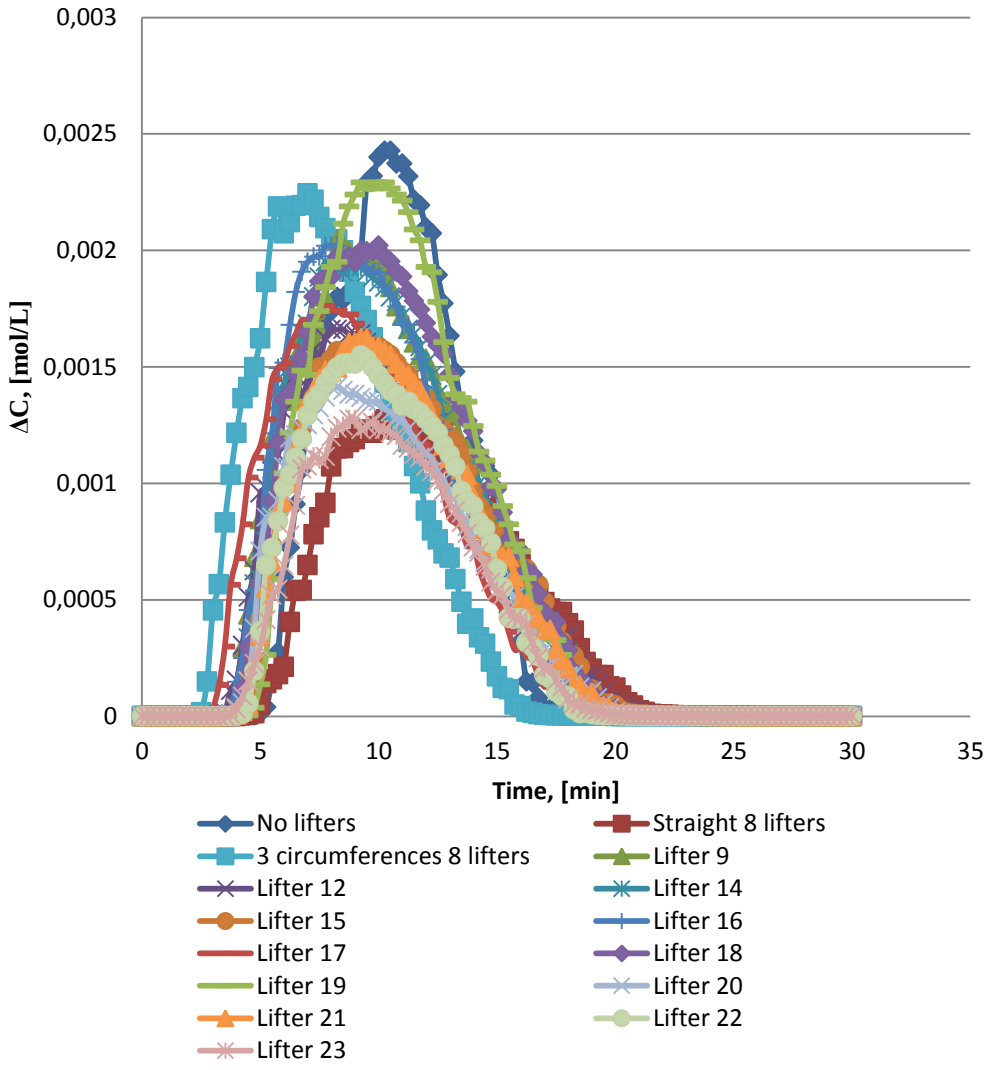

Figure 34 Concentration curves with different lifter geometries (8 lifters on one circumference) at 2 rpm and 0.001 m/s axial flow velocity.

Average of CoV numbers (included repetitions) at 2 rpm and 0.001 m/s axial flow velocity with different lifter designs are shown in Figure 35. In these experiments 8 lifters on one circumference were used. The CoV values are presented from lowest to highest.

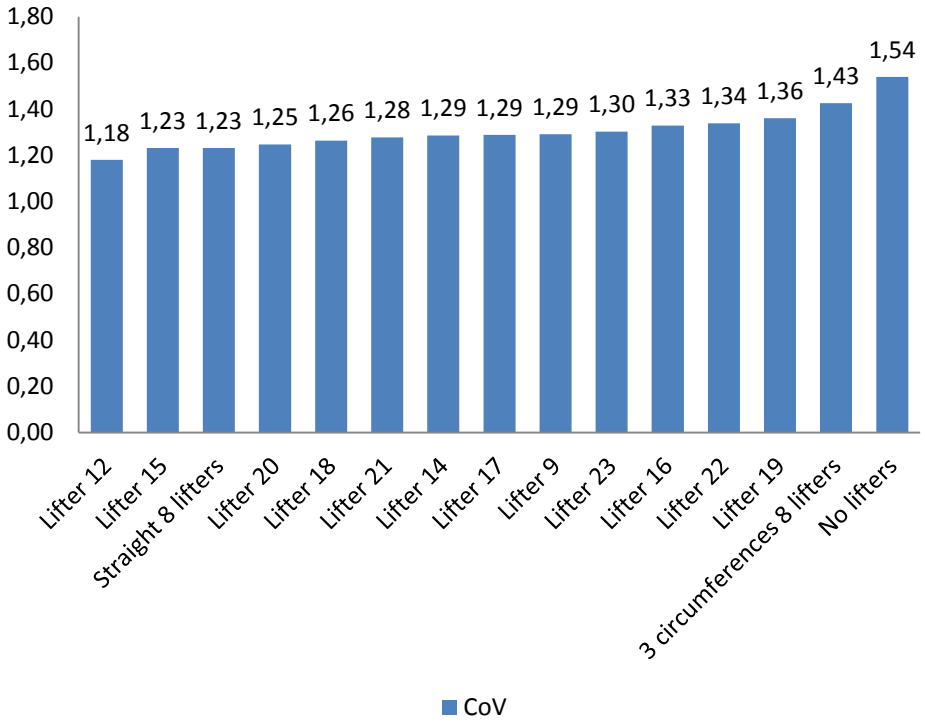

Figure 35 CoV numbers with different lifter geometries (8 lifters on one circumference) at 2 rpm and 0.001 m/s axial flow velocity.

Concentration curves at 2 rpm and 0.001 m/s axial flow velocity with different lifter designs is presented in Figure 36 In these experiments 4 lifters on one circumference were used. The CoV values are presented from lowest to highest in Figure 37.

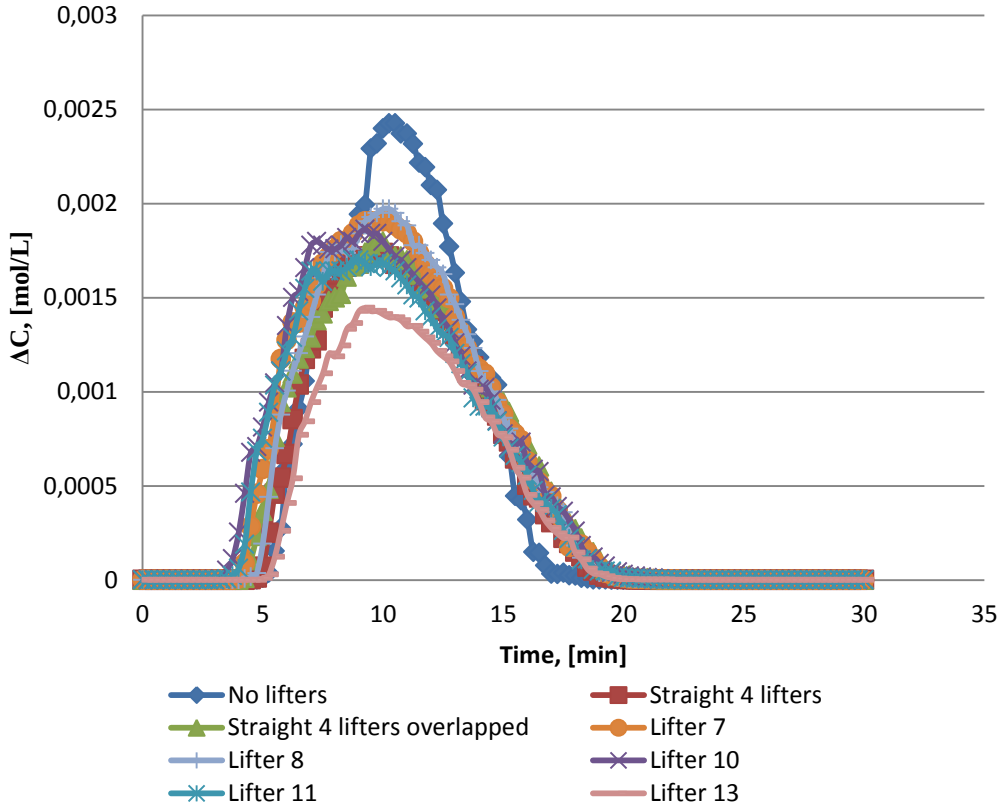

Figure 36 Concentration curves with different lifter geometries (4 lifters on one circumference) at 2 rpm and 0.001 m/s axial flow velocity.

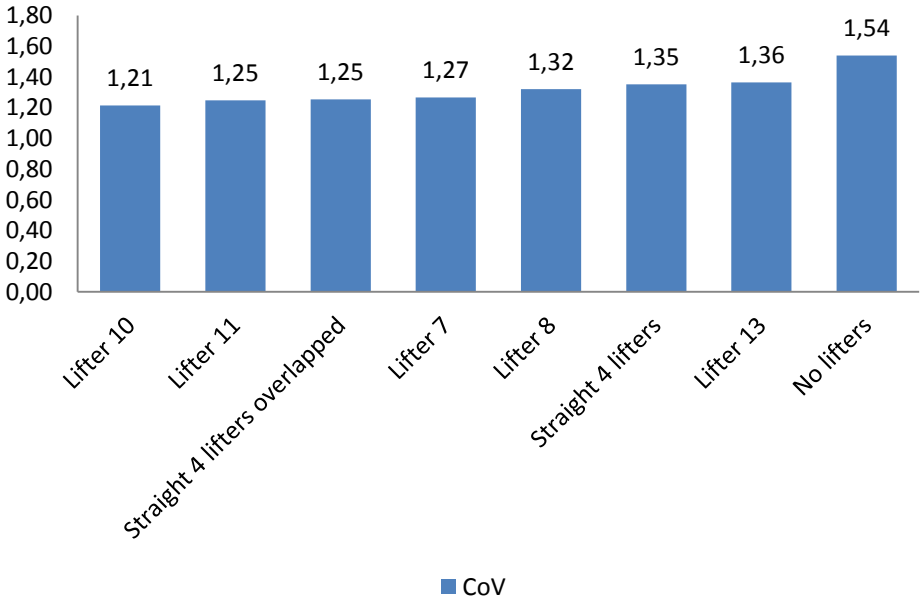

Figure 37 CoV numbers with different lifter geometries (4 lifters on one circumference) at 2 rpm and 0.001 m/s axial flow velocity.

Concentration curves at 4 rpm and 0.001 m/s axial flow velocity with different lifter designs is presented in Figure 38. In these experiments 8 lifters on one

circumference were used. The CoV values are presented from lowest to highest in Figure 39.

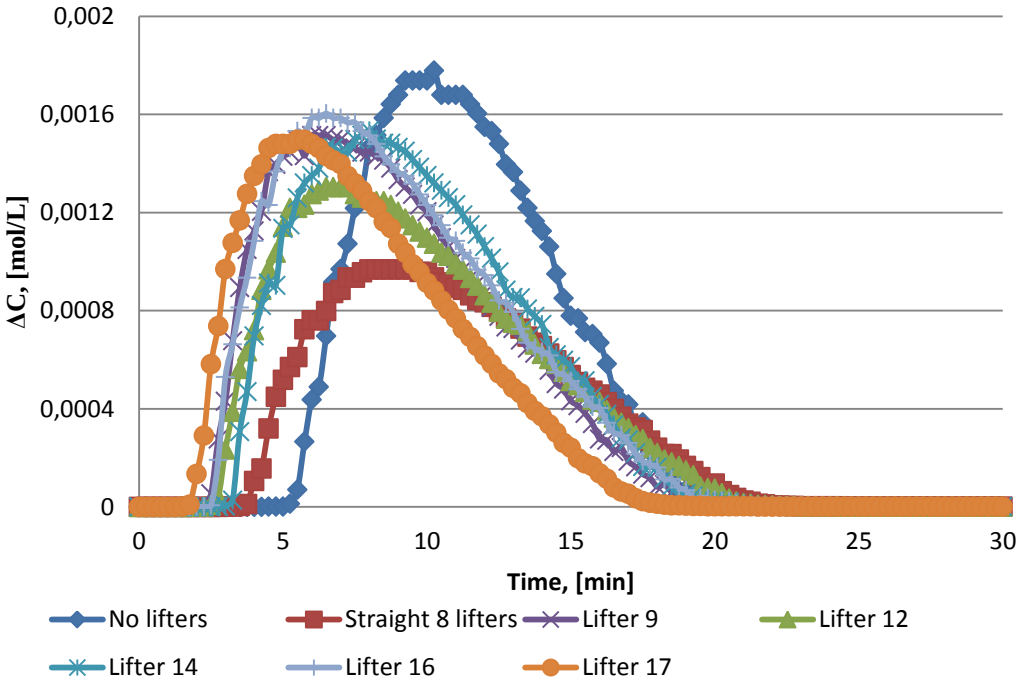

Figure 38 Concentration curves with different lifter geometries (8 lifters on one circumference) at 4 rpm and 0.001 m/s axial flow velocity.

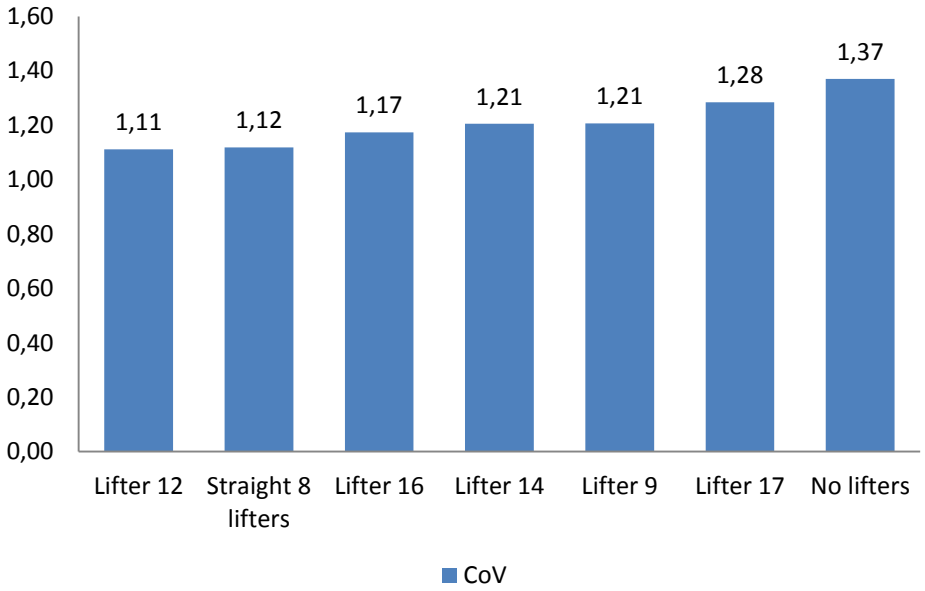

Figure 39 CoV numbers with different lifter geometries (8 lifters on one circumference) at 4 rpm and 0.001 m/s axial flow velocity.

Average of CoV numbers (included repetitions) using different lifter designs and process parameters are presented in Tables 10 and 11.

Table 10 CoV numbers with different lifter designs and process parameters.

	Process parameter		
	2 rpm 0,001 m/s	**4 rpm 0,001 m/s**	**4 rpm 0,002 m/s**
Lifter design	**CoV, -**		
No lifters	1.54	1.37	2.50
Straight 2 lifters	1.46	1.24	2.32
Straight 4 lifters	1.35	1.17	2.15
Straight 4 lifters overlapped	1.25	-	-
Straight 8 lifters	1.23	1.12	2.06
3 circumferences 8 lifters	1.43	-	-
Lifter 7	1.27	-	-
Lifter 8	1.32	-	-
Lifter 9	1.29	1.21	-
Lifter 10	1.21	-	-
Lifter 11	1.25	-	-
Lifter 12	1.18	1.11	-
Lifter 13	1.36	1.22	2.21
Lifter 14	1.29	1.21	-
Lifter 15	1.23	-	-
Lifter 16	1.33	1.17	-
Lifter 17	1.29	1.28	-
Lifter 18	1.26	-	-
Lifter 19	1.36	-	-
Lifter 20	1.25	-	-
Lifter 21	1.28	-	-
Lifter 22	1.34	-	-
Lifter 23	1.30	-	-

Mixing between lifter structures were normalized by applying Equation 5. Mixing variable used in Eq. 5 was CoV value. The higher the homogeneity value M is, the better the mixing is. Poor mixing is when M is 0. In Eq. 5 for example, X_0 was set based on the worst mixing in case of no lifters. As well, X_1 was set based on the best case. In each column in Table 11 the worst and the best CoV were selected for X_0 and X_1 respectively. Results are shown in Tables 11 and 12.

Table 11 Mixing between lifter structures based on homogeneity value. CoV values 1.54 (2 rpm 0.001 m/s), 1.37 (4 rpm 0.001 m/s) and 2.50 (4 rpm 0.002 m/s) were given for mixing variable X_0. CoV values 1.18 (2 rpm 0.001 m/s), 1.11 (4 rpm 0.001 m/s) and 2.06 (4 rpm 0.002 m/s) were given for variable X_1.

	Process parameter		
	2 rpm 0,001 m/s	**4 rpm 0,001 m/s**	**4 rpm 0,002 m/s**
Lifter design	**Homogeneity, -**		
No lifters	0.00	0.00	0.00
Straight 2 lifters	0.22	0.50	0.41
Straight 4 lifters	0.52	0.77	0.80
Straight 4 lifters overlapped	0.81	-	-
Straight 8 lifters	0.86	0.97	1.00
3 circumferences 8 lifters	0.30	-	-
Lifter 7	0.76	-	-
Lifter 8	0.61	-	-
Lifter 9	0.70	0.64	-
Lifter 10	0.91	-	-
Lifter 11	0.80	-	-
Lifter 12	1.00	1.00	-
Lifter 13	0.49	0.58	0.66
Lifter 14	0.69	0.62	-
Lifter 15	0.86	-	-
Lifter 16	0.59	0.76	-
Lifter 17	0.70	0.33	-
Lifter 18	0.77	-	-
Lifter 19	0.50	-	-
Lifter 20	0.81	-	-
Lifter 21	0.73	-	-
Lifter 22	0.56	-	-
Lifter 23	0.66	-	-

Table 12 Mixing between lifter structures based on homogeneity value. CoV values 1.54 (2 rpm 0.001 m/s), 1.37 (4 rpm 0.001 m/s) and 2.50 (4 rpm 0.002 m/s) were given for mixing variable X_0. Value 0 was given for variable X_1 because CoV = 0 is for perfect mixing.

	Process parameter		
	2 rpm 0,001 m/s	**4 rpm 0,001 m/s**	**4 rpm 0,002 m/s**
Lifter design	**Homogeneity, -**		
No lifters	0.00	0.00	0.00
Straight 2 lifters	0.05	0.09	0.07
Straight 4 lifters	0.12	0.15	0.14
Straight 4 lifters overlapped	0.19	-	-
Straight 8 lifters	0.20	0.18	0.18
3 circumferences 8 lifters	0.07	-	-
Lifter 7	0.18	-	-
Lifter 8	0.14	-	-
Lifter 9	0.16	0.12	-
Lifter 10	0.21	-	-
Lifter 11	0.19	-	-
Lifter 12	0.23	0.19	-
Lifter 13	0.11	0.11	0.12
Lifter 14	0.16	0.12	-
Lifter 15	0.20	-	-
Lifter 16	0.14	0.14	-
Lifter 17	0.16	0.06	-
Lifter 18	0.18	-	-
Lifter 19	0.12	-	-
Lifter 20	0.19	-	-
Lifter 21	0.17	-	-
Lifter 22	0.13	-	-
Lifter 23	0.15	-	-

10.1.2 Dispersion Coefficient

Dispersion coefficients were calculated according to Equation 13. Dispersion coefficients for without lifters geometry and for straight lifter structures are presented in Figures 40–43. The high values of the dispersion coefficient represent better mixing. It is noted that calculated dispersion coefficients between repetition runs are almost similar despite the differences in impulse response curves.

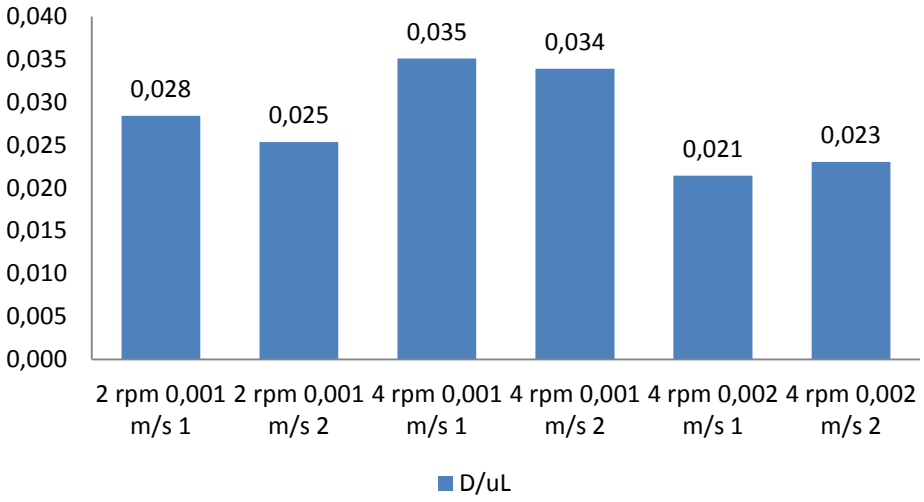

Figure 40 Dispersion coefficients without lifters including repetion runs.

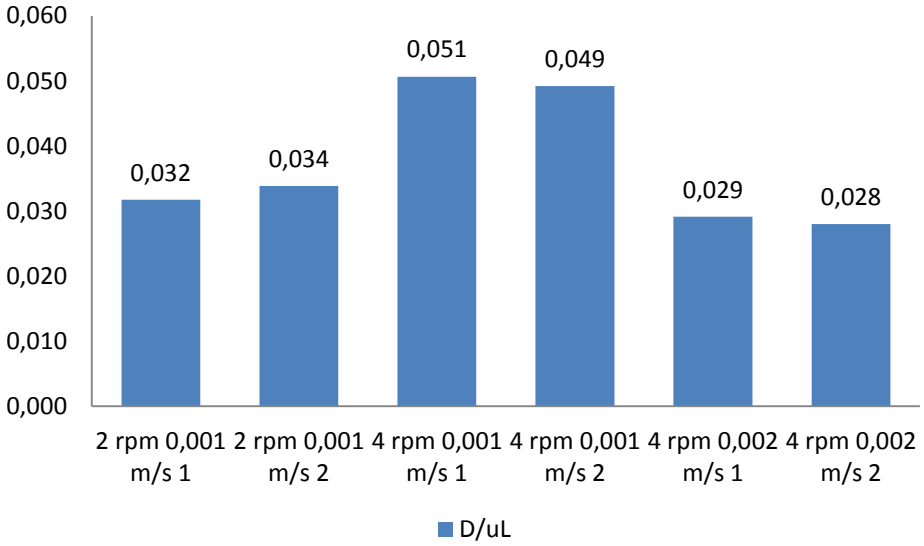

Figure 41 Dispersion coefficients for straight lifter geometry using 2 lifters on one circumference including repetion runs.

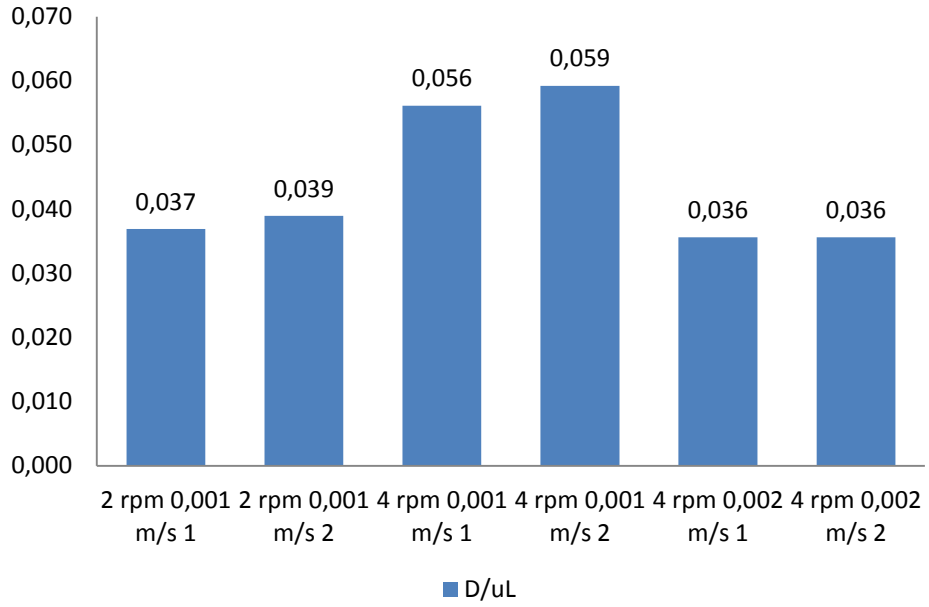

Figure 42 Dispersion coefficients for straight lifter geometry using 4 lifters on one circumference including repetion runs.

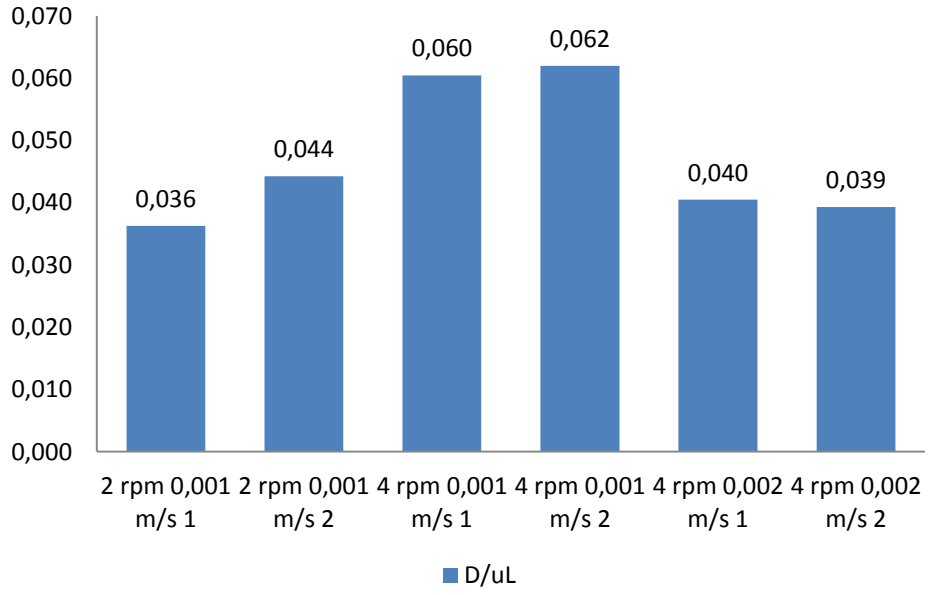

Figure 43 Dispersion coefficients for straight lifter geometry using 8 lifters on one circumference including repetion runs.

Average of dispersion coefficients (included repetitions) using straight lifters and different process parameters are shown in Table 13.

Table 13 Dispersion coefficients for straight lifter designs using different process parameters.

	Dispersion coefficient, -		
Lifters on one circumference, -	**2 rpm 0.001 m/s**	**4 rpm 0.001 m/s**	**4 rpm 0.002 m/s**
0	0.027	0.034	0.022
2	0.033	0.050	0.029
4	0.038	0.058	0.036
8	0.040	0.061	0.040

It is noted that dispersion coefficient increases when the amount of lifters increases. This is shown in Figure 44 using different process parameters.

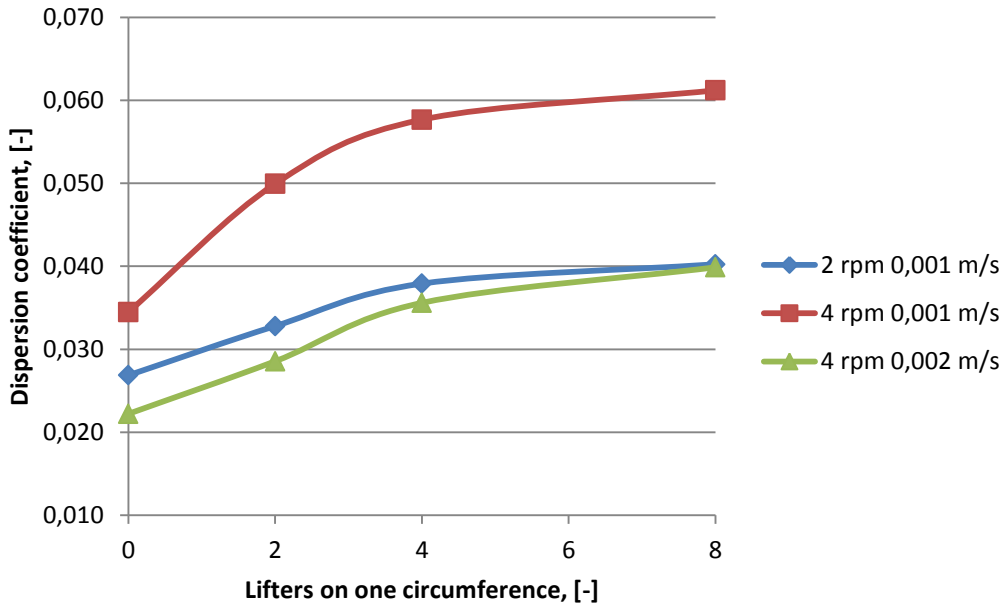

Figure 44 The effect of amount of lifters on dispersion coefficient using different process parameters. Dispersion coefficient increases when the amount of lifters on one circumference increases. Experiments were carried out using straight lifters.

Average of dispersion coefficients (included repetitions) at 2 rpm and 0.001 m/s axial flow velocity with different lifter designs are shown in Figure 45. In these experiments 8 lifters on one circumference were used. The dispersion coefficients are presented from highest to lowest.

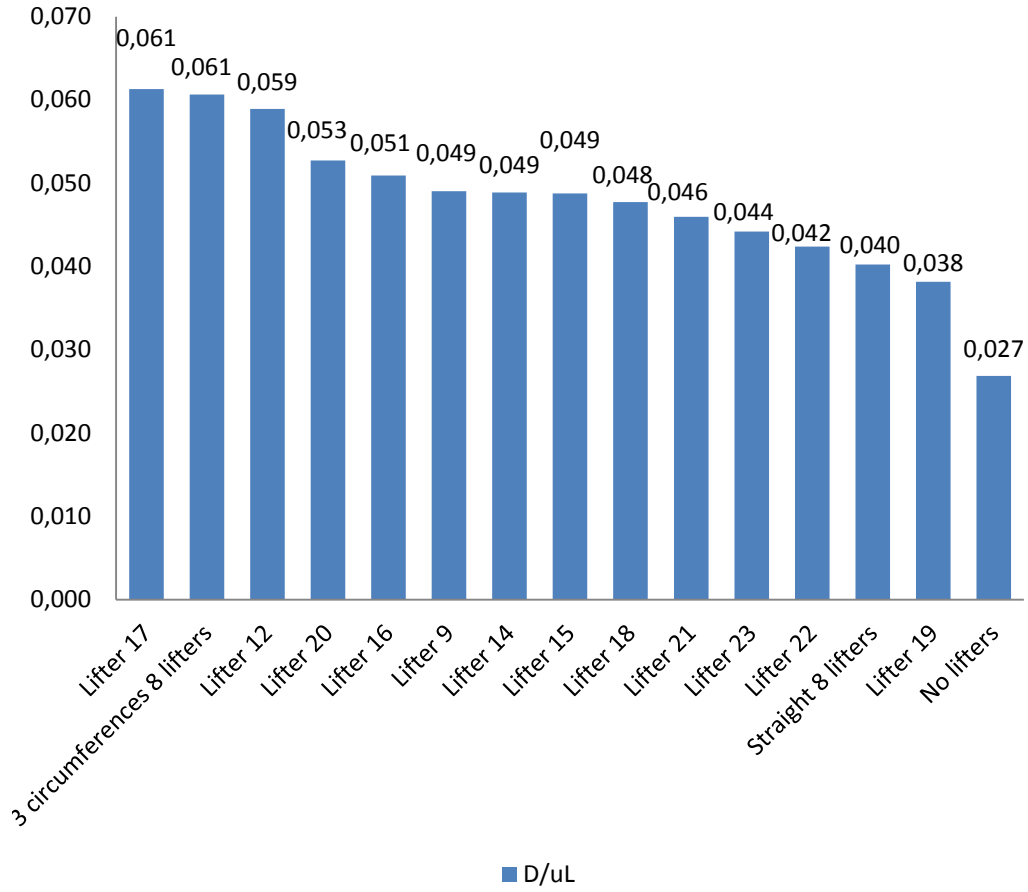

Figure 45 Dispersion coefficients with different lifter geometries (8 lifters on one circumference) at 2 rpm and 0.001 m/s axial flow velocity.

Average of dispersion coefficients (included repetitions) at 2 rpm and 0.001 m/s axial flow velocity with different lifter designs (4 lifters on one circumference) is shown in Figure 46. The dispersion coefficients are presented from highest to lowest.

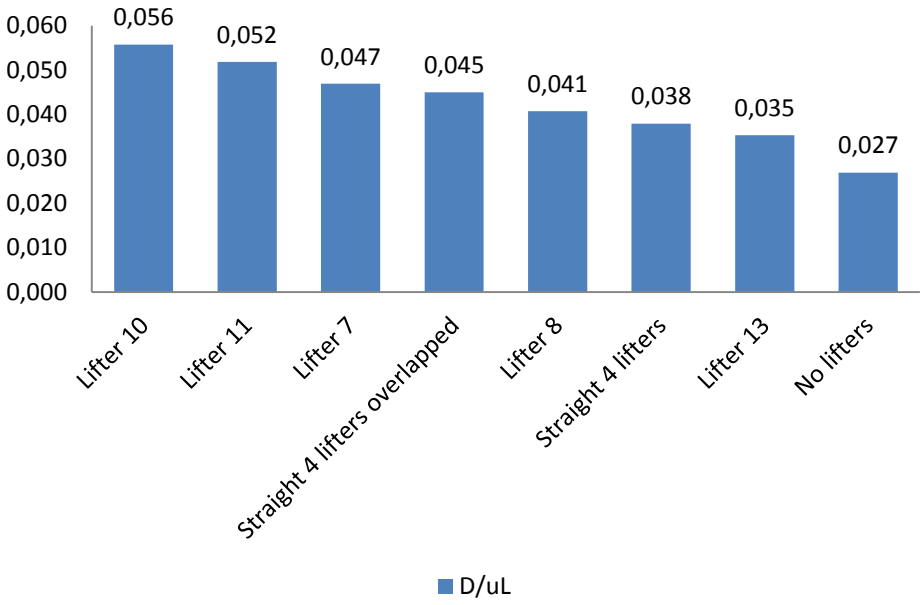

Figure 46 Dispersion coefficients with different lifter geometries (4 lifters on one circumference) at 2 rpm and 0.001 m/s axial flow velocity.

Average of dispersion coefficients (included repetitions) at 4 rpm and 0.001 m/s axial flow velocity with different lifter designs (8 lifters on one circumference) is shown Figure 47. The dispersion coefficients are presented from highest to lowest.

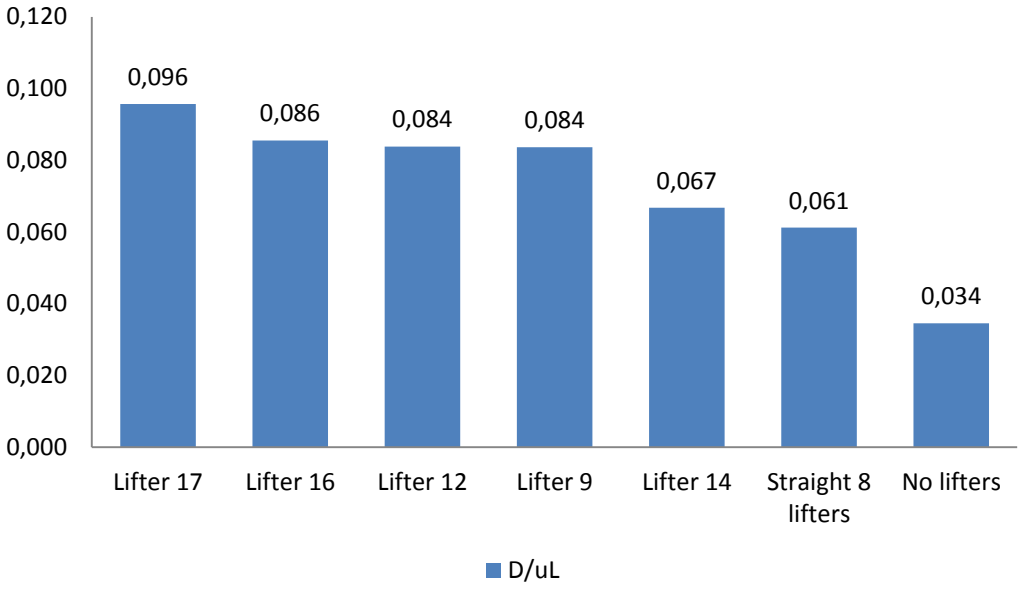

Figure 47 Dispersion coefficients with different lifter geometries (8 lifters on one circumference) at 4 rpm and 0.001 m/s axial flow velocity.

Average of dispersion coefficients (included repetitions) using different lifter designs and process parameters are shown in Table 14.

Table 14 Dimensionless dispersion coefficient with different lifter designs using different process parameters.

	Process parameter		
	2 rpm 0.001 m/s	**4 rpm 0.001 m/s**	**4 rpm 0.002 m/s**
Lifter design	**Dispersion coefficient, -**		
No lifters	0.027	0.034	0.022
Straight 2 lifters	0.033	0.050	0.029
Straight 4 lifters	0.038	0.058	0.036
Straight 4 lifters overlapped	0.045	-	-
Straight 8 lifters	0.040	0.061	0.040
3 circumferences 8 lifters	0.061	-	-
Lifter 7	0.047	-	-
Lifter 8	0.041	-	-
Lifter 9	0.049	0.084	-
Lifter 10	0.056	-	-
Lifter 11	0.052	-	-
Lifter 12	0.059	0.084	-
Lifter 13	0.035	0.058	0.035
Lifter 14	0.049	0.067	-
Lifter 15	0.049	-	-
Lifter 16	0.051	0.086	-
Lifter 17	0.061	0.096	-
Lifter 18	0.048	-	-
Lifter 19	0.038	-	-
Lifter 20	0.053	-	-
Lifter 21	0.046	-	-
Lifter 22	0.042	-	-
Lifter 23	0.044	-	-

However, due to analysis shown in Appendix VII 2(4) in Table 38 it can be stated that results are not reliable comparing to CoV value. Minor differences in volume and in concentrations have effect on results.

10.1.3 Video Analysis

Videos were analyzed by using machine vision method which is based on saturation. CoV numbers were calculated according to Equation 2. CoV was calculated after each lifter circumference as shown in Figure 71 in Appendix VII 3(4). Rotational speed 2 rpm and axial flow velocity 0.001 m/s were mainly used in these experiments. CoV numbers for every lifter design after each lifter circumference are shown in Table 15. Saturation curves for experiments are shown in Appendix X.

Table 15 CoV numbers for every lifter design after each lifter circumference.

	CoV based on saturation, -			
	Lifter circumference			
Lifter design	**1**	**2**	**3**	**4**
No lifters 2 rpm 0.001 m/s	1.397	1.171	0.917	0.676
Straight 4 lifters	1.336	1.034	0.781	0.603
Straight 4 lifters overlapped	1.342	0.984	0.721	0.592
Straight 8 lifters	1.241	0.952	0.672	0.549
Lifter 7	1.018	0.774	0.611	0.503
Lifter 8	1.076	0.820	0.642	0.487
Lifter 9	1.021	0.795	0.606	0.513
Lifter 10	1.003	0.773	0.590	0.513
Lifter 11	1.019	0.792	0.603	0.527
Lifter 12	0.938	0.694	0.510	0.442
Lifter 14	1.181	0.889	0.656	0.601
Lifter 15	1.218	0.861	0.603	0.491
Lifter 16	1.020	0.722	0.542	0.485
Lifter 17	1.017	0.775	0.608	0.547
Lifter 20	1.165	0.880	0.662	0.528
Lifter 21	1.114	0.834	0.670	0.560
Lifter 22	1.265	0.929	0.735	0.638
Lifter 23	1.094	0.838	0.641	0.541
Lifter 24	1.147	0.873	0.645	0.568
Lifter 25	1.184	0.889	0.654	0.540
Lifter 12 4 rpm 0.001 m/s	0.817	0.625	0.489	0.428
No lifters 4 rpm 0.001 m/s	1.375	1.091	0.824	0.606
No lifters 4 rpm 0.002 m/s	2.157	1.886	1.645	1.407

It is noted that CoV number decreases as a distance from the feed increases. This is shown for different lifters structures in Figures 48–52. CoV decrease for all experiments as a distance from the feed increases (Figure 48).

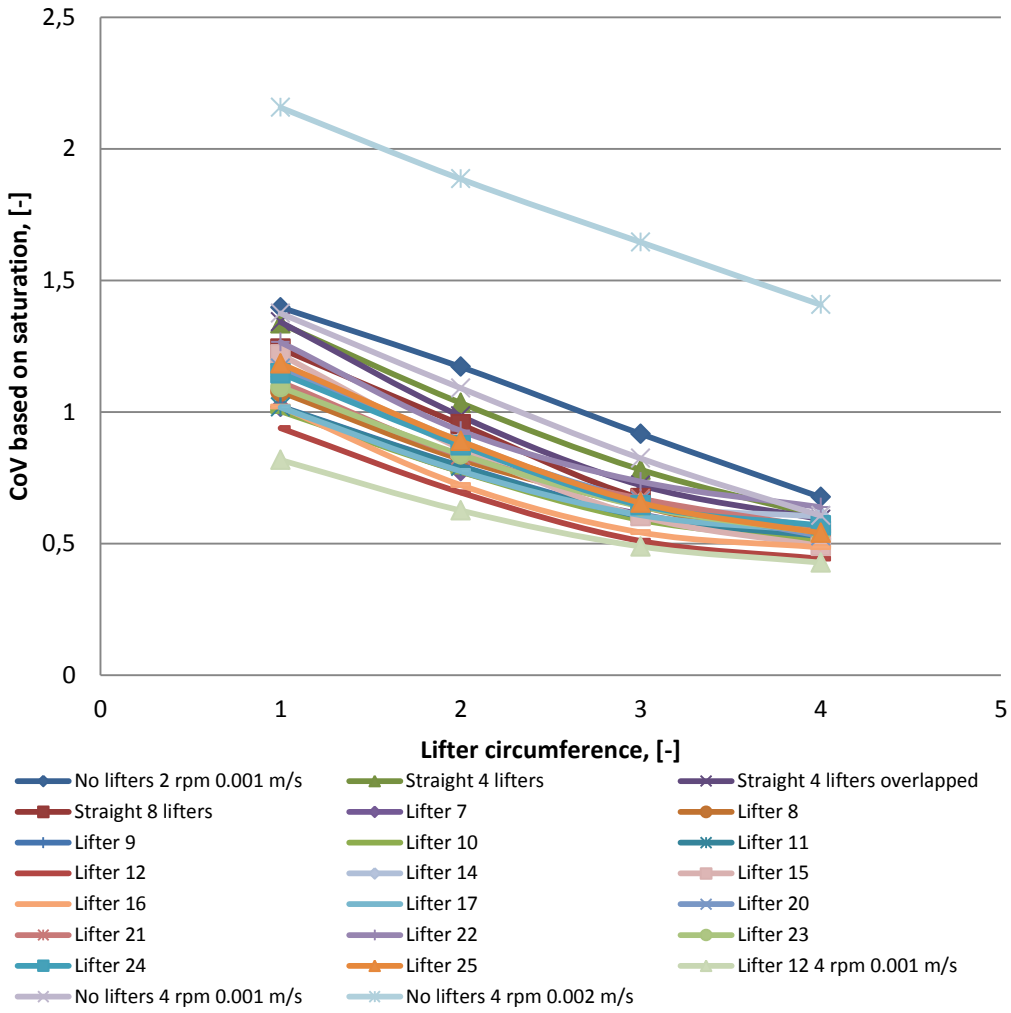

Figure 48 CoV decrease for all experiments. CoV decreases as a distance from the feed increases.

CoV decrease without lifters as a distance from the feed increases (Figure 49).

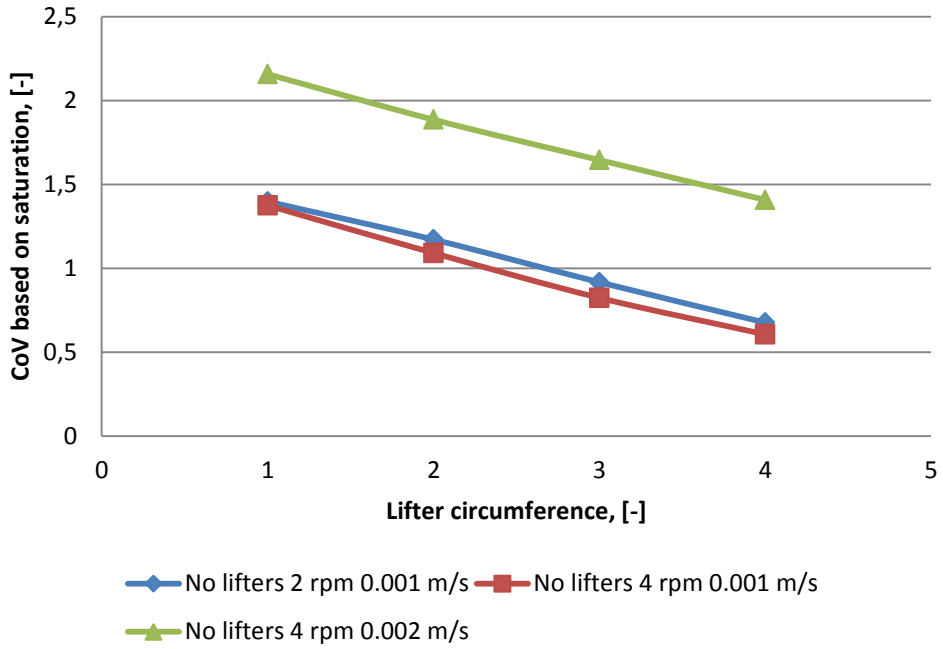

Figure 49 CoV after each lifter circumference distance without lifters.

CoV decrease with straight lifter structures as a distance from the feed increases (Figure 50).

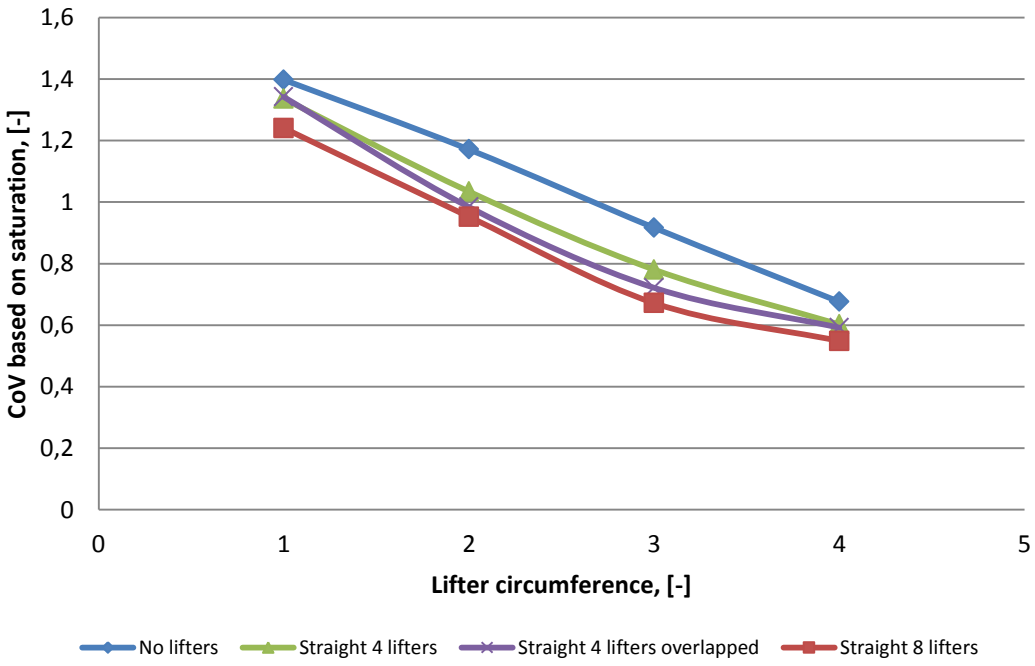

Figure 50 CoV after each lifter circumference distance with straight lifter structures.

CoV decrease with 8 lifters on one circumference structures as a distance from the feed increases (Figure 51).

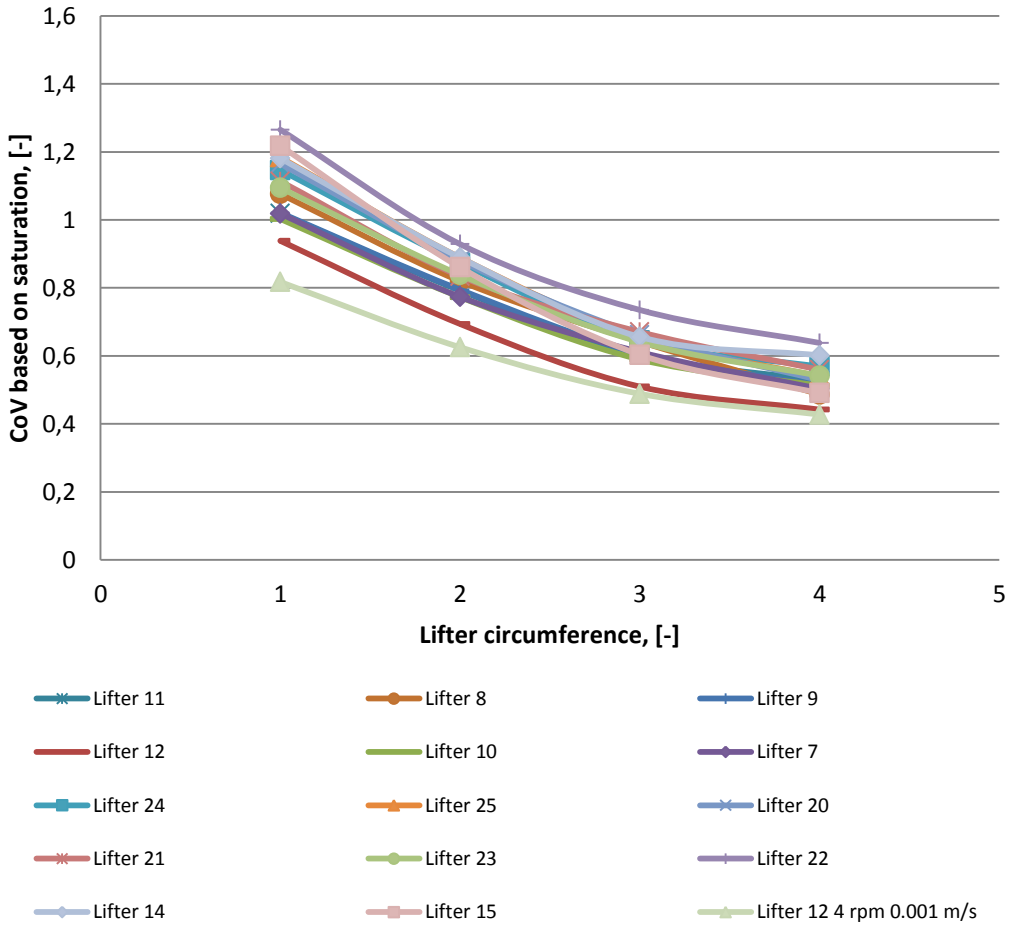

Figure 51 CoV after each lifter circumference distance with 8 lifters on one circumference.

CoV decrease with 4 lifters on one circumference structures as a distance from the feed increases (Figure 52).

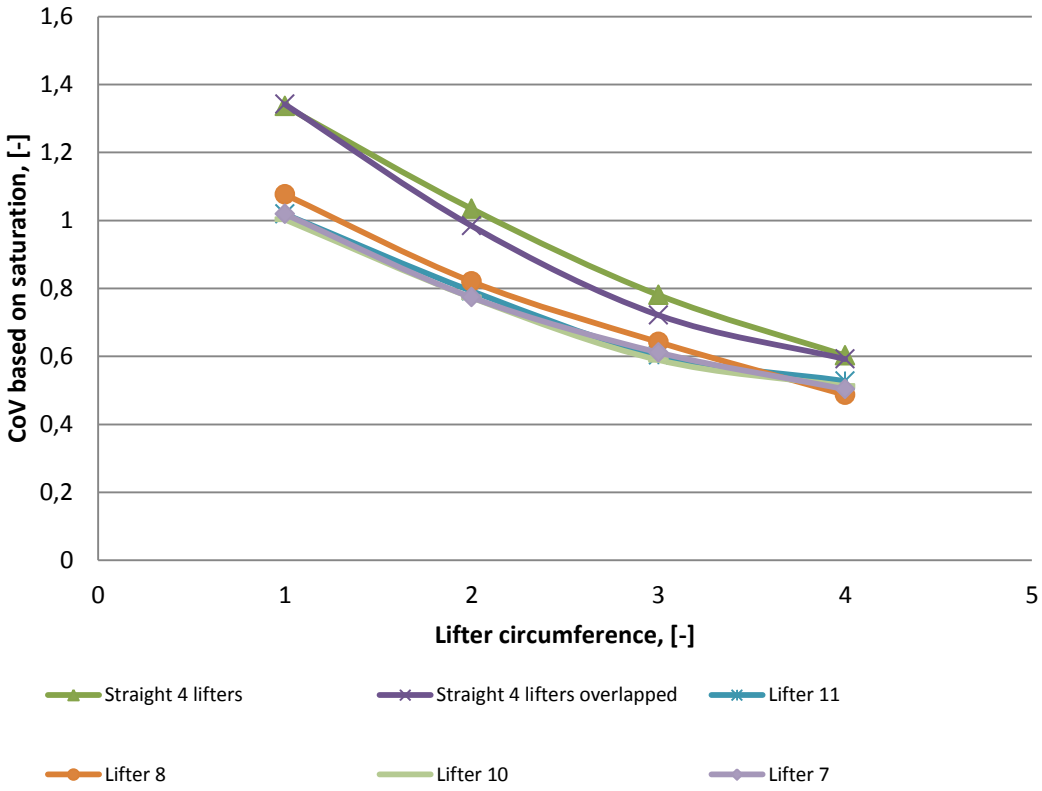

Figure 52 CoV after each lifter circumference distance with structures with 4 lifters on one circumference.

Based on CoV values different lifter structures can be ranked. Results are shown in table 16.

Table 16 Lifter structure rankings based on CoV values from machine vision analysis after 4th lifter circumference.

Rank	Lifter structure	CoV based on saturation, -
1	Lifter 12 4 rpm 0.001 m/s	0.428
2	Lifter 12	0.442
3	Lifter 16	0.485
3	Lifter 8	0.487
3	Lifter 15	0.491
6	Lifter 7	0.503
7	Lifter 10	0.513
7	Lifter 9	0.513
9	Lifter 11	0.527
9	Lifter 20	0.528
11	Lifter 25	0.540
11	Lifter 23	0.541
12	Lifter 17	0.547
12	Straight 8 lifters	0.549
14	Lifter 21	0.560
16	Lifter 24	0.568
15	Straight 4 lifters overlapped	0.592
16	Lifter 14	0.601
16	Straight 4 lifters	0.603
18	No lifters 4 rpm 0.001 m/s	0.606
19	Lifter 22	0.638
20	No lifters 2 rpm 0.001 m/s	0.676
21	No lifters 4 rpm 0.002 m/s	1.407

Mixing between lifter structures were normalized by applying Equation 5. Mixing variable used in Eq. 5 was CoV value. The higher the homogeneity value M is, the better the mixing is. Poor mixing is when M is 0. In Eq. 5 for example, X_0 was set based on the worst mixing in case of no lifters. As well, X_1 was set based on the best case. In each column in Table 21 the worst and the best CoV were selected for X_0 and X_1 respectively. Results are shown in Tables 17 and 18.

Table 17 Mixing between lifter structures based on homogeneity value. CoV value 1.397 was given for mixing variable X_0. Value 0.442 was given for variable X_1.

	CoV based on saturation, -			
	Lifter circumference			
Lifter design	**1**	**2**	**3**	**4**
No lifters 2 rpm 0.001 m/s	0.00	0.24	0.50	0.76
Straight 4 lifters	0.06	0.38	0.65	0.83
Straight 4 lifters overlapped	0.06	0.43	0.71	0.84
Straight 8 lifters	0.16	0.47	0.76	0.89
Lifter 7	0.40	0.65	0.82	0.94
Lifter 8	0.34	0.60	0.79	0.95
Lifter 9	0.39	0.63	0.83	0.93
Lifter 10	0.41	0.65	0.85	0.93
Lifter 11	0.40	0.63	0.83	0.91
Lifter 12	0.48	0.74	0.93	1.00
Lifter 14	0.23	0.53	0.78	0.83
Lifter 15	0.19	0.56	0.83	0.95
Lifter 16	0.40	0.71	0.90	0.95
Lifter 17	0.40	0.65	0.83	0.89
Lifter 20	0.24	0.54	0.77	0.91
Lifter 21	0.30	0.59	0.76	0.88
Lifter 22	0.14	0.49	0.69	0.79
Lifter 23	0.32	0.59	0.79	0.90
Lifter 24	0.26	0.55	0.79	0.87
Lifter 25	0.22	0.53	0.78	0.90

Table 18 Mixing between lifter structures based on homogeneity value. CoV value 1.397 was given for mixing variable X_0 g. Value 0 was given for variable X_1 because CoV = 0 is for perfect mixing.

	CoV based on saturation, -			
	Lifter circumference			
Lifter design	**1**	**2**	**3**	**4**
No lifters 2 rpm 0.001 m/s	0.00	0.16	0.34	0.52
Straight 4 lifters	0.04	0.26	0.44	0.57
Straight 4 lifters overlapped	0.04	0.30	0.48	0.58
Straight 8 lifters	0.11	0.32	0.52	0.61
Lifter 7	0.27	0.45	0.56	0.64
Lifter 8	0.23	0.41	0.54	0.65
Lifter 9	0.27	0.43	0.57	0.63
Lifter 10	0.28	0.45	0.58	0.63
Lifter 11	0.27	0.43	0.57	0.62
Lifter 12	0.33	0.50	0.64	0.68
Lifter 14	0.15	0.36	0.53	0.57
Lifter 15	0.13	0.38	0.57	0.65
Lifter 16	0.27	0.48	0.61	0.65
Lifter 17	0.27	0.45	0.57	0.61
Lifter 20	0.17	0.37	0.53	0.62
Lifter 21	0.20	0.40	0.52	0.60
Lifter 22	0.09	0.34	0.47	0.54
Lifter 23	0.22	0.40	0.54	0.61
Lifter 24	0.18	0.38	0.54	0.59
Lifter 25	0.15	0.36	0.53	0.61

10.1.4 Correlation between CoV Results

Correlation between CoV values from acid experiments and machine vision was also studied to prove that machine vision and saturation values can be used in CMC experiments. CoV results based on acid experiments and machine vision are shown in Appendix VI. The correlation was found between the impulse response test experiments and machine vision analysis.

10.2 CMC Experiments

CMC experiments were mainly carried out by using a colored CMC as an impulse. In this case degree of mixing was analyzed using CoV number calculated with machine vision based on saturation values. CMC experiments were also carried out by using HNO_3 as acid impulse. Mixing was measured based on concentration values which were collected using pH meter and analyzed with CoV number.

10.2.1 Coefficient of Variation

CoV numbers were calculated according to Equation 2. Concentration curves and CoV numbers for no lifters geometry are shown in Figures 53 and 54. It is noted based on repetition runs that there is uncertainty in results comparing to water experiments.

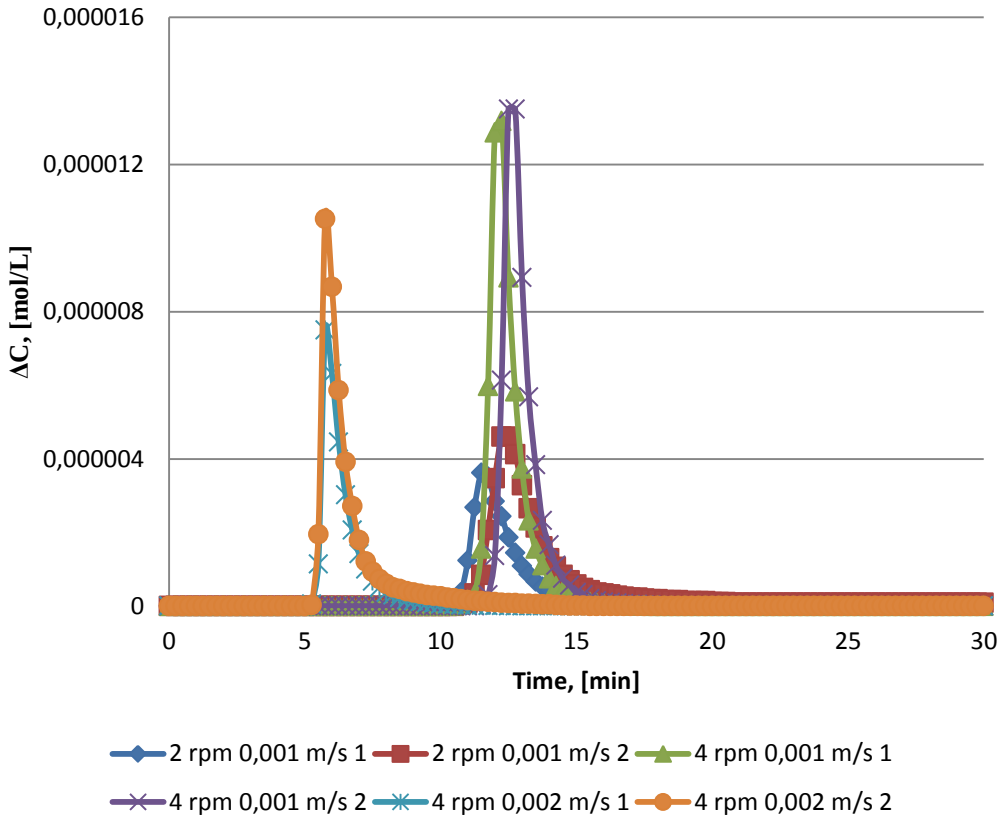

Figure 53 Concentration curves for no lifters geometry including repetion runs.

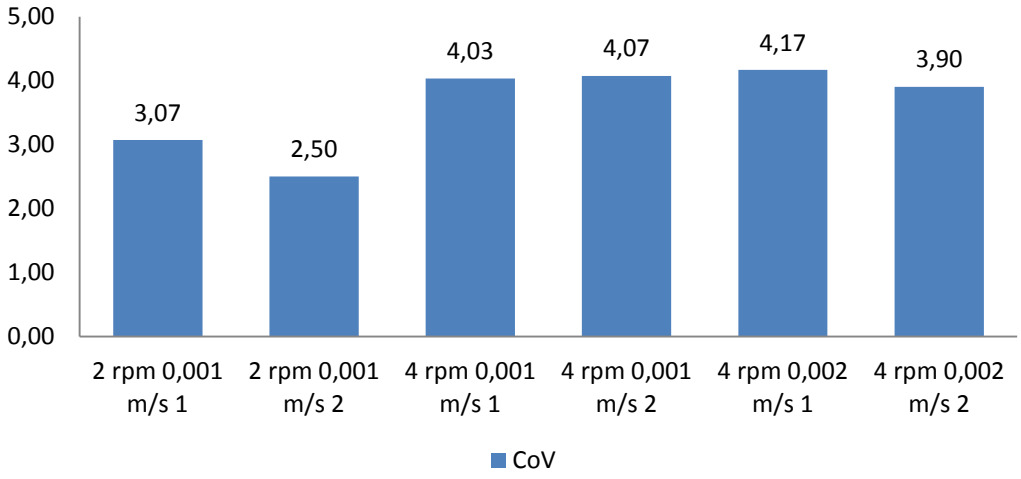

Figure 54 CoV numbers for no lifters geometry including repetion runs.

Uncertainty increases as lifters were added in experiments. Concentration curves and CoV numbers for lifter 12 at 2 rpm and 0.001 m/s axial flow velocity are presented in Figures 55 and 56.

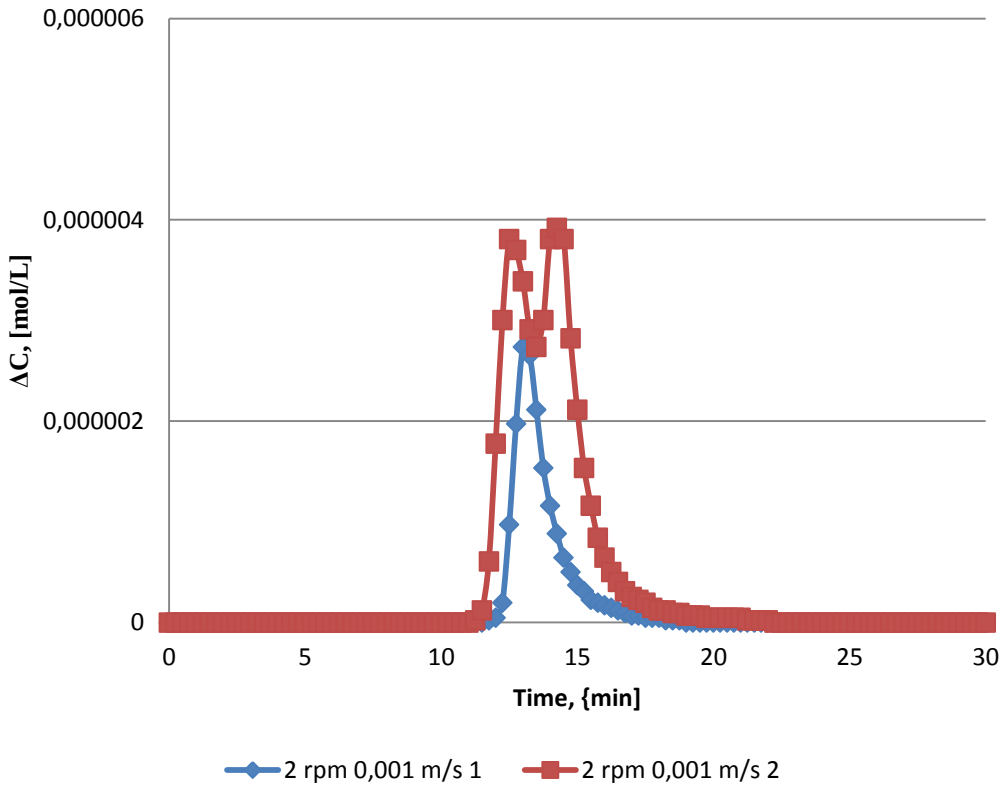

Figure 55 Concentration curves for lifter 12 geometry including repetion runs.

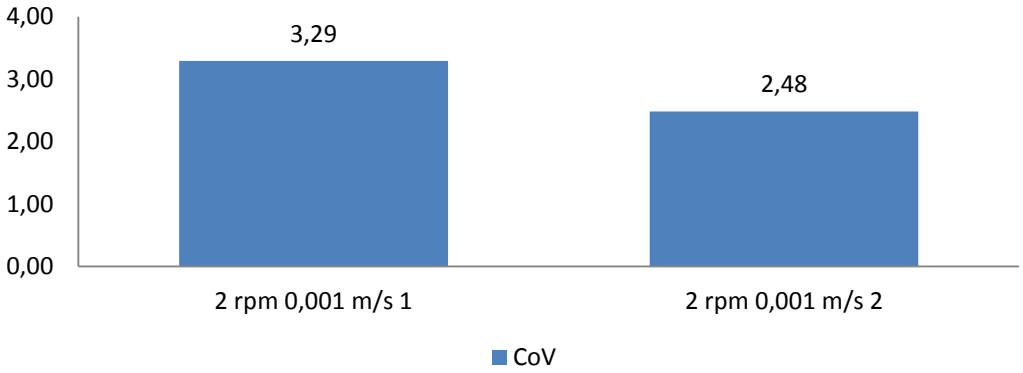

Figure 56 CoV numbers for lifter 12 geometry including repetion runs.

Uncertainty is also noted in results using straight lifters (8 lifters on one circumference). Concentration curves and CoV numbers for straight lifter geometry using all process parameters are shown in Figures 57 and 58.

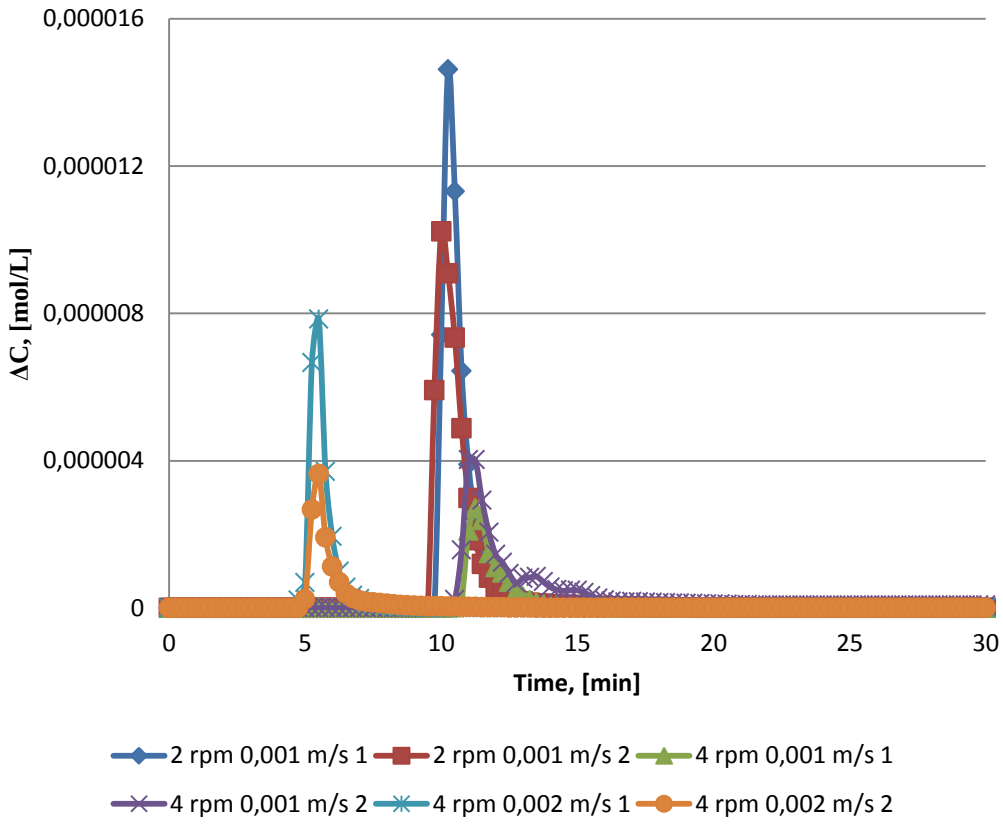

Figure 57 Concentration curves for straight lifter geometry including repetion runs.

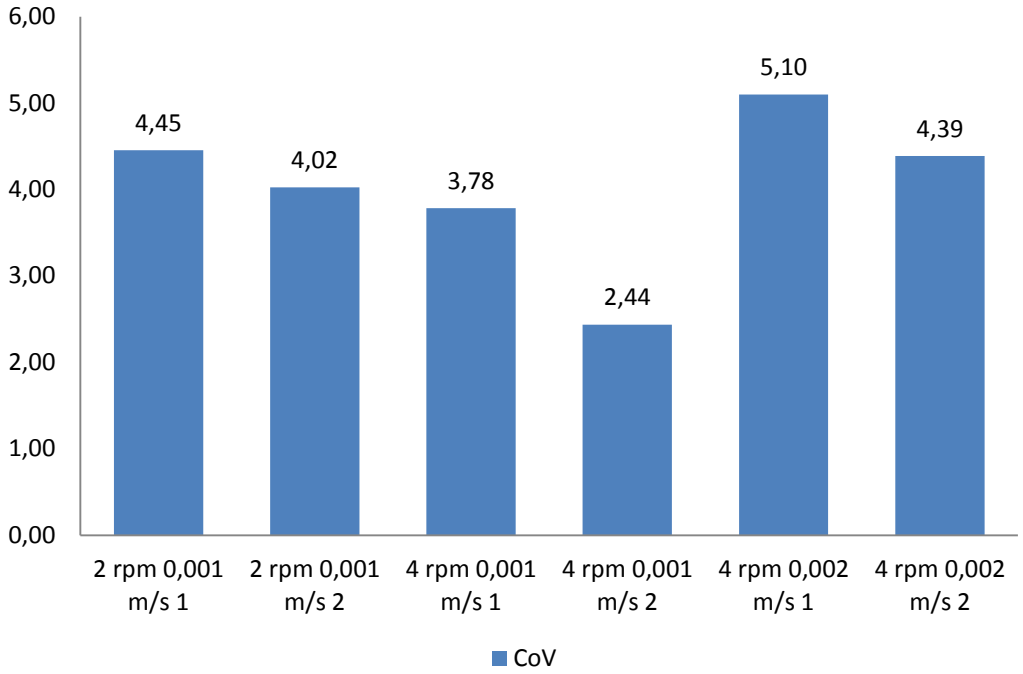

Figure 58 CoV numbers for straight lifter geometry including repetion runs.

CoV numbers from acid experiments using different lifter designs and operational parameters are shown in Table 19. It is noted based on repetition runs that there is uncertainty in results and lifters only increase the uncertainty. The rest of the experiments were analyzed by using machine vision technique.

Table 19 CoV numbers with different lifter designs using different process parameters. A repetition experiment was carried out using every process parameter.

	CoV, -		
	Lifter design		
Operational parameter	**No lifters**	**Straight 8 lifters**	**Lifter 12**
2 rpm 0.001 m/s test 1	3.07	4.45	3.29
2 rpm 0.001 m/s test 2	2.50	4.02	2.48
4 rpm 0.001 m/s test 1	4.03	3.78	-
4 rpm 0.001 m/s test 2	4.07	2.44	-
4 rpm 0.002 m/s test 1	4.17	5.10	-
4 rpm 0.002 m/s test 2	3.90	4.39	-

10.2.2 Video Analysis

Videos were analyzed by using machine vision method which is based on saturation. CoV numbers were calculated according to Equation 2. CoV values were calculated for three lifter circumferences as shown in Figure 71 in Appendix VII 3(4). Rotational speed 2 rpm and axial flow velocity 0.001 m/s were mainly used in these experiments. CoV numbers for every lifter design after each lifter circumference are shown in Tables 20 and 21. Duration of each calculation time was limited to 1 000 seconds. Some deviations in results carried out with modified lifters were found. Due to this results from modified lifter experiments were analyzed separately. Saturation curves with residence times for experiments are also shown in Appendix XI. CoV numbers for every lifter design after each lifter circumference are shown in Table 20.

Table 20 CoV numbers for every lifter design after each lifter circumference.

	CoV, -		
	Lifter circumference		
Lifter design	**1. lifter**	**2. lifter**	**3. lifter**
No lifters 2 rpm 0.001 m/s	2.134	1.861	1.516
No lifters 4 rpm 0.001 m/s	1.870	1.674	1.458
No lifters 4 rpm 0.002 m/s	2.128	1.822	1.605
Straight 2 lifters	1.761	1.410	1.318
Straight 4 lifters	1.747	1.303	1.138
Straight 4 lifters overlapped	1.332	0.896	0.821
Straight 8 lifters 1	1.649	1.297	1.129
Straight 8 lifters 2	1.274	0.935	0.859
Lifter 7	1.296	0.846	0.620
Lifter 8	1.383	0.880	0.816
Lifter 9	0.938	0.665	0.575
Lifter 10	1.359	1.243	1.118
Lifter 11	1.621	1.344	1.291
Lifter 12	1.614	1.303	1.075
Lifter 13	1.379	1.163	1.198
Lifter 14	1.453	1.275	1.186
Lifter 15	1.298	1.195	1.062
Lifter 16	2.213	1.374	0.875
Lifter 17	1.873	1.103	0.764
Lifter 18	1.715	1.472	1.057
Lifter 19	1.474	1.217	1.140
Lifter 20	1.121	0.854	0.772
Lifter 21	1.381	1.158	1.088
Lifter 22	0.940	0.642	0.613
Lifter 23	1.657	1.355	1.244
Lifter 24	1.000	0.669	0.561
Lifter 25	1.442	1.166	1.105

Modified structures were analyzed separately due to uncertainty in results. CoV numbers for every modified lifter design after each lifter circumference are shown in Table 21.

Table 21 CoV numbers for every modified lifter design after each lifter circumference.

	CoV, -		
	Lifter circumference		
Lifter design	**1. lifter**	**2. lifter**	**3. lifter**
M Straight 4 lifters	0.946	0.790	0.735
M Straight 4 lifters overlapped	0.927	0.868	0.827
M Straight 8 lifters	1.071	0.897	0.822
Lifter 20	1.403	1.076	0.791
Lifter 21	1.731	1.405	1.266
Lifter 22	1.132	0.671	0.517
Lifter 23	1.832	1.331	1.063
Lifter 24	1.228	0.818	0.529
Lifter 25	1.630	1.455	1.343

It is noted that CoV number decreases after each lifter circumference. This is shown for different lifters structures in Figures 59–62. CoV decrease for all experiments as a distance from the feed increases (Figure 59).

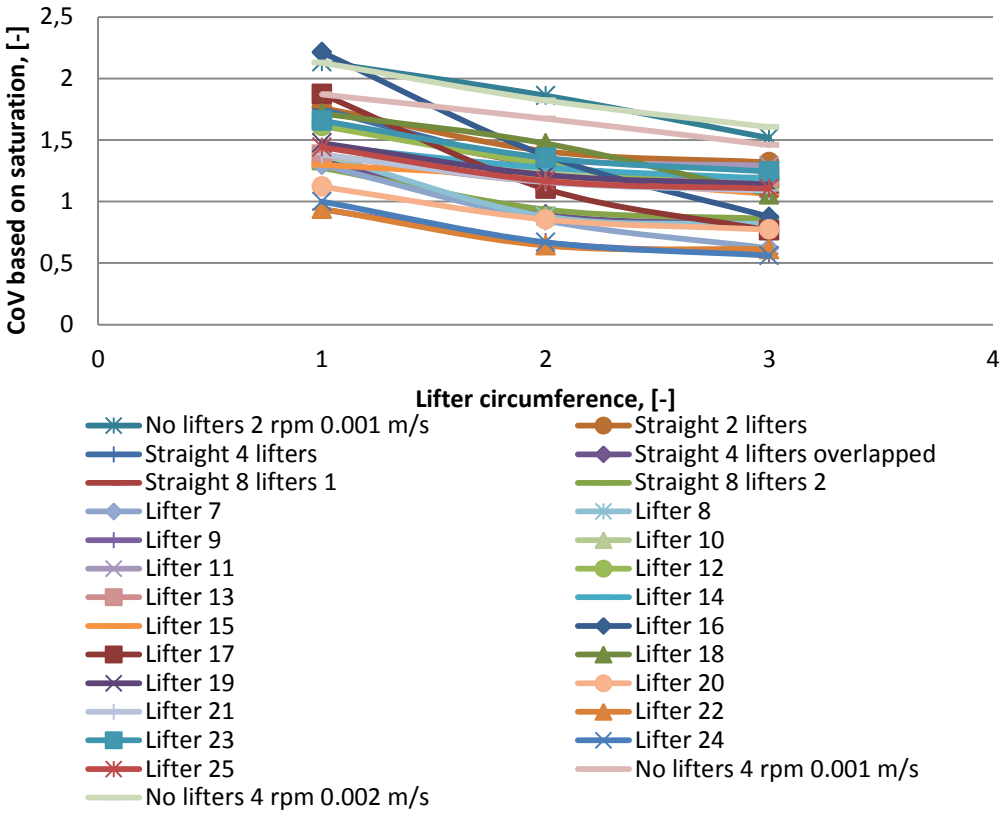

Figure 59 CoV decrease for all experiments. CoV decreases as a distance from the feed increases.

CoV decrease without lifters as a distance from the feed increases (Figure 60).

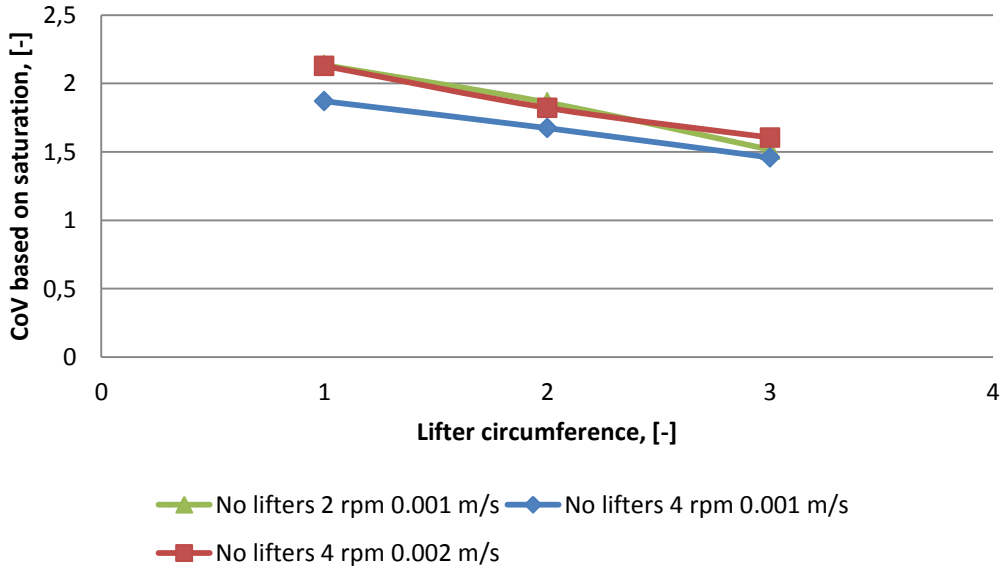

Figure 60 CoV after each lifter circumference distance without lifters.

CoV decrease with straight lifter structures as a distance from the feed increases (Figure 61).

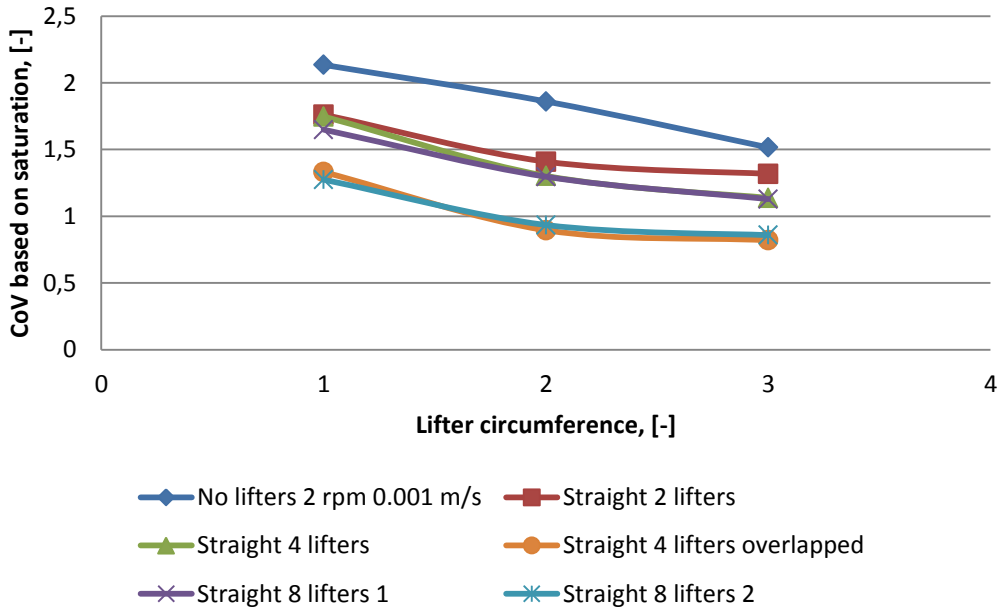

Figure 61 CoV after each lifter circumference distance with straight lifter structures.

CoV decrease with modified straight structures as a distance from the feed increases (Figure 62).

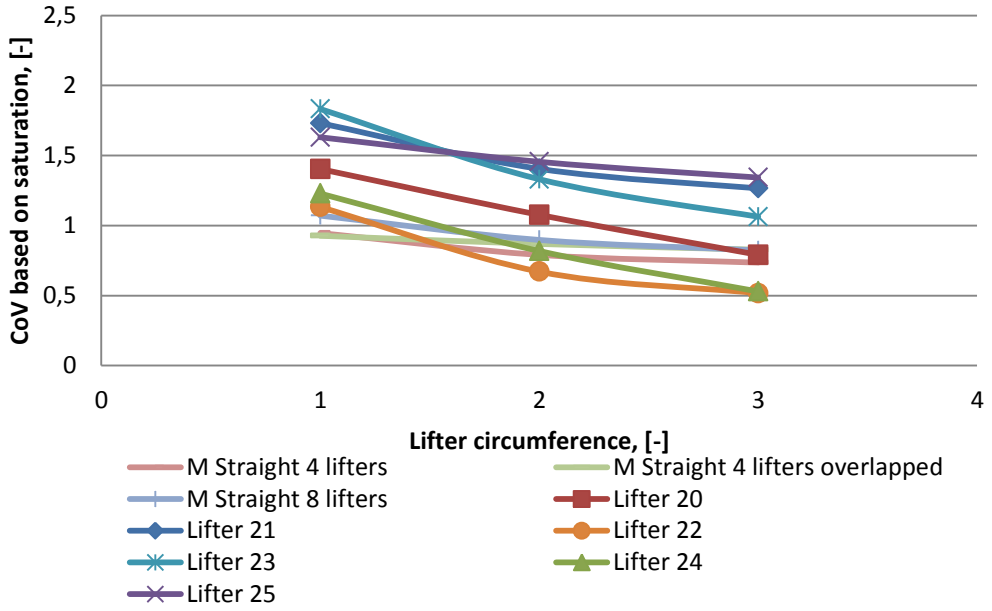

Figure 62 CoV after each lifter circumference distance with modified lifter structures.

Based on CoV values different lifter structures can be ranked. Results are presented in Table 22.

Table 22 Lifter structure rankings based on CoV values from machine vision analysis.

Rank	Lifter design	CoV, -
1	Lifter 24	0.561
2	Lifter 9	0.575
3	Lifter 22	0.613
4	Lifter 7	0.620
5	Lifter 17	0.764
6	Lifter 20	0.772
7	Lifter 8	0.816
8	Straight 4 lifters overlapped	0.821
9	Straight 8 lifters 2	0.859
10	Lifter 16	0.875
11	Lifter 18	1.057
12	Lifter 15	1.062
13	Lifter 12	1.075
14	Lifter 21	1.088
15	Lifter 25	1.105
16	Lifter 10	1.118
17	Straight 8 lifters 1	1.129
18	Straight 4 lifters	1.138
19	Lifter 19	1.140
20	Lifter 14	1.186
21	Lifter 15	1.198
22	Lifter 23	1.244
23	Lifter 11	1.291
24	Straight 2 lifters	1.318
25	No lifters 4 rpm 0.001 m/s	1.458
26	No lifters 2 rpm 0.001 m/s	1.516
27	No lifters 4 rpm 0.002 m/s	1.605

Modified structures were analyzed separately due to uncertainty in results. Based on CoV values different modified lifter structures were ranked. Results are presented in Table 23.

Table 23 Modified lifter structure rankings based on CoV values from machine vision analysis.

Rank	**Lifter design**	**CoV, -**
1	Lifter 22	0.517
2	Lifter 24	0.529
3	M Straight 4 lifters	0.735
4	Lifter 20	0.791
5	M Straight 8 lifters	0.822
6	M Straight 4 lifters overlapped	0.827
7	Lifter 23	1.063
8	Lifter 21	1.266
9	Lifter 25	1.343

Mixing between lifter structures were normalized by applying Equation 5. Mixing variable used in Eq. 5 was CoV value. The higher the homogeneity value M is, the better the mixing is. Poor mixing is when M is 0. In Eq. 5 for example, X_0 was set based on the worst mixing. As well, X_1 was set based on the best case. In each column in Table 24 the worst and the best CoV were selected for X_0 and X_1 respectively. Results are shown in Tables 24–27.

Table 24 Mixing between lifter structures based on homogeneity value. CoV value 2.213 was given for mixing variable X_0. Value 0.561 was given for variable X_1.

	Homogeneity, -		
	Lifter circumference		
Lifter design	**1. lifter**	**2. lifter**	**3. lifter**
No lifters 2 rpm 0.001 m/s	0.05	0.21	0.42
No lifters 4 rpm 0.001 m/s	0.21	0.33	0.46
No lifters 4 rpm 0.002 m/s	0.05	0.24	0.37
Straight 2 lifters	0.27	0.49	0.54
Straight 4 lifters	0.28	0.55	0.65
Straight 4 lifters overlapped	0.53	0.80	0.84
Straight 8 lifters 1	0.34	0.55	0.66
Straight 8 lifters 2	0.57	0.77	0.82
Lifter 7	0.55	0.83	0.96
Lifter 8	0.50	0.81	0.85
Lifter 9	0.77	0.94	0.99
Lifter 10	0.52	0.59	0.66
Lifter 11	0.36	0.53	0.56
Lifter 12	0.36	0.55	0.69
Lifter 13	0.50	0.64	0.61
Lifter 14	0.46	0.57	0.62
Lifter 15	0.55	0.62	0.70
Lifter 16	0.00	0.51	0.81
Lifter 17	0.21	0.67	0.88
Lifter 18	0.30	0.45	0.70
Lifter 19	0.45	0.60	0.65
Lifter 20	0.66	0.82	0.87
Lifter 21	0.50	0.64	0.68
Lifter 22	0.77	0.95	0.97
Lifter 23	0.34	0.52	0.59
Lifter 24	0.73	0.93	1.00
Lifter 25	0.47	0.63	0.67

Table 25 Mixing between modified lifter structures based on homogeneity value. CoV value 2.213 was given for mixing variable X_0. Value 0.517 was given for variable X_1.

	Homogeneity, -		
	Lifter circumference		
Lifter design	**1. lifter**	**2. lifter**	**3. lifter**
M Straight 4 lifters	0.75	0.84	0.87
M Straight 4 lifters overlapped	0.76	0.79	0.82
M Straight 8 lifters	0.67	0.78	0.82
Lifter 20	0.48	0.67	0.84
Lifter 21	0.28	0.48	0.56
Lifter 22	0.64	0.91	1.00
Lifter 23	0.22	0.52	0.68
Lifter 24	0.58	0.82	0.99
Lifter 25	0.34	0.45	0.51

Table 26 Mixing between lifter structures based on homogeneity value. CoV value 2.213 was given for mixing variable X_0. Value 0 was given for variable X_1 because CoV = 0 is for perfect mixing.

	Homogeneity, -		
	Lifter circumference		
Lifter design	**1. lifter**	**2. lifter**	**3. lifter**
No lifters 2 rpm 0.001 m/s	0.04	0.16	0.31
No lifters 4 rpm 0.001 m/s	0.15	0.24	0.34
No lifters 4 rpm 0.002 m/s	0.04	0.18	0.27
Straight 2 lifters	0.20	0.36	0.40
Straight 4 lifters	0.21	0.41	0.49
Straight 4 lifters overlapped	0.40	0.60	0.63
Straight 8 lifters 1	0.25	0.41	0.49
Straight 8 lifters 2	0.42	0.58	0.61
Lifter 7	0.41	0.62	0.72
Lifter 8	0.38	0.60	0.63
Lifter 9	0.58	0.70	0.74
Lifter 10	0.39	0.44	0.49
Lifter 11	0.27	0.39	0.42
Lifter 12	0.27	0.41	0.51
Lifter 13	0.38	0.47	0.46
Lifter 14	0.34	0.42	0.46
Lifter 15	0.41	0.46	0.52
Lifter 16	0.00	0.38	0.60
Lifter 17	0.15	0.50	0.65
Lifter 18	0.23	0.34	0.52
Lifter 19	0.33	0.45	0.48
Lifter 20	0.49	0.61	0.65
Lifter 21	0.38	0.48	0.51
Lifter 22	0.58	0.71	0.72
Lifter 23	0.25	0.39	0.44
Lifter 24	0.55	0.70	0.75
Lifter 25	0.35	0.47	0.50

Table 27 Mixing between modified lifter structures based on homogeneity value. CoV value 2.213 was given for mixing variable X_0. Value 0 was given for variable X_1 because CoV = 0 is for perfect mixing.

	Homogeneity, -		
	Lifter circumference		
Lifter design	**1. lifter**	**2. lifter**	**3. lifter**
M Straight 4 lifters	0.57	0.64	0.67
M Straight 4 lifters overlapped	0.58	0.61	0.63
M Straight 8 lifters	0.52	0.59	0.63
Lifter 20	0.37	0.51	0.64
Lifter 21	0.22	0.37	0.43
Lifter 22	0.49	0.70	0.77
Lifter 23	0.17	0.40	0.52
Lifter 24	0.44	0.63	0.76
Lifter 25	0.26	0.34	0.39

Residence time of tracer impulse in each lifter circumference was also analyzed. Results are shown in Table 28.

Table 28 Residence time of tracer pulse in each lifter circumference.

	Residence time, s		
	Lifter circumference		
Lifter design	**1. lifter**	**2. lifter**	**3. lifter**
No lifters 2 rpm 0.001 m/s	84	168	247
No lifters 4 rpm 0.001 m/s	120	166	218
No lifters 4 rpm 0.002 m/s	66	92	127
Straight 2 lifters	217	310	357
Straight 4 lifters	205	310	394
Straight 4 lifters overlapped	227	330	376
Straight 8 lifters 1	221	348	478
Straight 8 lifters 2	257	416	538
Lifter 7	144	260	517
Lifter 8	132	322	472
Lifter 9	230	370	541
Lifter 10	158	260	338
Lifter 11	141	265	433
Lifter 12	172	283	425
Lifter 13	171	306	424
Lifter 14	178	302	429
Lifter 15	169	314	427
Lifter 16	113	268	506
Lifter 17	114	197	383
Lifter 18	111	213	324
Lifter 19	151	237	311
Lifter 20	184	378	471
Lifter 21	167	323	443
Lifter 22	355	633	678
Lifter 23	160	292	411
Lifter 24	290	652	718
Lifter 25	223	342	468

10.3 Solid Experiments

Mixing and transverse bed motion were examined with machine vision and visually. It was seen that the tangential bed motion was the most intensive with straight lifters. Mixing was noted as cascading. With lifter designs 9, 12, 16 and 17 it was noted that mixing in tangential bed motion is not that intensive comparing to straight lifter. Motion was more like rolling type. Without lifters the mixing was hardly seen. Based on machine vision results, it was noted that with lifter design 9 and 16 the residence time of the tracer increases. With lifter designs 12 and 16 the effect is opposite. Residence time results are shown in Appendix VIII. When studying the lifting height it is noted that lifters 9 and 12 lift the dust the highest before dust drops to bed. Comparison between results is shown in Table 29.

Table 29 Comparison between transverse bed motion, residence time and lift height using different lifter structures.

Structure	**Tangential bed motion**	**Residence time**	**Lift height**
No lifters	Slumping	Normal	4. highest
Straight	Cascading	Normal	3. highest
Lifter 9	Rolling	Increases	1. highest
Lifter 12	Rolling	Decreases	1. highest
Lifter 16	Rolling	Increases	2. highest
Lifter 17	Rolling	Decreases	2. highest

11 CONCLUSIONS

In this research of the mixing in the rotating drum different materials, different process parameters and different methods for analyzing the results were used. Water was chosen as low viscous material and CMC was chosen as more viscous material due to the rheology studies of lime mud dust to the material characterization. Minor part of the experiments was also carried out with solid lime mud dust. Rotation speed of the drum and the linearized flow rate were the main operational parameters in the experiments. Rotation speeds used were 2 rpm and 4 rpm. The linearized flow rates used were 0.001 m/s and 0.002 m/s. Different lifter designs were used in the experiments. The straight lifter structure was installed horizontally to x-direction of the drum.

Observations were made from the water experiments. It was noted that when the rotation speed increases the CoV value decreases. When the flow rate decreases the CoV value decreases. Increase of the lifters on one circumference decreases the CoV value. The concentration curves decrease steeper from the peak with some lifter geometries than with other structures. Results also show that it is better to use overlapping structure with straight lifters compare to normal structure.

Lifter structures were compared according to homogeneity calculated with Equation 5. From Tables 11–12 it is noted that the lifter 12 structure is a dominant structure. With normalization from 0 to 1 it can be noted that lifter 12 structure is far from perfect mixing. Also all homogeneity values are between 0.00 and 0.23 so it can be said that the efficiency between the lifters in case of water is minimal. Results are shown in Tables 11 and 12.

In machine vision experiments carried out with water CoV values were calculated for all four lifter circumferences. It is noted that CoV value decreases as a distance from the feed increases. However, it is noted that differences are not large. This is presented in Figure 48. Also in machine vision experiments lifter 12 is the dominant lifter geometry. Lifter structures were compared according to homogeneity calculated with Equation 5. The homogeneity values after last lifter

circumference are between 0.52 and 0.68 so it can be said that efficiency between lifters in case of water is minimal. Results are shown in Tables 17 and 18.

CoV values were calculated for only three lifter circumferences in machine vision experiments with CMC. It was noted that CoV values behave differently compared to water experiments. The lifter design has more influence on CoV value with CMC. Results are presented in Figures 59–62. It was also noted that the residence time of impulse increases while the number of lifters on one circumference increases. Residence time results are shown in Table 28.

The lifter structures were compared according to homogeneity calculated with Equation 5. With normalization from 0 to 1 it can be noted that the differences are larger compared to water experiments. Homogeneity values after last lifter circumference are between 0.31 and 0.75. So, it can be said that lifter structures have influence on mixing in case of a viscous material. Results are presented in Tables 24–27.

Differences in results are explained by the movement of molecules. Molecules are able to move rapidly and randomly in case of low viscous water. The mixing improves when lifters are arranged densely. Straight lifters are in horizontal direction so the mixing improves when the lifters are organized densely in an overlapping structure. In case of a high viscous material the lifter structures have more important role. Molecules are not able to move rapidly and randomly in case of high viscous CMC. In case of CMC lifter geometries have effect on residence times and mixing.

When comparing the residence times of different lifter structures it is noted that with some lifter structures the residence time of tracer impulse increases. It is also noted that when the amount of lifters on one circumference increases the residence time increases. With 8 straight lifters on one circumference the residence time was doubled comparing to geometry without lifters. The residence time was increased even more with some random lifter geometries. Mixing and tangential bed motion were also examined with solid lime mud dust. It was noted that the most intensive tangential bed motion was reached with straight lifter

structure. However, based on residence time results it was noted that with lifter 9 and lifter 16 structures the residence time was increased by 25 % compared to straight lifters.

Final conclusion from the mixing experiments is that lifter structure in lime kiln must be planned carefully. It is noted that the residence time can be increased and the mixing improved with the right choice of lifter geometry. Random lifter geometries tend to increase the residence time and mixing is improved compared to geometry without lifters. Also the tangential bed motion was observed the most intensive with straight lifters. Next step in experiments would be the optimization of the lifter structures. The experiments and analyzes of the optimal gas velocity to avoid the lime mud particles being pick up from the particle bed were excluded from this master's thesis and will be performed separately. After these experiments it is more accurate to say how the operating efficiency of lime kiln is increased in the best possible way.

REFERENCES

Andritz Oy. 2014. [Online document]. [Accessed 31 January 2014]. Available at http://www.andritz.com/group/gr-about-us.htm

Alopaeus, V., Laavi, H., *et al.* 2008. A Dynamic Model for Plug Flow Reactor State Profiles, *Computers and Chemical Engineering*, 32, pp. 1494–1506.

Arpalahti, O., Engdahl, H., *et al*. 1999. White Liquor Preparation, in Gullichsen, J., Fogelholm, C-J., Papermaking Science and Technology. Book 6, A Chemical Pulping. Helsinki: Fapet Oy.

Aubin, J., Fletcher, D.F., *et al*. 2003. Characterization of the Mixing Quality in Micromixers. *Chemical Engineering Technology*, 26, pp. 1263-1264.

Barr, P.V., Brimacombe, J.K., Watkinson, A.P. 1989. A Heat-Transfer Model for the Rotary Kiln: Part II. Development of the Cross-Section Model. *Metallurgical Transactions*, vol. 20 B, pp. 403-404.

Barr, P.V., Boateng, A.A. 1997. Granular Flow Behaviour in the Transverse Plane of a Partially Filled Rotating Cylinder. *Journal of Fluid Mechanics*, vol. 330, pp. 233-249.

Björk, M. 2002. Effects of Process Variation on Ring Formation in Lime Kilns. Karlstad: Stora Enso.

Boateng, A.A. 2008. Rotary Kilns, Elsevier, Amsterdam: Elsevier

Boateng, A.A. 1993. Rotary Kiln Transport Phenomena: Study of the Bed Motion and Heat Transfer. PhD Dissertation. Vancouver: University of British Columbia.

Boyden, J.W. 1991. Lime Sludge Kiln, U.S. Patent No. 4993942, February 19.

Boynton, R.S. 1980. Chemistry and Technology of Lime and Limestone. 2nd ed., New York: Wiley & Sons.

Brimacombe, J.K., Watkinson, A.P. 1978. Heat Transfer in a Direct Fired Rotary Kiln: Part 1. Pilot Plant and Experimentation. *Metallurgical Transactions*, vol. 9B, pp. 201-202.

Brown, D.A.R., Jones, P.N., *et al.* 2004. Experimental Methods in Paul, E.L., Atiemo-Obeng, V.A., Kresta, S.M., (Eds.). Handbook of Industrial Mixing – Science and Practice. New Jersey: John Wiley & Sons Inc.

CPKelco. 2014. [Online document]. [Accessed 15 October 2014]. Available at http://cpkelco.com/

Cussler, E.L. 2009. Diffusion: Mass Transfer in Fluid Systems. 3rd Ed., New York: Cambridge University Press.

Davies, P.R., Norton, M.J.S., et al. 2010. Gas Flow in Rotary Kilns. *Particuology*, vol. 8, pp. 613-616.

Dhanjal, S.S., Barr, P.V., et al. 2004. The Rotary Kiln: An investigation of Bed Heat Transfer in the Transverse Plane. *Metallurgical and Materials Transactions*, vol. 35B, pp. 1059-1070.

deBeus, A.J. 1987. Heat Exchange Apparatus and Process for Rotary Kilns. U.S. Patent No. 4676740, June 30.

Dillman, B.A. 2008. Low Profile Flights for Use in a Drum. U.S. Patents No. 7343697, March 18.

Ellis, K. 1989. Ring Formation in a NCG Burning Lime Kiln. Tappi Environmental Conference Proceeding, Tappi Press, pp. 115.

Etchells III, A.W. 2004. Mixing in Pipelines in Paul, E.L., Atiemo-Obeng, V.A., Kresta, S.M., (Eds.). Handbook of Industrial Mixing – Science and Practice. New Jersey: John Wiley & Sons Inc.

Ferron, L.T., Singh, D.K. 1991. Rotary Kiln Transport Processes. *AIChE Journal*, 5, pp. 774-758.

Flemming, E.J. 1970. Rotary Kilns with Cooler Tubes. U.S. Patents No. 3547418, December 15.

Gorog, J.P., Brimacombe, J.K, *et al*. 1981. Radiative Heat Transfer in Rotary Kilns. *Metallurgical Transactions*, vol. 12B, pp. 55-56.

Hassibi, M. 2009. An Overview of Lime Slaking and Factors That Affect the Process, Chemco Systems.

He, M. 2005. Slurry Rheology of Limestone and Its Effects on Wet ultra-fine Grinding. Licentiate Thesis, Luleå: Luleå University of Technology.

Henein, H. 1991. Radial Segregation in Rotary Kilns, *The Minerals, Metals and Materials Society*, pp. 311-329.

Henein, H. 1980. Bed Behavior in Rotary Cylinders with Applications to Rotary Kilns. PhD Dissertation, Vancouver: University of British Columbia.

Honghi, T. 2008. Lime Kiln Chemistry and Effects on Kiln Operations. Tappi Kraft Recovery Short Course, Florida, January 7 – January 10, Toronto, Canada.

Kottila, Mika. 2014. Andritz Oy, Oral information.

Lacey, P.M.C. 1954. Developments in the Theory of Particulate Mixing. *Journal of Applied Chemistry*, 4, pp.257-268.

Levenspiel, O. 1999. Chemical Reaction Engineering, 3rd Ed., New York: John Wiley & Sons.

Lou, H.H., Chandrasekaran, J., *et al.* 2006. Large-scale Dynamic Simulation for Security Assessment of an Ethylene Oxide Manufacturing Process. *Computers and Chemical Engineering*, 30, pp. 1102–1118.

Malahat, F. 2010. Modeling Dust Formation in Lime Kilns. PhD Thesis, Department of Mechanical and Industrial Engineering, Toronto: University of Toronto.

Marte, U. 2000. Rheology, in Hentrich, P., ed., Handbook of Mixing. Schopfheim: EKATO Ruhr- und Mischtechnic GmbH.

Miner, R., Upton, B. 2002. Methods for Estimating Greenhouse Gas Emissions from Lime Kilns at Kraft Pulp Mills. *Energy*, 27, pp. 729-738.

Muzzio, F.J., Alexander, A., *et al.* 2004. Solids Mixing in Paul, E.L., Atiemo-Obeng, V.A., Kresta, S.M., (Eds.). Handbook of Industrial Mixing – Science and Practice. New Jersey: John Wiley & Sons Inc.

Nyström, L.H.E. 1978. On the Steady and Disturbed Flow of Material through Rotary Kilns. PhD Dissertation, Turku: Åbo Akademi.

Perry, R.H., Green, D. 1984. Chemical Engineering Handbook. 6th ed. New York: McGraw-Hill.

Porter, H.F., Schurr, G.A., *et al.* 1973. Solids Drying and Gas-Solid Systems, in Perry, RH., ed., Perry's Chemical Engineers' Handbook, 6th ed. New York: McGraw-Hill Book Co.

Senegacnik, A., Oman, J., *et al*. 2008. Annular Shaft Kiln for Lime Burning with Kiln Gas Recirculation. *Applied Thermal Engineering*, 28, pp. 785-792.

Schulze D. 2008. Powders and Bulk Solids. Berlin: Springer-Verlag.

Seppälä, M.J., Klemetti, U., *et al*. 2001. Paperimassan Valmistus. 2nd ed. Saarijärvi: Opetushallitus.

Shamlou, P.A. 1988. Handling of Bulk Solids – Theory and Practice, Tiptree: Butterworth & CO.

Sunnergren, C.E., Simms, J.K., *et al.* 1979. Mixer Block for Use in Rotary Drums. U.S. Patent No. 4136965, January 30.

The McIlvaine Company. 2014. [Online document]. [Accessed 12 February 2014]. Available at http://www.mcilvainecompany.com/lime/subscriber/mfg%20proc/mfg%20process.htm.

Vakkilainen, E. 1999. Chemical Recovery, in Gullichsen, J., Fogelholm, C-J., Papermaking Science and Technology. Book 6, A Chemical Pulping. Helsinki: Fapet Oy

Venäläinen, Nina. 2014, Andritz Oy, Oral information.

Yin, H., Zhang, M., *et al*. 2014. Numerical Simulation of Three-dimensional Unsteady Granular Flows in Rotary Kiln. *Powder Technology*, 253, pp. 138-145.

The Rotation Speed

To scale down the rotation speed of the pilot-scale rotating drum from industrial drum speeds it was noted that the rotation speed slows down when diameter of the kiln grows up as shown in Figure 63. Rotation speed 2 rpm was linearly extrapolated for diameter 0.3 m based on the data from industrial rotary drums (See Table 1).

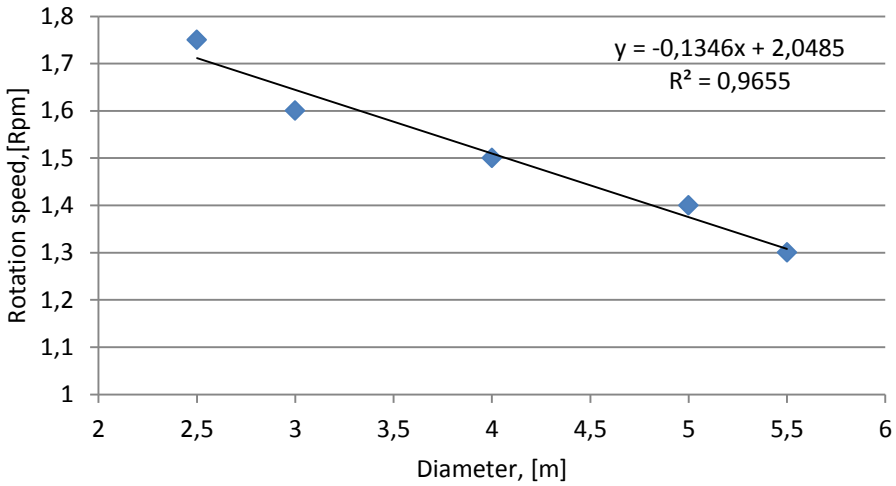

Figure 63 Rotation speed at different drum diameters (Venäläinen, 2014).

Rotational speed was also calculated according to Froude Number (Eq. 20). At first rotational speed 5 rpm was determined for pilot scale drum based on equal Froude numbers from industrial drums. However, based on the experiments the rotational speed was adjusted to 4 rpm.

The Linearized Volumetric Flow Rate

To scale down the linearized volumetric flow rate of the pilot-scale rotating drum from industrial drum rates the TIP speeds were determined. With TIP speeds the linearized flow rates for pilot scale drum with rotational speeds 2 rpm and 4 rpm were determined. Results are shown in Table 30.

Table 30 Linearized flow rates for pilot scale drum with rotational speeds 2 rpm and 4 rpm. Residence time of industrial lime kiln was 2.7 h.

Lime kiln	Diameter, m	Length, m	n, rpm	TIPS, m/s	V, m/s
Industrial	3.0	80.00	1.6	0.25	0.0082
Pilot 1	0.3	1.15	2.0	0.03	0.0011
Pilot 2	0.3	1.15	4.0	0.06	0.0022

However, the slope of the drum needs to be taken into account. With the linearized flow rate 0.0011 m/s the flow rate at the beginning of the lifter network is 0.0026 m/s and at the end of the lifter network 0.0010 m/s. The average flow rate at the lifter network is 0.0018 m/s. With the linearized flow rate 0.0022 m/s the average flow rate at the lifter network is 0.0038 m/s. However, it was decided that to simplify the measurements the linearized flow rate was used in the measurements. As a result of scale up the linearized flow rate 0.0011 m/s was chosen for measurements with rotational speed 2 rpm. With rotational speed 4 rpm the linearized flow rate 0.0022 m/s was used.

Results of the rotameter calibration for water measurements are presented in Figure 64.

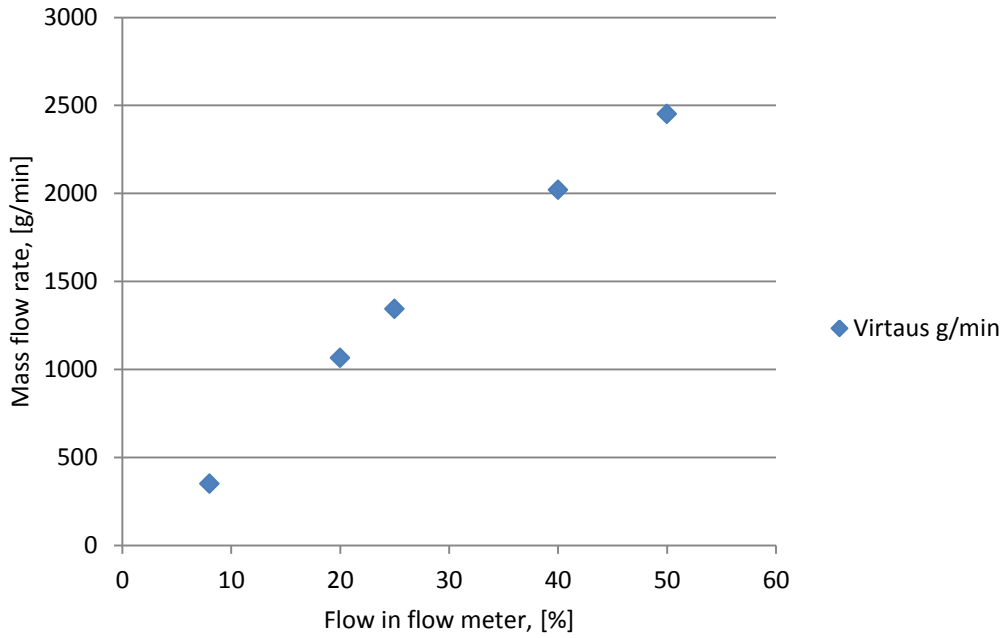

Figure 64 Calibration results for the rotameter in water measurements.

Rheology of Lime Mud

The temperature in the lime kiln's lifter network varies from 300 °C to 500 °C. Due to the high operating temperature the lime mud is replaced in measurements by the substance with the same viscous properties in lower temperatures.

The rheology of lime mud dust was analyzed using Anton Paar's modular compact rheometer 302. Cup from standard measuring system CC27/T200/AL was used with stirrer ST24-2D/2V/2V-30/109. Electrically heated temperature device with temperature range from 0 °C to 300 °C was used in measurements. The wanted rheology level at temperatures from 300 °C to 500 °C was analyzed with the results from these measurements.

The rheology studies were carried out at temperatures 75 °C, 100 °C, 125 °C, 150 °C, 175 °C, 200°C, 250 °C and 300 °C. The lime mud was first dried in the oven over the night. At the beginning of the measurement the temperature of the device was set to wanted temperature and the device was heated for 20 minutes before starting the measurements to raise the temperature of the lime mud to wanted level. The shear rate region used was from 2.14 1/s to 100 1/s. Rheology data from measurements is shown in Table 31.

Table 31 Rheology data from measurements at temperatures 75 °C, 100 °C, 125 °C, 150 °C, 175 °C, 200°C, 250 °C and 300 °C.

	Temperature, °C							
Shear rate, 1/s	75 °C	100 °C	125 °C	150 °C	175 °C	200 °C	250 °C	300 °C
	Viscosity, mPas							
2.14	234000	185000	182000	164000	66400	64300	65600	66700
4.18	115000	97700	90000	80800	36600	35700	34700	28500
6.22	74900	66700	58200	54700	39300	26700	24400	17400
8.25	57000	48300	43800	40200	28500	33400	17600	11700
10.30	45900	38500	35800	31600	22500	23900	13300	33400
12.30	36900	31900	29700	25700	18000	19200	14700	28600
14.40	31700	26900	24600	21500	17700	15500	5830	22300
16.40	27500	22600	22600	20100	15600	12600	6480	21400
18.40	24600	20800	19500	17900	14800	10800	8420	15700
20.50	21900	18700	17100	15800	11900	9710	10400	14000
22.50	19500	16700	15500	13300	12400	8900	10300	10900
24.60	17700	15800	14600	12700	10900	8790	7620	8950
26.60	16300	14100	13000	12400	9170	8100	7760	7850
28.60	15000	13100	12000	10900	9030	7370	7300	8180
30.70	13900	12100	11500	10400	8640	6530	7650	6540
32.70	13200	10900	10500	9400	8040	5860	6730	6290
34.80	12200	10400	9910	8810	9120	5610	5960	5370
36.80	11400	9840	9940	8410	8070	5550	6190	5420
38.80	10600	8870	9320	8130	7080	5380	6760	5390
40.90	9970	8600	8790	7600	7320	5500	5480	4950
42.90	9730	8200	8170	7240	6870	5220	4820	4380
45.00	9750	7950	8210	6980	6480	4850	5640	4300
47.00	9110	7350	7950	6910	5620	5310	4830	4180
49.00	8540	7340	7490	6550	5090	4790	5090	3300
51.10	8060	7260	6980	5880	5130	4610	4410	3020
53.10	7820	6890	6670	6040	4900	3710	4480	3150
55.10	7550	6680	6300	5770	5230	3870	4160	2710
57.20	7040	6170	6130	5440	5590	4160	4480	2140

59.20	6750	6170	5480	5530	4930	3700	4360	2580
61.30	6690	5790	5360	5050	4470	3100	4170	2580
63.30	6620	5840	5130	4850	3900	2920	3860	2150
65.30	6370	5710	5040	4820	3860	3420	3740	2990
67.40	6180	5400	4800	4730	3930	2990	4050	3030
69.40	6010	5180	4670	4550	3560	2870	3710	3150
71.50	6010	5310	4580	4360	3410	2850	3420	3050
73.50	5710	5240	4380	4250	3240	2640	3130	2480
75.50	5610	4930	4430	4440	3700	2380	3170	2710
77.60	5280	4760	4300	4510	3340	2130	3380	2750
79.60	5060	4710	4140	3960	3160	2330	2930	2540
81.70	4920	4590	3880	3870	3160	2240	2770	2160
83.70	4930	4400	3980	3940	2960	2250	2720	2340
85.70	4890	4470	3790	3830	2810	2180	2790	2380
87.80	4930	4340	3680	3850	2760	1980	3080	2030
89.80	4760	4130	3680	3560	3240	2050	2520	2230
91.80	4570	4090	3590	3470	2960	1880	2460	1920
93.90	4370	4030	3550	3490	3000	2080	2610	2390
95.90	4410	3960	3430	3460	3010	2370	2480	2610
98.00	4300	3830	3350	3300	2940	2460	2360	2880
100.00	4140	3690	3320	3340	2780	2100	2330	3320

Viscosity curves for lime mud at different temperatures are shown in Figure 65.

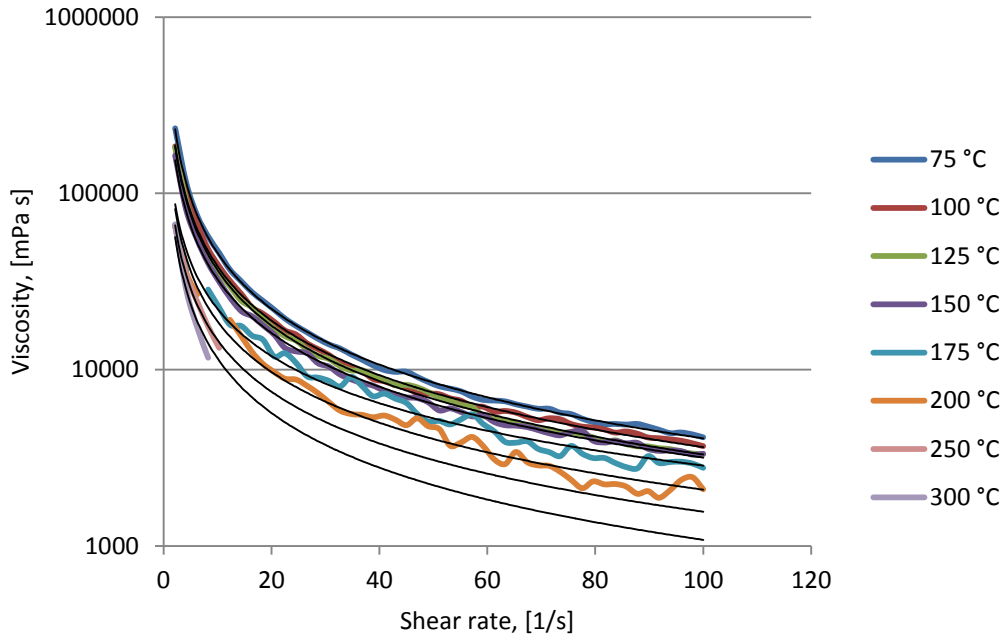

Figure 65 Viscosity curves for lime mud at different temperatures.

The viscosity curves for lime mud at temperatures 400 °C and 500 °C were extrapolated based on the angular coefficient data from rheology studies. The results are presented in Figure 66.

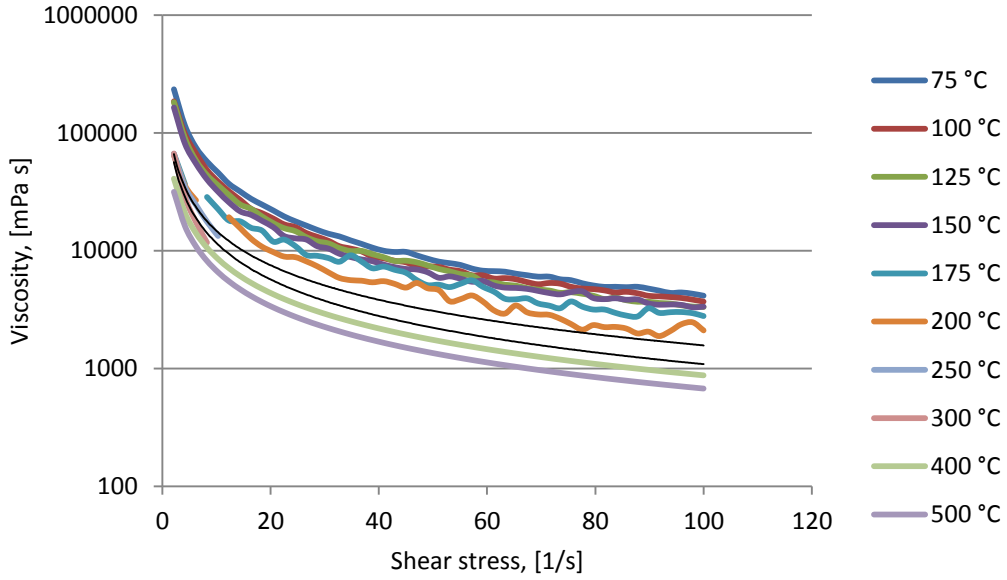

Figure 66 Results to predict the viscosity curves for lime mud at temperatures 400 °C and 500 °C.

Simulant Materials

Sodium carboxymethylcellulose (CMC) was chosen as a simulant material. CMC solutions are especially useful for performing mixing experiments because they are inexpensive and the viscosity is relatively intensive to small changes in temperature and dilution.

For rheology studies different CMC solutions were studied. To find optimal simulant material with same rheological properties as lime mud three high viscosity products were dissolved to different mass concentrations. The chosen products were Finnfix 50 000, Finnfix 30 and Cekol 30 000.

In these measurements the bob from standard measuring system CC27/T200/AL was used instead of stirrer ST24-2D/2V/2V-30/109. The shear rate region was from 2.14 1/s to 100 1/s. Viscosity curves with different CMC solutions and concentrations are shown in Figure 67.

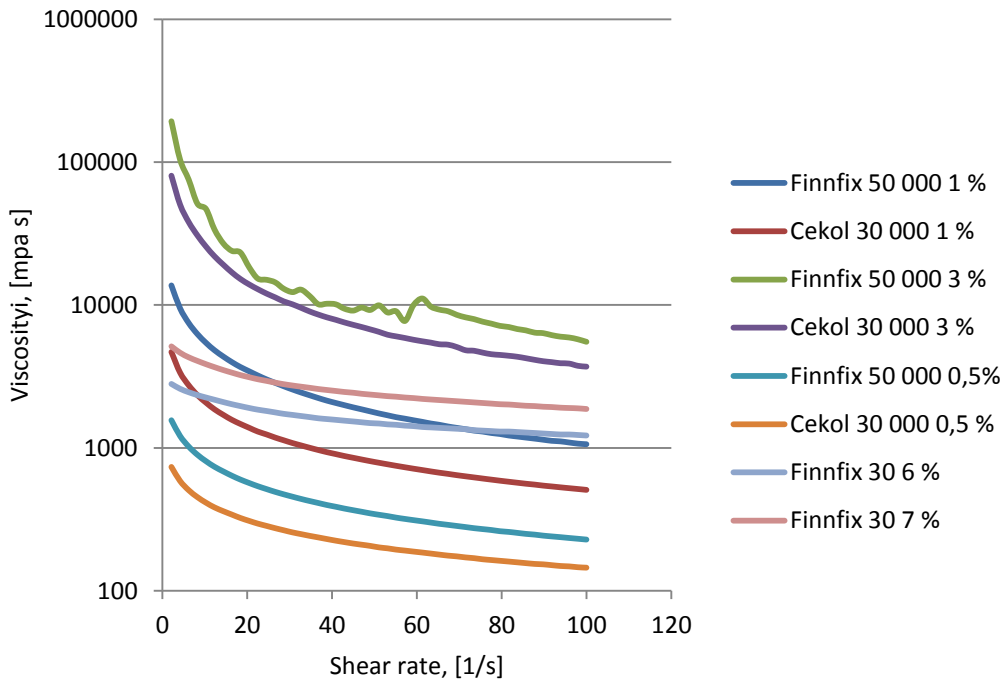

Figure 67 Viscosity curves with different CMC solutions and concentrations.

These results were compared to rheology studies made with lime mud (see Figure 66) to find similar viscosity curves. Results for similar viscosity curves in wanted temperature region from 300 °C to 500 °C are presented in Figure 68.

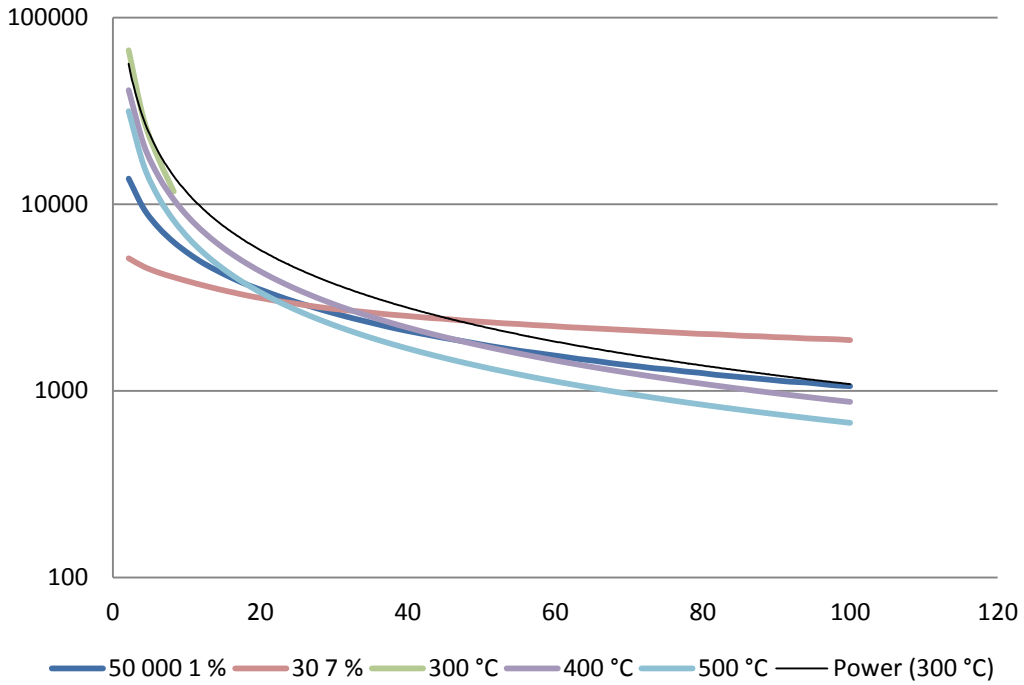

Figure 68 Similar viscosity curves in wanted temperature region from 300 °C to 500 °C.

As a result Finnfix 50 000 with mass concentration 1 % and Finnfix 30 with mass concentration 7 % were chosen for closer comparison. It was noted that it is much easier to achieve a batch of 90 kg with wanted concentration with Finnfix 50 000 concentration of 1 by mass than with Finnfix 30 concentration of 7 by mass. There were some difficulties to dissolve the Finnfix 30 to wanted viscosity level. Also the Finnfix 30 was much challenging as material due to its sticky nature. The biggest advance of Finnfix 50 000 was the amount of required powder. As a result the Finnfix 50 000 with mass concentration 1 % was chosen as a high viscous material.

The contamination of CMC was followed for couple of days to study if there are any changes in viscosity. Also the viscosity of more acid type CMC was tested. Typically the pH of CMC solutions is from 6–8. It was known that when the pH drops under the 3 the viscosity decreases. Viscosity also decreases when pH increases above 9. PH of CMC was dropped from 7 to 4 and it was noted that there is not major difference in viscosity curves. Also when the viscosity of pure CMC was followed for a week it was noted that there are not major differences in viscosity curves.

Table 32 Process parameters used with different lifter designs in water acid experiments.

	Process parameter		
Lifter design	**2 rpm 0.001 m/s**	**4 rpm 0.001 m/s**	**4 rpm 0.002 m/s**
No lifters	x	x	x
Straight 2 lifters	x	x	x
Straight 4 lifters	x	x	x
Straight 4 lifters overlapping	x		
Straight 8 lifters	x	x	x
Straight 3 Circumferences	x		
Lifter 7	x		
Lifter 8	x		
Lifter 9	x	x	
Lifter 10	x		
Lifter 11	x		
Lifter 12	x	x	
Lifter 13	x	x	x
Lifter 14	x	x	
Lifter 15	x		
Lifter 16	x	x	
Lifter 17	x	x	
Lifter 18	x		
Lifter 19	x		
Lifter 20	x		
Lifter 21	x		
Lifter 22	x		
Lifter 23	x		

Table 33 Process parameters used with different lifter designs in water machine vision experiments.

Lifter design	**Process parameter**
No lifters	2 rpm; 0.001 m/s
Straight 4 lifters	2 rpm; 0.001 m/s
Straight 4 lifters overlapping	2 rpm; 0.001 m/s
Straight 8 lifters	2 rpm; 0.001 m/s
Lifter 7	2 rpm; 0.001 m/s
Lifter 8	2 rpm; 0.001 m/s
Lifter 9	2 rpm; 0.001 m/s
Lifter 10	2 rpm; 0.001 m/s
Lifter 11	2 rpm; 0.001 m/s
Lifter 12	2 rpm; 0.001 m/s
Lifter 14	2 rpm; 0.001 m/s
Lifter 15	2 rpm; 0.001 m/s
Lifter 16	2 rpm; 0.001 m/s
Lifter 17	2 rpm; 0.001 m/s
Lifter 20	2 rpm; 0.001 m/s
Lifter 21	2 rpm; 0.001 m/s
Lifter 22	2 rpm; 0.001 m/s
Lifter 23	2 rpm; 0.001 m/s
Lifter 24	2 rpm; 0.001 m/s
Lifter 25	2 rpm; 0.001 m/s
No lifters	4 rpm; 0.001 m/s
No lifters	4 rpm; 0.002 m/s
Lifter 12	4 rpm; 0.001 m/s

Table 34 Process parameters used with different lifter designs in CMC machine vision experiments.

Lifter design	**Process parameter**
No lifters	2 rpm; 0.001 m/s
Straight 2 lifters	2 rpm; 0.001 m/s
Straight 4 lifters	2 rpm; 0.001 m/s
Straight 4 lifters overlapping	2 rpm; 0.001 m/s
Straight 8 lifters 1	2 rpm; 0.001 m/s
Straight 8 lifters 2	2 rpm; 0.001 m/s
Lifter 7	2 rpm; 0.001 m/s
Lifter 8	2 rpm; 0.001 m/s
Lifter 9	2 rpm; 0.001 m/s
Lifter 10	2 rpm; 0.001 m/s
Lifter 11	2 rpm; 0.001 m/s
Lifter 12	2 rpm; 0.001 m/s
Lifter 13	2 rpm; 0.001 m/s
Lifter 14	2 rpm; 0.001 m/s
Lifter 15	2 rpm; 0.001 m/s
Lifter 16	2 rpm; 0.001 m/s
Lifter 17	2 rpm; 0.001 m/s
Lifter 18	2 rpm; 0.001 m/s
Lifter 19	2 rpm; 0.001 m/s
Lifter 20	2 rpm; 0.001 m/s
Lifter 21	2 rpm; 0.001 m/s
Lifter 22	2 rpm; 0.001 m/s
Lifter 23	2 rpm; 0.001 m/s
Lifter 24	2 rpm; 0.001 m/s
Lifter 25	2 rpm; 0.001 m/s
No lifters	4 rpm; 0.001 m/s
No lifters	4 rpm; 0.002 m/s
Modified lifters	
Straight 4 lifters	2 rpm; 0.001 m/s
Straight 4 lifters overlapping	2 rpm; 0.001 m/s
Straight 8 lifters	2 rpm; 0.001 m/s
Lifter 20	2 rpm; 0.001 m/s
Lifter 21	2 rpm; 0.001 m/s
Lifter 22	2 rpm; 0.001 m/s
Lifter 23	2 rpm; 0.001 m/s
Lifter 24	2 rpm; 0.001 m/s
Lifter 25	2 rpm; 0.001 m/s

Table 35 CoV results based on acid experiments and saturation values using different lifter structures

	CoV	
Lifter structure	**Acid test**	**Saturation**
No lifters 2 rpm 0.001 m/s	1.54	0.676
Straight 4 lifters	1.35	0.603
Straight 4 lifters overlapped	1.25	0.592
Straight 8 lifters	1.23	0.549
Lifter 7	1.27	0.503
Lifter 8	1.32	0.487
Lifter 9	1.29	0.513
Lifter 10	1.21	0.513
Lifter 11	1.25	0.527
Lifter 12	1.18	0.442
Lifter 14	1.29	0.601
Lifter 15	1.23	0.491
Lifter 16	1.33	0.485
Lifter 17	1.29	0.547
Lifter 20	1.25	0.528
Lifter 21	1.28	0.560
Lifter 22	1.34	0.638
Lifter 23	1.30	0.541
Lifter 24	-	0.568
Lifter 25	-	0.540
Lifter 12 4 rpm 0.001 m/s	1.11	0.428
No lifters 4 rpm 0.001 m/s	1.37	0.606
No lifters 4 rpm 0.002 m/s	2.50	1.407

Curve fitting shown in Figure 69 indicates that there is a dependency between results from acid and saturation experiments.

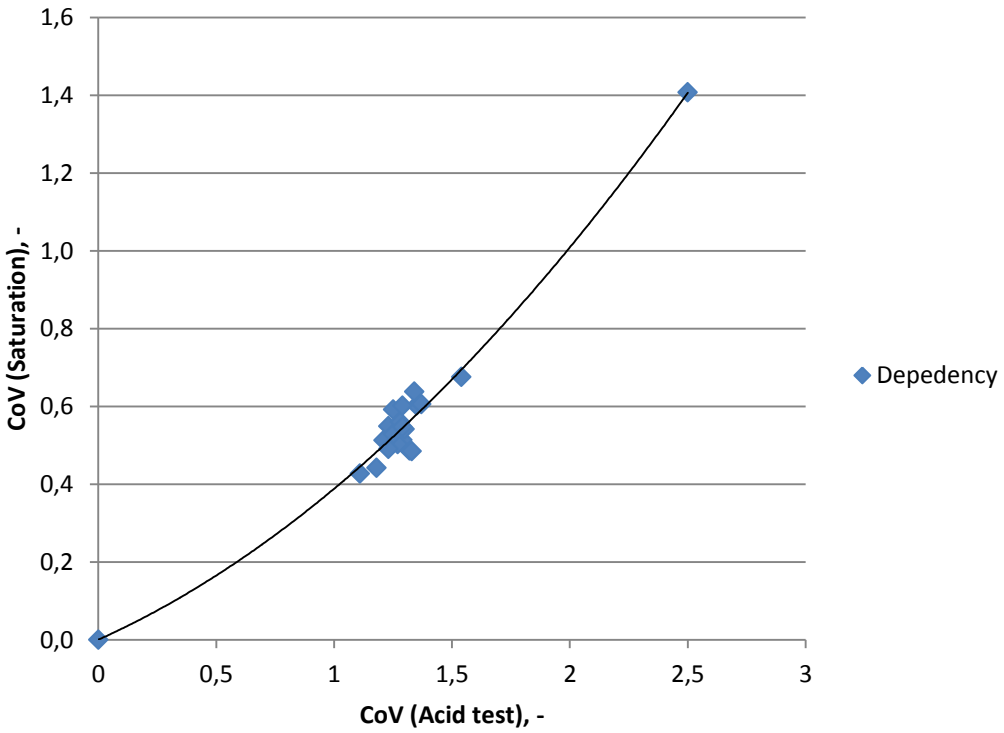

Figure 69 Dependency between the results from acid and saturation measurements. X-axis shows the CoV number based on acid experiments and y-axis the corresponding number based on saturation measurements.

Based on CoV values from acid experiments and machine vision different lifter structures can be ranked. Results are shown in Table 36.

Table 36 Lifter structure rankings based on CoV values from acid experiments and machine vision experiments.

Rank	Lifter structure
1	Lifter 12 4 rpm 0.001 m/s
2	Lifter 12
3	Lifter 15
4	Lifter 10
5	Lifter 11
6	Lifter 7
7	Straight 8 lifters
8	Lifter 20
9	Lifter 9
10	Lifter 8
11	Lifter 16
12	Straight 4 lifters overlapped
13	Lifter 17
14	Lifter 21
15	Lifter 14
16	Lifter 23
17	Straight 4 lifters
18	Lifter 22
19	No lifters 4 rpm 0.001 m/s
20	No lifters 2 rpm 0.001 m/s
21	No lifters 4 rpm 0.002 m/s

Coefficient of Variation

CoV number was calculated according to Equation 2. It was used to examine the mixing with HNO_3 acid in water and CMC experiments. CoV number was also used in machine vision analyses. Basic idea of CoV number is that when CoV number decreases the mixing improves.

In statistics and probability theory, the CoV is a normalized measure of dispersion of frequency distribution or a probability distribution. This has a benefit when analyzing the results, because of the small differences in concentration of the acid impulse does not matter. This is proven in Figure 70 and in Table 37. There is a same amount (150 ml) of HNO_3 but in different concentrations. From figure it is noted that the spreading is a little bit wider with lower pH value but as it can be seen from Table 37 the CoV number is almost the same.

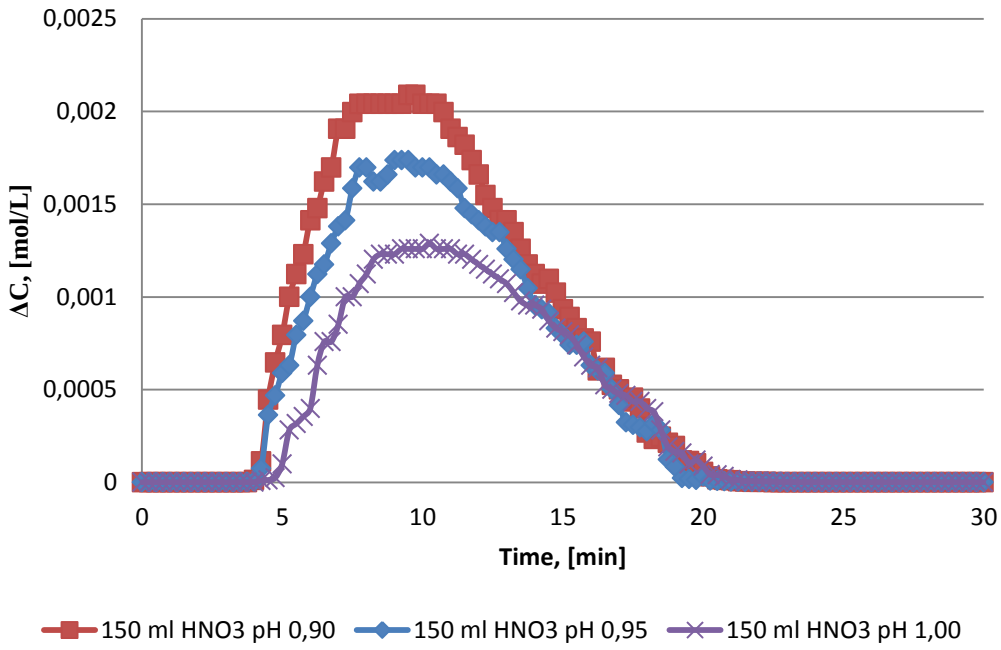

Figure 70 Concentration curves with different concentration impulses of 150 ml HNO3.

Table 37 CoV value with same amount of HNO_3 (150 ml) but with different concentrations.

pH, -	0.90	0.95	1.00
CoV value, -	1.23	1.24	1.20

Dispersion Coefficient

Dispersion coefficient or the dimensionless $\frac{D}{uL}$ was calculated according to Equation 13. It was used to examine the mixing with HNO_3 acid in water experiments. For high viscous CMC experiments this model is not suitable because of for high viscous fluids it is assumed that each element of fluid slides past its neighbor with no interaction by molecular diffusion. Due to this the spread in residence times is caused only by the velocity variations. Basic idea of dimensionless $\frac{D}{uL}$ number is that when $\frac{D}{uL}$ number increases the mixing improves. (Levenspiel, 1999.)

In case of dimensionless $\frac{D}{uL}$ the same effect in small differences in concentration of the acid impulse is noted comparing to CoV number. However, it is noted that there is a bigger and also linear difference between pH values 0.90 and 1.00. Due to this it is seen that there might be more errors with results in case of $\frac{D}{uL}$ comparing to CoV. Dimensionless $\frac{D}{uL}$ with different pH values are shown at Table 38.

Table 38 Dimensionless $\frac{D}{uL}$ with same amount of HNO_3 (150 ml) but in different concentrations.

pH, -	0.90	0.95	1.00
Dispersion coefficient, -	0.053	0.049	0.044

Video Analysis

Video material was analyzed by Machine Vision and Pattern Recognition laboratory in Lappeenranta University of Technology. Matlab was used to analyze the mixing results and to calculate the CoV value. The analyzation area was limited manually according to figure 71. The area from every video frame was scaled to one pixel row and rows from all frames were stacked to one image. The image was converted to HSV color space and the CoV value was calculated for each cell based on the saturation value.

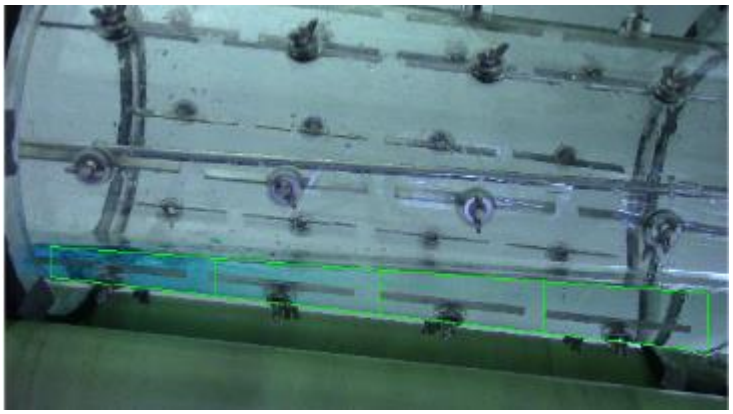

Figure 71 The whole simulation area and each calculation cells in which areas the CoV numbers were calculated.

Species Transport Equation

Diffusion effecting on mixing in water HNO_3 experiments was studied with Equation 7. As a result it was noted that diffusion coefficients in this case are relatively low and do not have effect on mixing. Diffusion coefficients are typically approximately $1 \cdot 10^{-5}$ cm^2/s (Cussler, 2009). So according to Equation 7 mixing occurs only due to convection. Comparing was made to water acid experiments shown in figure 70. Similarity is seen between concentration curves and when changing the diffusion coefficient between $1 \cdot 10^{-4}$ m^2/s and $1 \cdot 10^{-9}$ m^2/s the change in curve's shape is relatively low. Results are shown in figure 72.

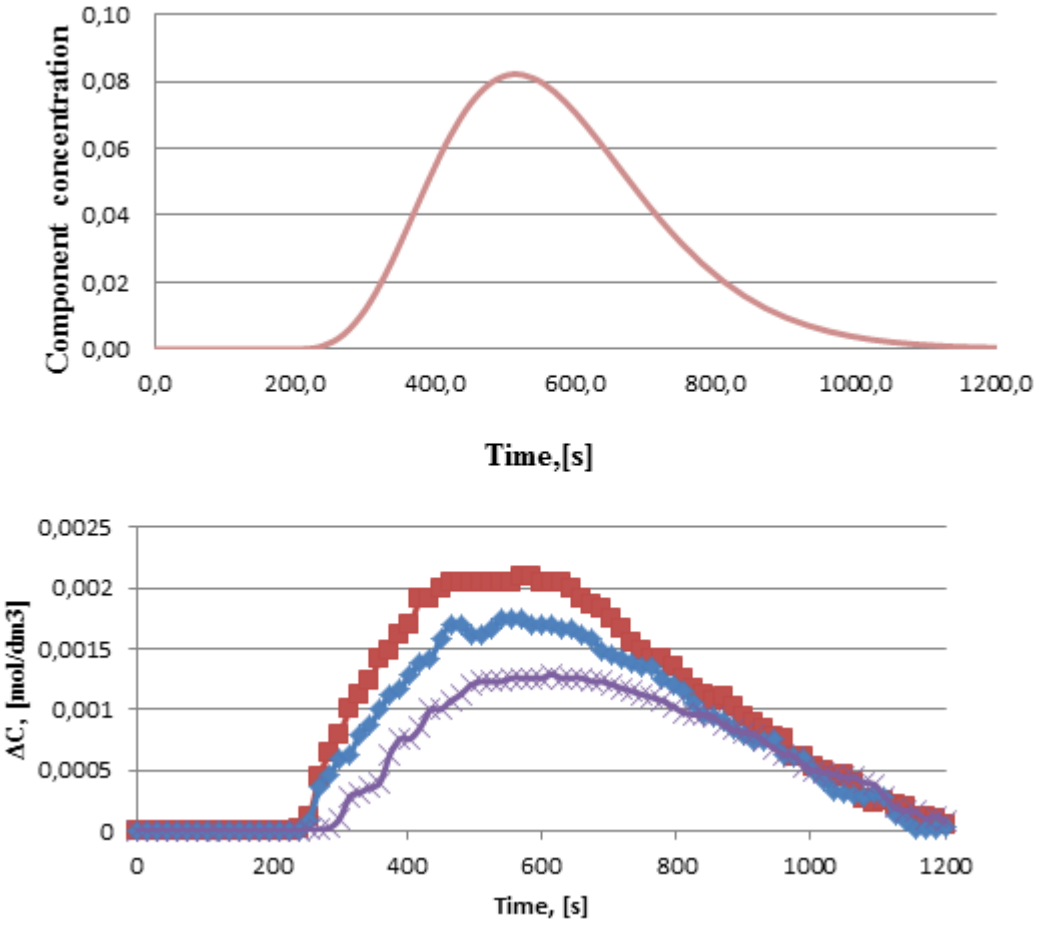

Figure 72 Diffusion effecting on mixing in water HNO_3 experiments. The curve in upper figure is calculated based on equation 7 and the lower figure is from water acid experiments.

Also according the Stokes Einstein (Eq. 8) it can be stated that diffusion coefficient has remained constant because of temperature, solute radius and viscosity have remain same in all repetition experiments with same material.

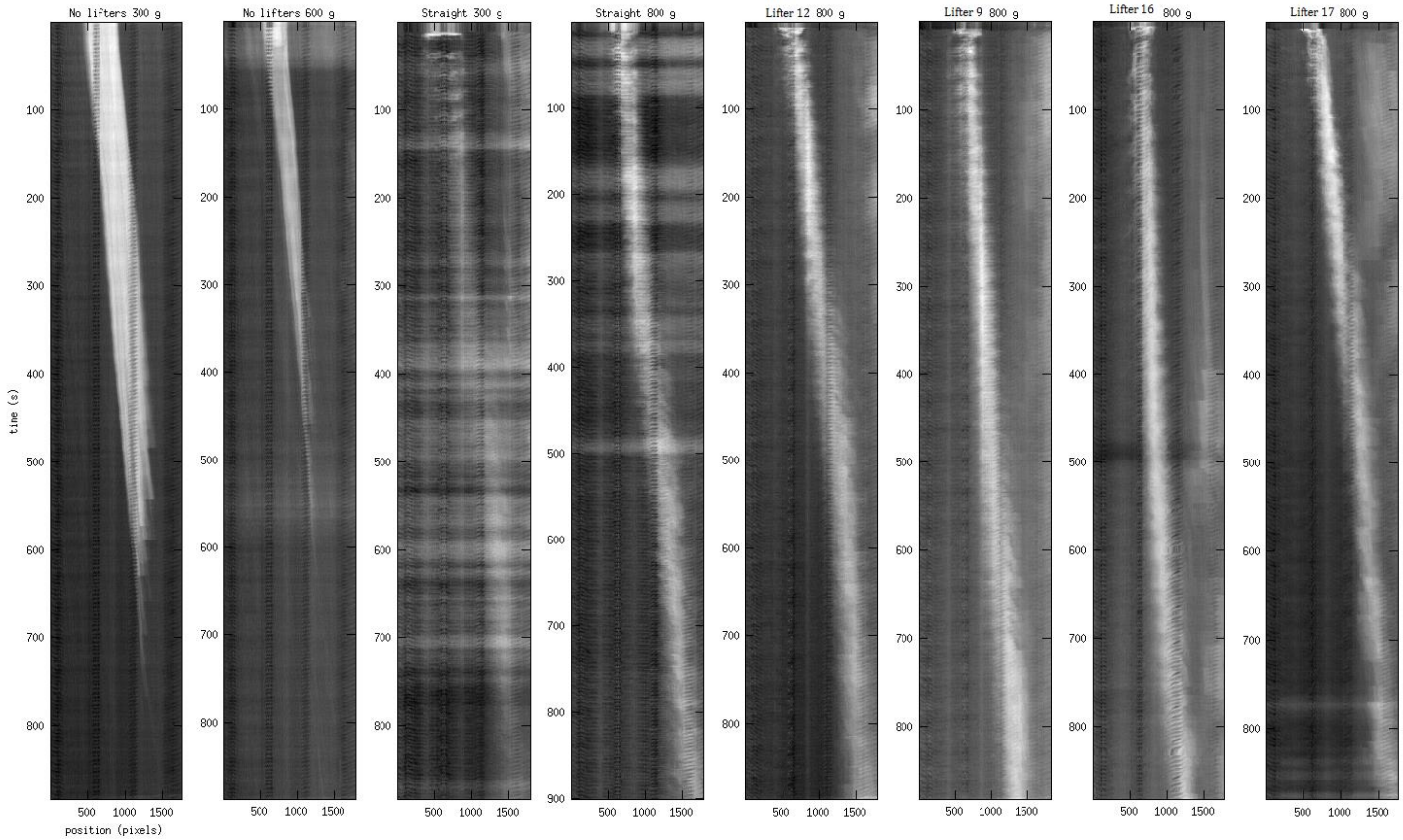

Figure 73 Residence time results for solid experiments. Experiment time was 15 minutes.

No lifters – 2 rpm 0.001 m/s

Time [min]	pH	Time [min]	pH	Time [min]	pH
0	7,50	10	2,61	20	5,90
0,25	7,50	10,25	2,61	20,25	5,92
0,5	7,50	10,5	2,61	20,5	6,00
0,75	7,50	10,75	2,62	20,75	6,05
1	7,50	11	2,62	21	6,15
1,25	7,50	11,25	2,63	21,25	6,20
1,5	7,50	11,5	2,63	21,5	6,25
1,75	7,50	11,75	2,63	21,75	6,29
2	7,50	12	2,64	22	6,32
2,25	7,50	12,25	2,65	22,25	6,35
2,5	7,50	12,5	2,68	22,5	6,38
2,75	7,45	12,75	2,70	22,75	6,40
3	7,20	13	2,74	23	6,42
3,25	7,10	13,25	2,77	23,25	6,42
3,5	7,05	13,5	2,82	23,5	6,44
3,75	7,00	13,75	2,85	23,75	6,46
4	6,92	14	2,88	24	6,48
4,25	6,80	14,25	2,92	24,25	6,51
4,5	6,74	14,5	2,94	24,5	6,53
4,75	6,62	14,75	2,96	24,75	6,57
5	6,53	15	3,03	25	6,58
5,25	6,11	15,25	3,13	25,25	6,60
5,5	4,91	15,5	3,21	25,5	6,63
5,75	4,07	15,75	3,20	25,75	6,65
6	3,42	16	3,30	26	6,69
6,25	3,31	16,25	3,63	26,25	6,70
6,5	3,14	16,5	3,60	26,5	6,73
6,75	3,10	16,75	3,86	26,75	6,75
7	2,97	17	4,30	27	6,76
7,25	2,87	17,25	4,30	27,25	6,78
7,5	2,85	17,5	4,20	27,5	6,80
7,75	2,83	17,75	4,42	27,75	6,82
8	2,76	18	4,43	28	6,83
8,25	2,74	18,25	4,70	28,25	6,85
8,5	2,71	18,5	4,91	28,5	6,87
8,75	2,71	18,75	5,30	28,75	6,89
9	2,66	19	5,50	29	6,90
9,25	2,64	19,25	5,62	29,25	6,92
9,5	2,63	19,5	5,67	29,5	6,95
9,75	2,62	19,75	5,76	29,75	6,95
				30	6,96

No lifters – 4 rpm 0.001 m/s

Time [min]	pH	Time [min]	pH	Time [min]	pH
0	7,50	10	2,76	20	4,60
0,25	7,50	10,25	2,75	20,25	4,85
0,5	7,50	10,5	2,79	20,5	5,08
0,75	7,50	10,75	2,79	20,75	5,11
1	7,50	11	2,78	21	5,22
1,25	7,50	11,25	2,78	21,25	5,30
1,5	7,50	11,5	2,79	21,5	5,32
1,75	7,50	11,75	2,80	21,75	5,40
2	7,50	12	2,81	22	5,45
2,25	7,50	12,25	2,81	22,25	5,60
2,5	7,50	12,5	2,82	22,5	5,71
2,75	7,50	12,75	2,86	22,75	5,79
3	7,50	13	2,87	23	5,78
3,25	7,48	13,25	2,88	23,25	5,81
3,5	7,47	13,5	2,89	23,5	5,86
3,75	7,45	13,75	2,90	23,75	5,93
4	7,41	14	2,92	24	5,99
4,25	7,32	14,25	2,95	24,25	6,05
4,5	7,20	14,5	2,98	24,5	6,07
4,75	7,01	14,75	3,01	24,75	6,12
5	6,49	15	3,04	25	6,16
5,25	5,00	15,25	3,05	25,25	6,18
5,5	4,14	15,5	3,10	25,5	6,20
5,75	4,02	15,75	3,11	25,75	6,22
6	3,38	16	3,15	26	6,25
6,25	3,50	16,25	3,21	26,25	6,30
6,5	3,30	16,5	3,34	26,5	6,30
6,75	3,08	16,75	3,35	26,75	6,31
7	3,05	17	3,36	27	6,33
7,25	2,99	17,25	3,41	27,25	6,36
7,5	2,93	17,5	3,36	27,5	6,39
7,75	2,93	17,75	3,65	27,75	6,43
8	2,87	18	3,62	28	6,46
8,25	2,84	18,25	3,64	28,25	6,47
8,5	2,80	18,5	3,72	28,5	6,48
8,75	2,78	18,75	4,07	28,75	6,50
9	2,78	19	4,20	29	6,52
9,25	2,77	19,25	4,43	29,25	6,54
9,5	2,77	19,5	4,20	29,5	6,56
9,75	2,76	19,75	4,33	29,75	6,57
				30	6,58

No lifters – 4 rpm 0.002 m/s

Time [min]	pH	Time [min]	pH	Time [min]	pH
0	7,50	10	5,90	20	7,21
0,25	7,50	10,25	6,02	20,25	7,22
0,5	7,50	10,5	6,09	20,5	7,23
0,75	7,50	10,75	6,15	20,75	7,24
1	7,50	11	6,22	21	7,24
1,25	7,50	11,25	6,30	21,25	7,25
1,5	7,50	11,5	6,37	21,5	7,25
1,75	7,50	11,75	6,43	21,75	7,26
2	7,50	12	6,48	22	7,27
2,25	7,47	12,25	6,51	22,25	7,27
2,5	6,50	12,5	6,55	22,5	7,28
2,75	5,10	12,75	6,60	22,75	7,28
3	4,45	13	6,66	23	7,28
3,25	3,40	13,25	6,70	23,25	7,29
3,5	3,05	13,5	6,73	23,5	7,29
3,75	2,86	13,75	6,78	23,75	7,30
4	2,78	14	6,80	24	7,30
4,25	2,70	14,25	6,84	24,25	7,31
4,5	2,58	14,5	6,88	24,5	7,31
4,75	2,54	14,75	6,90	24,75	7,31
5	2,52	15	6,91	25	7,31
5,25	2,52	15,25	6,94	25,25	7,32
5,5	2,52	15,5	6,96	25,5	7,32
5,75	2,53	15,75	6,98	25,75	7,33
6	2,54	16	7,00	26	7,33
6,25	2,55	16,25	7,02	26,25	7,33
6,5	2,65	16,5	7,04	26,5	7,33
6,75	2,70	16,75	7,06	26,75	7,33
7	2,75	17	7,08	27	7,34
7,25	2,86	17,25	7,10	27,25	7,34
7,5	3,00	17,5	7,11	27,5	7,34
7,75	3,30	17,75	7,12	27,75	7,34
8	3,60	18	7,13	28	7,35
8,25	3,59	18,25	7,14	28,25	7,35
8,5	3,60	18,5	7,15	28,5	7,35
8,75	4,15	18,75	7,17	28,75	7,36
9	4,75	19	7,18	29	7,36
9,25	5,30	19,25	7,19	29,25	7,36
9,5	5,55	19,5	7,20	29,5	7,36
9,75	5,80	19,75	7,20	29,75	7,36
				30	7,36

4 straight lifters – 2 rpm 0.001 m/s

Time [min]	pH	Time [min]	pH	Time [min]	pH
0	7,50	10	2,77	20	5,09
0,25	7,50	10,25	2,78	20,25	5,35
0,5	7,50	10,5	2,79	20,5	5,50
0,75	7,50	10,75	2,78	20,75	5,60
1	7,50	11	2,79	21	5,72
1,25	7,50	11,25	2,79	21,25	5,80
1,5	7,50	11,5	2,80	21,5	5,87
1,75	7,50	11,75	2,81	21,75	5,91
2	7,50	12	2,82	22	5,97
2,25	7,50	12,25	2,83	22,25	6,00
2,5	7,49	12,5	2,84	22,5	6,05
2,75	7,48	12,75	2,85	22,75	6,08
3	7,44	13	2,87	23	6,13
3,25	7,39	13,25	2,90	23,25	6,18
3,5	7,35	13,5	2,92	23,5	6,23
3,75	7,25	13,75	2,95	23,75	6,26
4	7,08	14	3,00	24	6,28
4,25	6,70	14,25	3,01	24,25	6,31
4,5	5,92	14,5	3,03	24,5	6,35
4,75	5,20	14,75	3,03	24,75	6,38
5	4,40	15	3,11	25	6,40
5,25	3,83	15,25	3,17	25,25	6,42
5,5	3,45	15,5	3,19	25,5	6,44
5,75	3,46	15,75	3,19	25,75	6,46
6	3,35	16	3,24	26	6,50
6,25	3,15	16,25	3,30	26,25	6,53
6,5	3,02	16,5	3,29	26,5	6,55
6,75	2,93	16,75	3,35	26,75	6,58
7	2,92	17	3,44	27	6,60
7,25	2,90	17,25	3,44	27,25	6,63
7,5	2,86	17,5	3,65	27,5	6,65
7,75	2,84	17,75	3,67	27,75	6,67
8	2,81	18	3,80	28	6,69
8,25	2,82	18,25	3,82	28,25	6,70
8,5	2,81	18,5	4,00	28,5	6,71
8,75	2,80	18,75	4,30	28,75	6,71
9	2,80	19	4,60	29	6,72
9,25	2,78	19,25	4,92	29,25	6,73
9,5	2,78	19,5	4,90	29,5	6,74
9,75	2,77	19,75	5,00	29,75	6,75
				30	6,77

4 straight lifters – 4 rpm 0.001 m/s

Time [min]	pH	Time [min]	pH	Time [min]	pH
0	7,50	10	3,01	20	4,25
0,25	7,50	10,25	3,01	20,25	4,40
0,5	7,50	10,5	3,02	20,5	4,50
0,75	7,50	10,75	3,02	20,75	4,71
1	7,50	11	3,03	21	4,89
1,25	7,50	11,25	3,04	21,25	5,04
1,5	7,50	11,5	3,06	21,5	5,16
1,75	7,49	11,75	3,07	21,75	5,19
2	7,46	12	3,07	22	5,30
2,25	7,41	12,25	3,08	22,25	5,44
2,5	7,35	12,5	3,09	22,5	5,53
2,75	7,26	12,75	3,10	22,75	5,57
3	7,13	13	3,13	23	5,62
3,25	6,88	13,25	3,14	23,25	5,65
3,5	6,39	13,5	3,15	23,5	5,72
3,75	5,52	13,75	3,17	23,75	5,76
4	4,86	14	3,19	24	5,80
4,25	3,93	14,25	3,20	24,25	5,85
4,5	3,66	14,5	3,21	24,5	5,89
4,75	3,55	14,75	3,25	24,75	5,95
5	3,43	15	3,27	25	6,00
5,25	3,34	15,25	3,31	25,25	6,03
5,5	3,24	15,5	3,32	25,5	6,06
5,75	3,17	15,75	3,33	25,75	6,10
6	3,16	16	3,34	26	6,12
6,25	3,10	16,25	3,37	26,25	6,14
6,5	3,08	16,5	3,42	26,5	6,17
6,75	3,01	16,75	3,50	26,75	6,20
7	3,01	17	3,49	27	6,22
7,25	2,99	17,25	3,51	27,25	6,24
7,5	3,00	17,5	3,57	27,5	6,26
7,75	2,99	17,75	3,66	27,75	6,29
8	2,99	18	3,67	28	6,31
8,25	2,99	18,25	3,65	28,25	6,33
8,5	2,99	18,5	3,82	28,5	6,35
8,75	2,99	18,75	3,84	28,75	6,37
9	2,99	19	3,87	29	6,39
9,25	3,00	19,25	3,90	29,25	6,42
9,5	3,00	19,5	4,00	29,5	6,44
9,75	3,00	19,75	4,20	29,75	6,47
				30	6,49

4 straight lifters – 4 rpm 0.002 m/s

Time [min]	pH	Time [min]	pH	Time [min]	pH
0	7,50	10	4,56	20	6,90
0,25	7,50	10,25	4,76	20,25	6,92
0,5	7,50	10,5	5,08	20,5	6,93
0,75	7,50	10,75	5,11	20,75	6,95
1	7,50	11	5,20	21	6,96
1,25	7,50	11,25	5,49	21,25	6,98
1,5	7,48	11,5	5,67	21,5	7,00
1,75	7,42	11,75	5,80	21,75	7,01
2	7,15	12	5,90	22	7,02
2,25	6,44	12,25	5,99	22,25	7,03
2,5	5,32	12,5	6,04	22,5	7,04
2,75	4,55	12,75	6,10	22,75	7,05
3	3,62	13	6,14	23	7,06
3,25	3,10	13,25	6,19	23,25	7,07
3,5	3,02	13,5	6,24	23,5	7,08
3,75	2,96	13,75	6,27	23,75	7,10
4	2,91	14	6,32	24	7,11
4,25	2,85	14,25	6,36	24,25	7,12
4,5	2,79	14,5	6,38	24,5	7,13
4,75	2,82	14,75	6,41	24,75	7,14
5	2,81	15	6,45	25	7,14
5,25	2,80	15,25	6,48	25,25	7,15
5,5	2,81	15,5	6,50	25,5	7,16
5,75	2,81	15,75	6,54	25,75	7,16
6	2,84	16	6,57	26	7,17
6,25	2,86	16,25	6,59	26,25	7,18
6,5	2,90	16,5	6,61	26,5	7,19
6,75	2,93	16,75	6,63	26,75	7,19
7	2,93	17	6,66	27	7,20
7,25	3,01	17,25	6,68	27,25	7,20
7,5	3,01	17,5	6,70	27,5	7,21
7,75	3,10	17,75	6,73	27,75	7,21
8	3,21	18	6,75	28	7,22
8,25	3,31	18,25	6,78	28,25	7,23
8,5	3,35	18,5	6,80	28,5	7,23
8,75	3,49	18,75	6,81	28,75	7,24
9	3,80	19	6,83	29	7,24
9,25	4,09	19,25	6,84	29,25	7,25
9,5	4,05	19,5	6,86	29,5	7,25
9,75	4,12	19,75	6,88	29,75	7,26
				30	7,26

8 straight lifters – 2 rpm 0.001 m/s

Time [min]	pH	Time [min]	pH	Time [min]	pH
0	7,50	10	2,90	20	4,06
0,25	7,50	10,25	2,89	20,25	4,37
0,5	7,50	10,5	2,90	20,5	4,40
0,75	7,50	10,75	2,90	20,75	4,50
1	7,50	11	2,90	21	4,82
1,25	7,50	11,25	2,91	21,25	4,92
1,5	7,50	11,5	2,91	21,5	5,20
1,75	7,50	11,75	2,92	21,75	5,19
2	7,50	12	2,93	22	5,25
2,25	7,48	12,25	2,94	22,25	5,30
2,5	7,42	12,5	2,95	22,5	5,44
2,75	7,39	12,75	2,96	22,75	5,55
3	7,31	13	2,97	23	5,65
3,25	7,23	13,25	2,99	23,25	5,74
3,5	7,12	13,5	3,01	23,5	5,80
3,75	6,95	13,75	3,02	23,75	5,85
4	5,92	14	3,02	24	5,88
4,25	5,03	14,25	3,03	24,25	5,90
4,5	4,88	14,5	3,06	24,5	5,93
4,75	4,60	14,75	3,08	24,75	5,96
5	4,00	15	3,09	25	6,00
5,25	3,55	15,25	3,10	25,25	6,05
5,5	3,50	15,5	3,13	25,5	6,07
5,75	3,45	15,75	3,17	25,75	6,09
6	3,40	16	3,20	26	6,13
6,25	3,20	16,25	3,21	26,25	6,15
6,5	3,12	16,5	3,28	26,5	6,18
6,75	3,12	16,75	3,30	26,75	6,20
7	3,07	17	3,32	27	6,23
7,25	3,00	17,25	3,33	27,25	6,27
7,5	3,00	17,5	3,36	27,5	6,30
7,75	2,97	17,75	3,36	27,75	6,32
8	2,95	18	3,40	28	6,34
8,25	2,92	18,25	3,42	28,25	6,37
8,5	2,91	18,5	3,55	28,5	6,40
8,75	2,91	18,75	3,72	28,75	6,41
9	2,91	19	3,78	29	6,42
9,25	2,90	19,25	3,80	29,25	6,44
9,5	2,90	19,5	4,00	29,5	6,47
9,75	2,90	19,75	3,92	29,75	6,48
				30	6,50

8 straight lifters – 4 rpm 0.001 m/s

Time [min]	pH	Time [min]	pH	Time [min]	pH
0	7,50	10	2,99	20	3,97
0,25	7,50	10,25	3,00	20,25	4,20
0,5	7,50	10,5	3,01	20,5	4,37
0,75	7,50	10,75	3,01	20,75	4,49
1	7,50	11	3,02	21	4,68
1,25	7,50	11,25	3,02	21,25	4,75
1,5	7,50	11,5	3,04	21,5	4,90
1,75	7,48	11,75	3,05	21,75	4,98
2	7,40	12	3,05	22	5,22
2,25	7,33	12,25	3,06	22,25	5,30
2,5	7,23	12,5	3,08	22,5	5,41
2,75	7,10	12,75	3,10	22,75	5,51
3	6,90	13	3,10	23	5,59
3,25	6,34	13,25	3,11	23,25	5,64
3,5	5,46	13,5	3,13	23,5	5,71
3,75	5,08	13,75	3,15	23,75	5,76
4	3,84	14	3,16	24	5,79
4,25	3,68	14,25	3,18	24,25	5,85
4,5	3,44	14,5	3,20	24,5	5,88
4,75	3,31	14,75	3,22	24,75	5,91
5	3,23	15	3,25	25	5,94
5,25	3,22	15,25	3,27	25,25	5,98
5,5	3,20	15,5	3,30	25,5	6,01
5,75	3,08	15,75	3,31	25,75	6,05
6	3,09	16	3,32	26	6,07
6,25	3,09	16,25	3,36	26,25	6,10
6,5	3,06	16,5	3,38	26,5	6,13
6,75	3,04	16,75	3,43	26,75	6,15
7	3,02	17	3,47	27	6,17
7,25	3,00	17,25	3,49	27,25	6,20
7,5	3,01	17,5	3,49	27,5	6,22
7,75	3,00	17,75	3,54	27,75	6,24
8	2,99	18	3,58	28	6,26
8,25	2,99	18,25	3,62	28,25	6,28
8,5	2,99	18,5	3,62	28,5	6,30
8,75	2,99	18,75	3,70	28,75	6,32
9	2,99	19	3,73	29	6,34
9,25	2,99	19,25	3,78	29,25	6,37
9,5	2,99	19,5	3,86	29,5	6,39
9,75	2,99	19,75	4,02	29,75	6,41
				30	6,43

8 straight lifters – 4 rpm 0.002 m/s

Time [min]	pH	Time [min]	pH	Time [min]	pH
0	7,50	10	4,15	20	6,83
0,25	7,50	10,25	4,75	20,25	6,84
0,5	7,50	10,5	4,90	20,5	6,86
0,75	7,50	10,75	5,09	20,75	6,88
1	7,50	11	5,25	21	6,90
1,25	7,50	11,25	5,45	21,25	6,92
1,5	7,50	11,5	5,60	21,5	6,94
1,75	7,45	11,75	5,65	21,75	6,96
2	7,30	12	5,72	22	6,98
2,25	6,20	12,25	5,78	22,25	6,99
2,5	4,99	12,5	5,85	22,5	7,00
2,75	3,90	12,75	5,90	22,75	7,01
3	3,40	13	5,96	23	7,02
3,25	3,20	13,25	6,01	23,25	7,03
3,5	3,03	13,5	6,07	23,5	7,04
3,75	2,99	13,75	6,11	23,75	7,06
4	2,92	14	6,16	24	7,07
4,25	2,89	14,25	6,20	24,25	7,08
4,5	2,84	14,5	6,25	24,5	7,09
4,75	2,83	14,75	6,29	24,75	7,10
5	2,83	15	6,32	25	7,12
5,25	2,84	15,25	6,35	25,25	7,12
5,5	2,84	15,5	6,38	25,5	7,13
5,75	2,85	15,75	6,42	25,75	7,14
6	2,86	16	6,45	26	7,15
6,25	2,90	16,25	6,48	26,25	7,16
6,5	2,90	16,5	6,50	26,5	7,17
6,75	2,95	16,75	6,53	26,75	7,18
7	2,98	17	6,57	27	7,18
7,25	3,03	17,25	6,59	27,25	7,19
7,5	3,05	17,5	6,61	27,5	7,19
7,75	3,10	17,75	6,63	27,75	7,20
8	3,20	18	6,66	28	7,20
8,25	3,20	18,25	6,69	28,25	7,21
8,5	3,25	18,5	6,71	28,5	7,21
8,75	3,30	18,75	6,73	28,75	7,22
9	3,45	19	6,75	29	7,22
9,25	3,55	19,25	6,77	29,25	7,22
9,5	3,65	19,5	6,79	29,5	7,23
9,75	3,90	19,75	6,81	29,75	7,23
				30	7,23

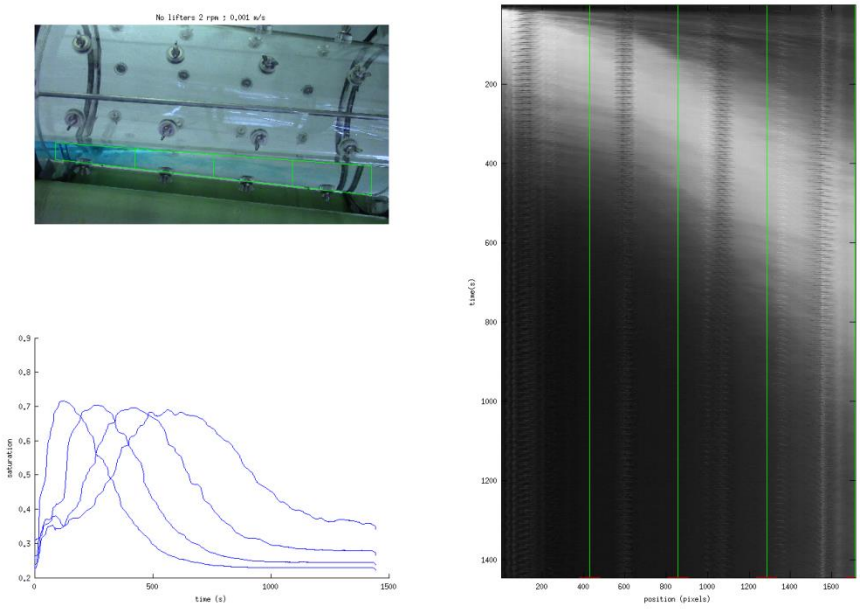
No lifters 2 rpm : 0,001 m/s
saturation
time (s)
time(s)
position (pixels)

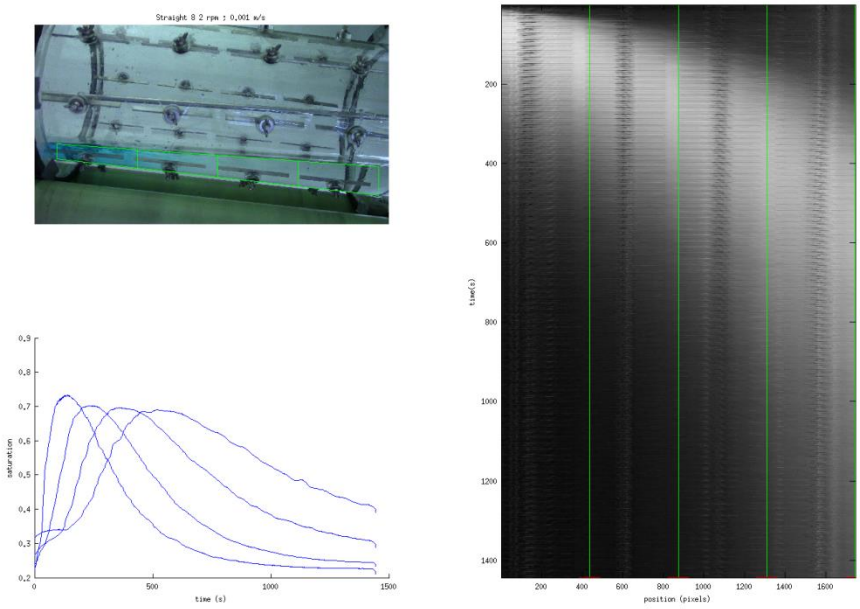
Straight 8 2 rpm : 0,001 m/s
saturation
time (s)
time(s)
position (pixels)

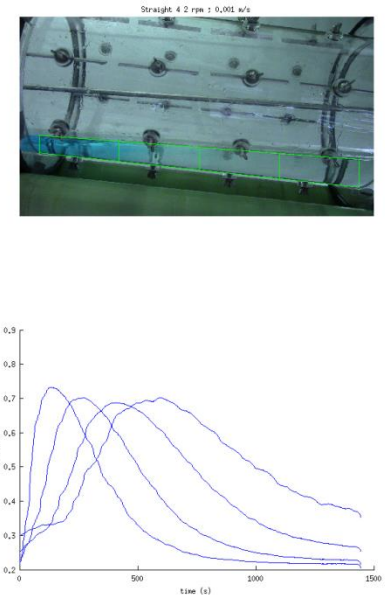
Straight 4 2 rpm : 0,001 m/s
saturation
time (s)

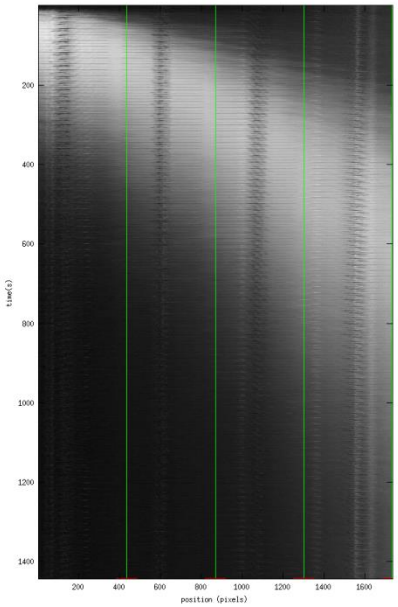
time(s)
position (pixels)

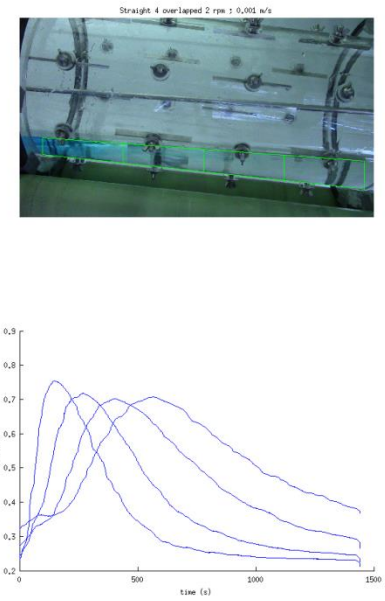
Straight 4 overlapped 2 rpm : 0,001 m/s
saturation
time (s)

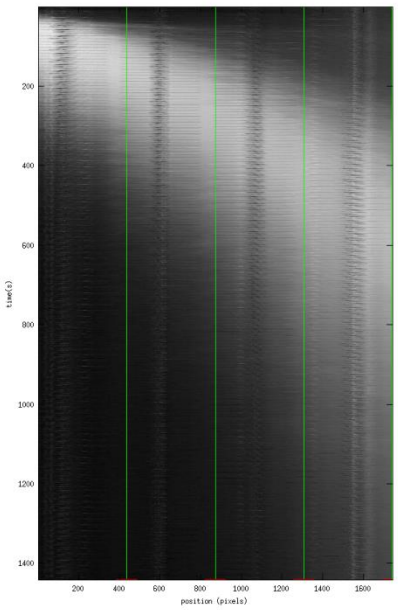
time(s)
position (pixels)

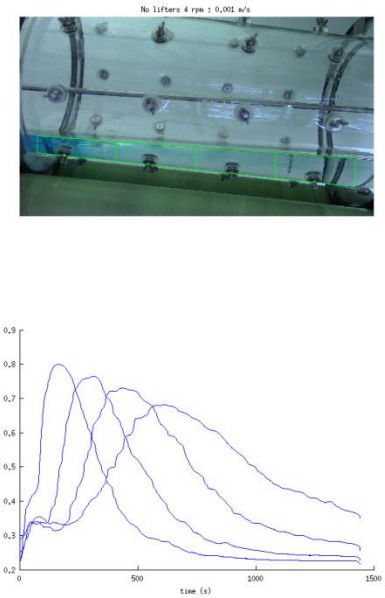
No lifters 4 rpm : 0,001 m/s
saturation
time (s)

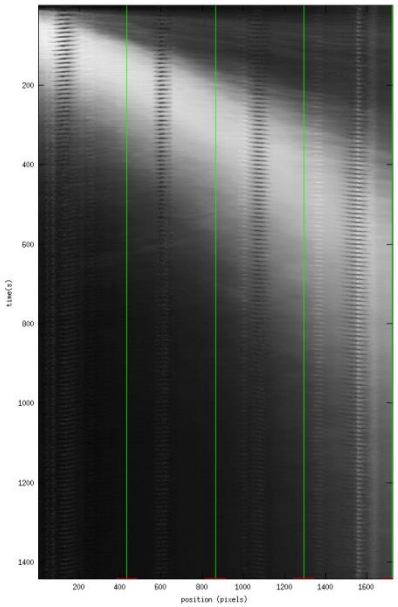
time(s)
position (pixels)

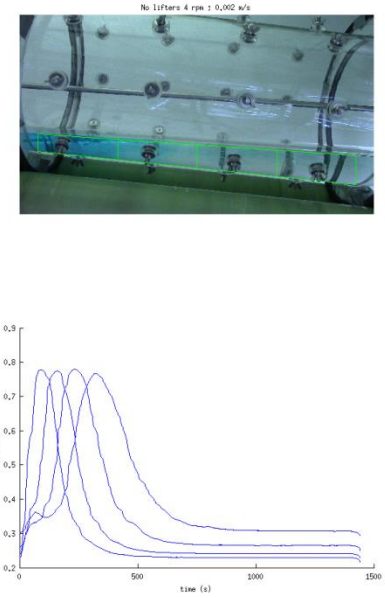
No lifters 4 rpm : 0,002 m/s
saturation
time (s)

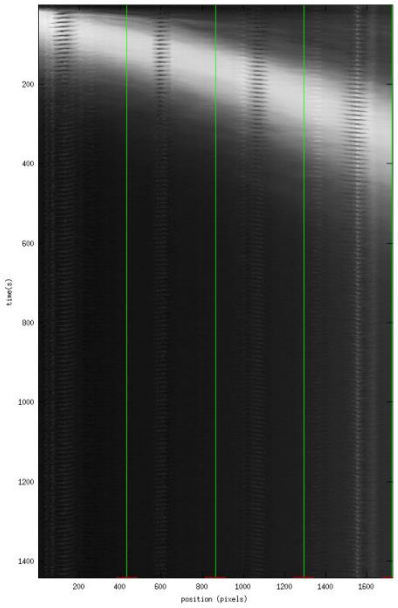
time(s)
position (pixels)

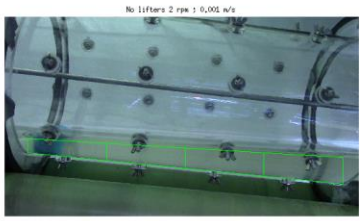
No lifters 2 rpm : 0,001 m/s

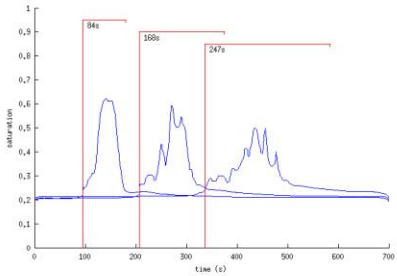
84s
168s
247s
saturation
time (s)

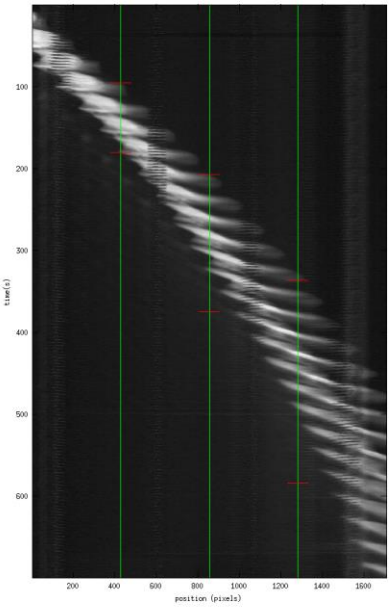
time(s)
position (pixels)

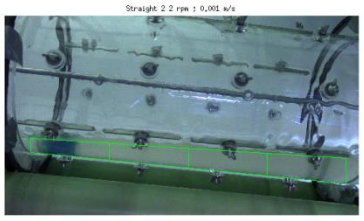
Straight 2 2 rpm : 0,001 m/s

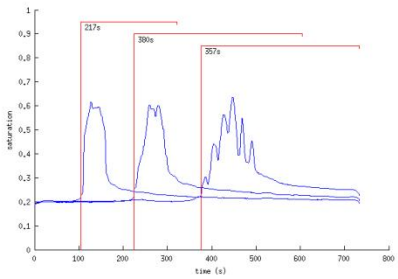
217s
390s
357s
saturation
time (s)

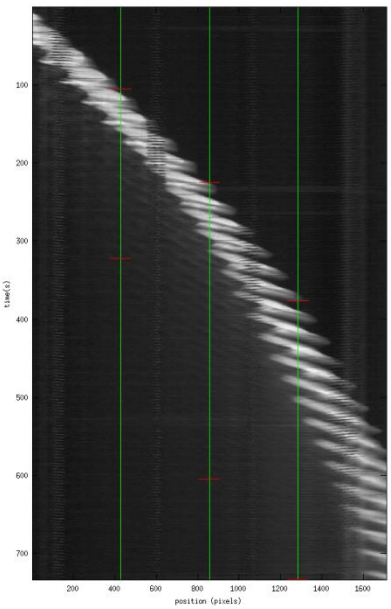
time(s)
position (pixels)

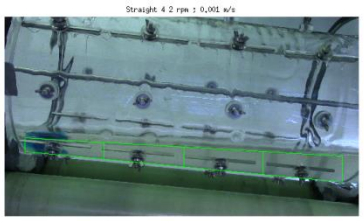
Straight 4 2 rpm ; 0,001 m/s

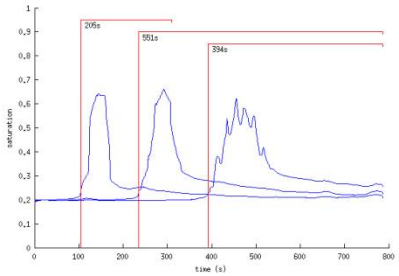
205s
551s
394s
saturation
time (s)

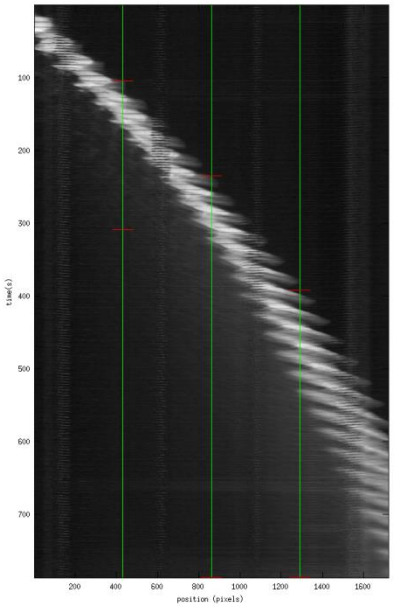
time(s)
position (pixels)

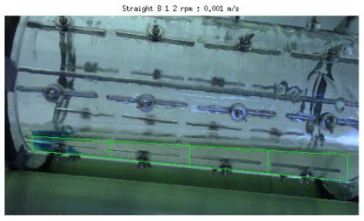
Straight 8 1 2 rpm ; 0,001 m/s

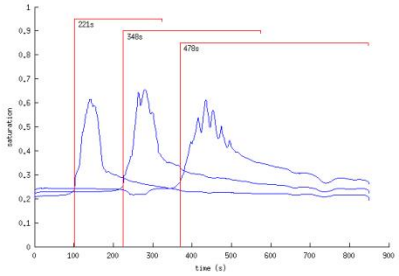
221s
348s
478s
saturation
time (s)

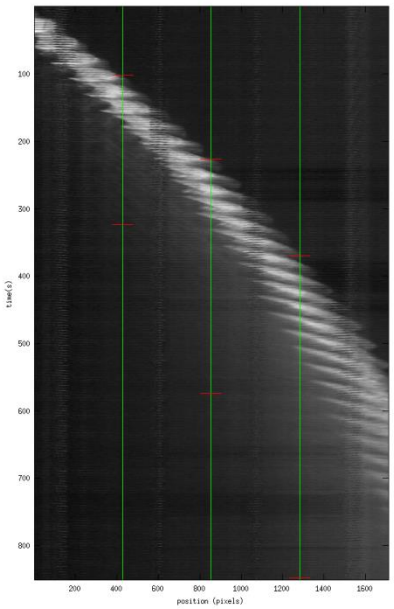
time(s)
position (pixels)

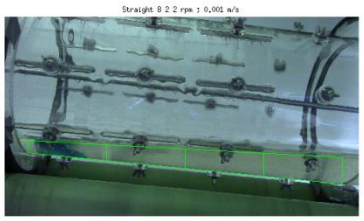
Straight 8 2 2 rpm : 0,001 m/s

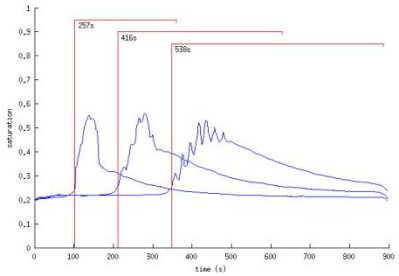
257s
416s
538s
saturation
time (s)

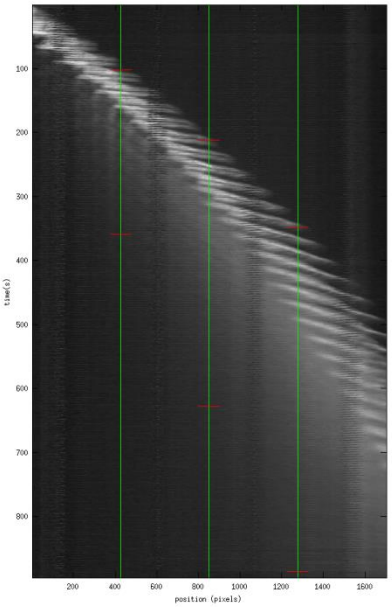
time(s)
position (pixels)

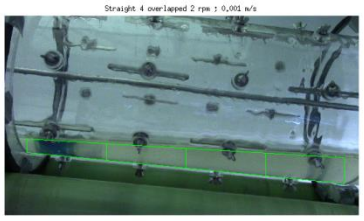
Straight 4 overlapped 2 rpm : 0,001 m/s

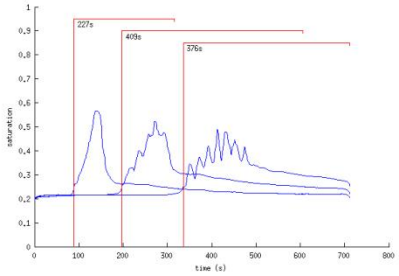
227s
409s
376s
saturation
time (s)

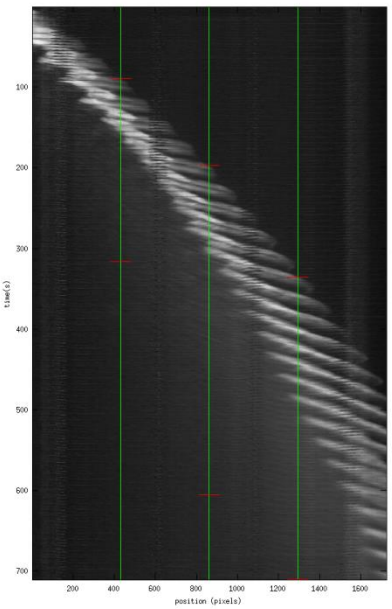
time(s)
position (pixels)

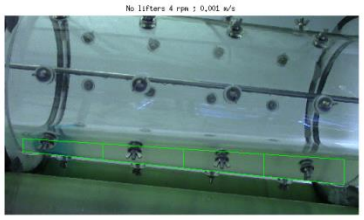
No lifters 4 rpm : 0,001 m/s

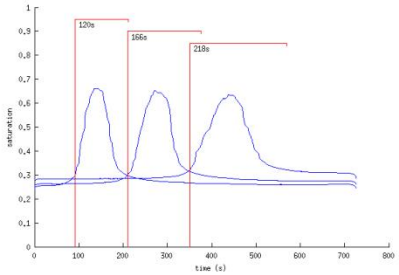
120s
168s
218s
saturation
time (s)

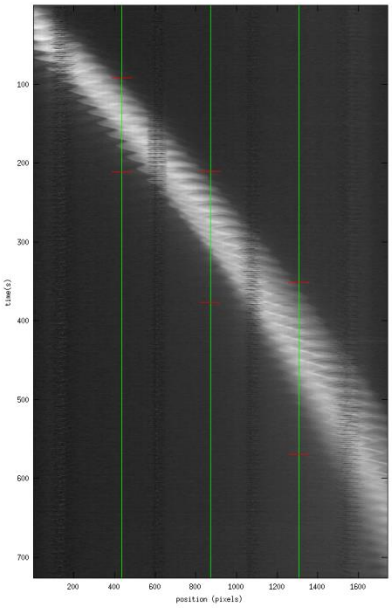
time(s)
position (pixels)

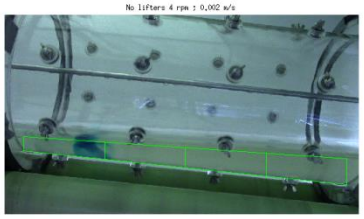
No lifters 4 rpm : 0,002 m/s

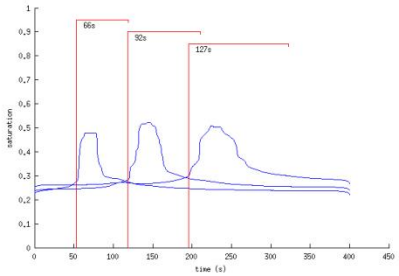
66s
92s
127s
saturation
time (s)

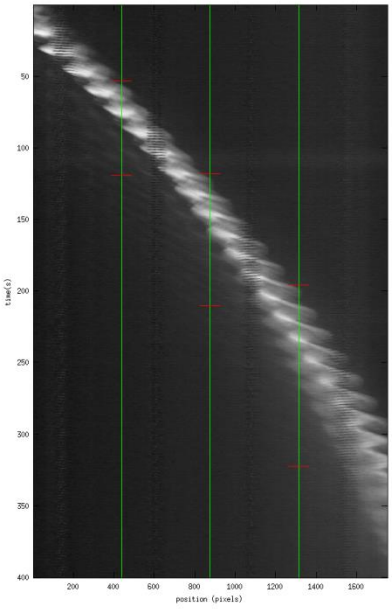
time(s)
position (pixels)

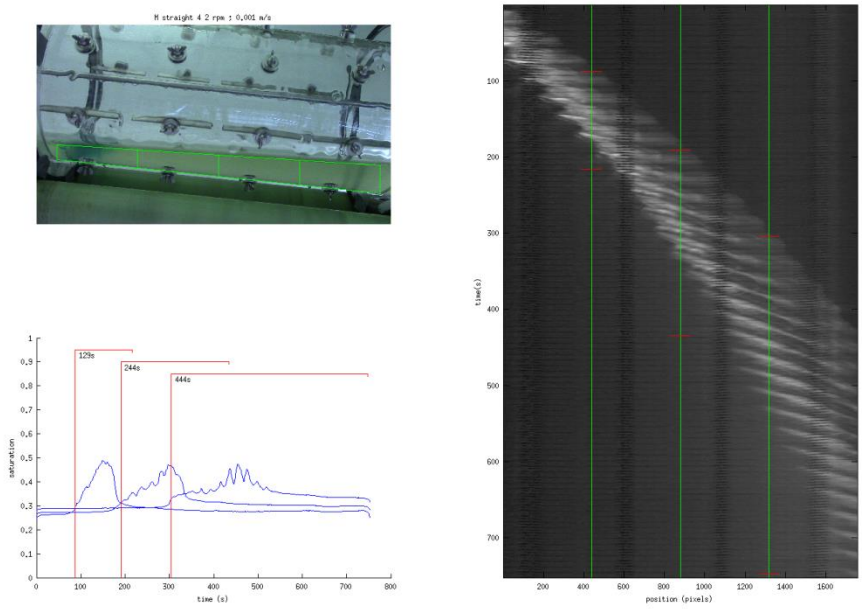
M straight 4 2 rpm ; 0,001 m/s
129s
244s
444s
saturation
time (s)
time(s)
position (pixels)

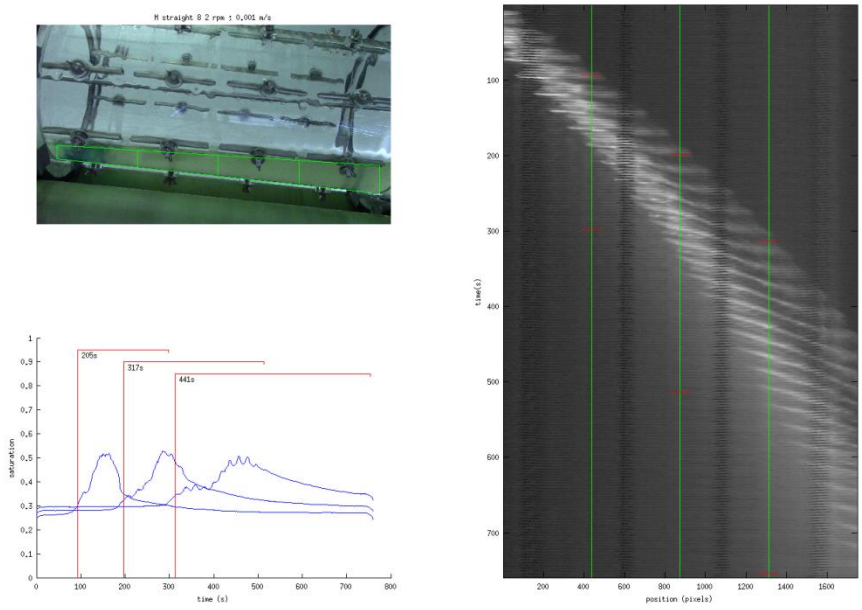
M straight 8 2 rpm ; 0,001 m/s
205s
317s
441s
saturation
time (s)
time(s)
position (pixels)

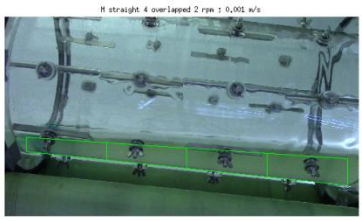
H straight 4 overlapped 2 rpm ; 0,001 m/s

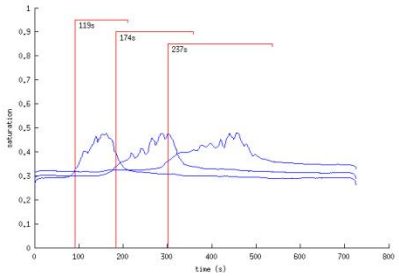
119s
174s
237s
saturation
time (s)

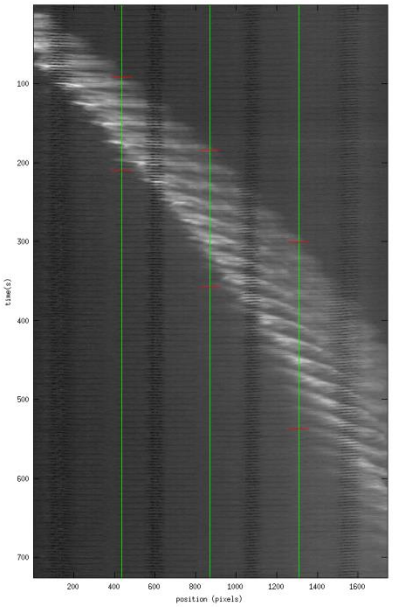
time(s)
position (pixels)

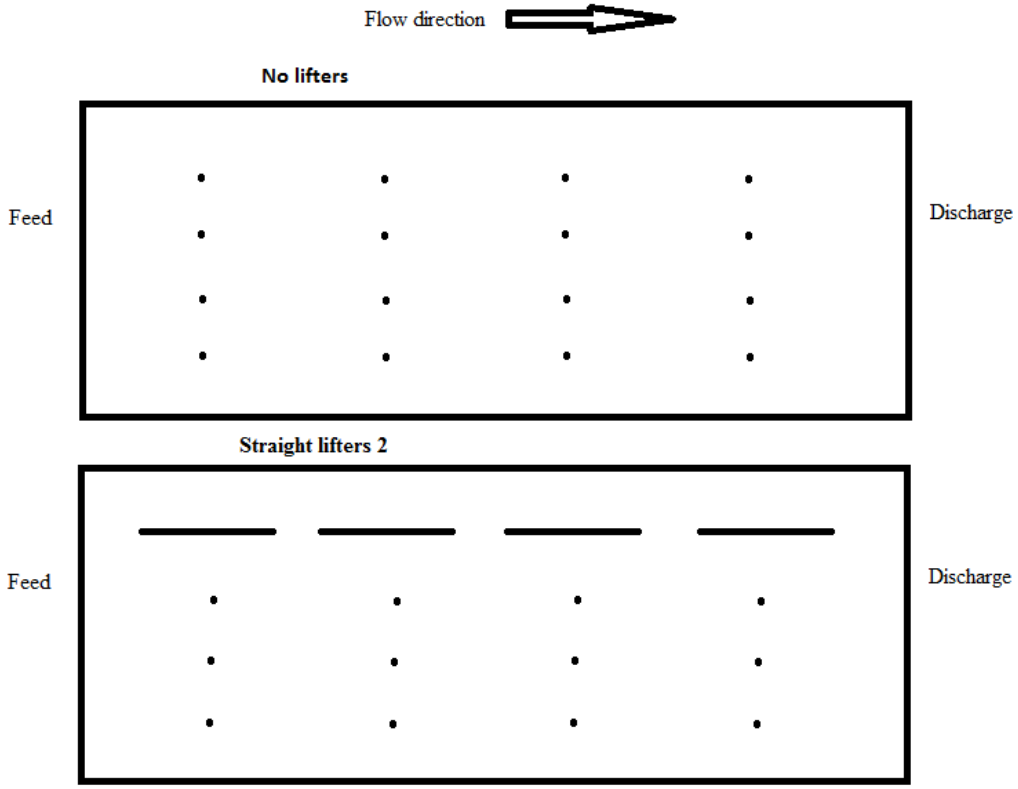
Flow direction
No lifters
Feed
Discharge
Straight lifters 2
Feed
Discharge

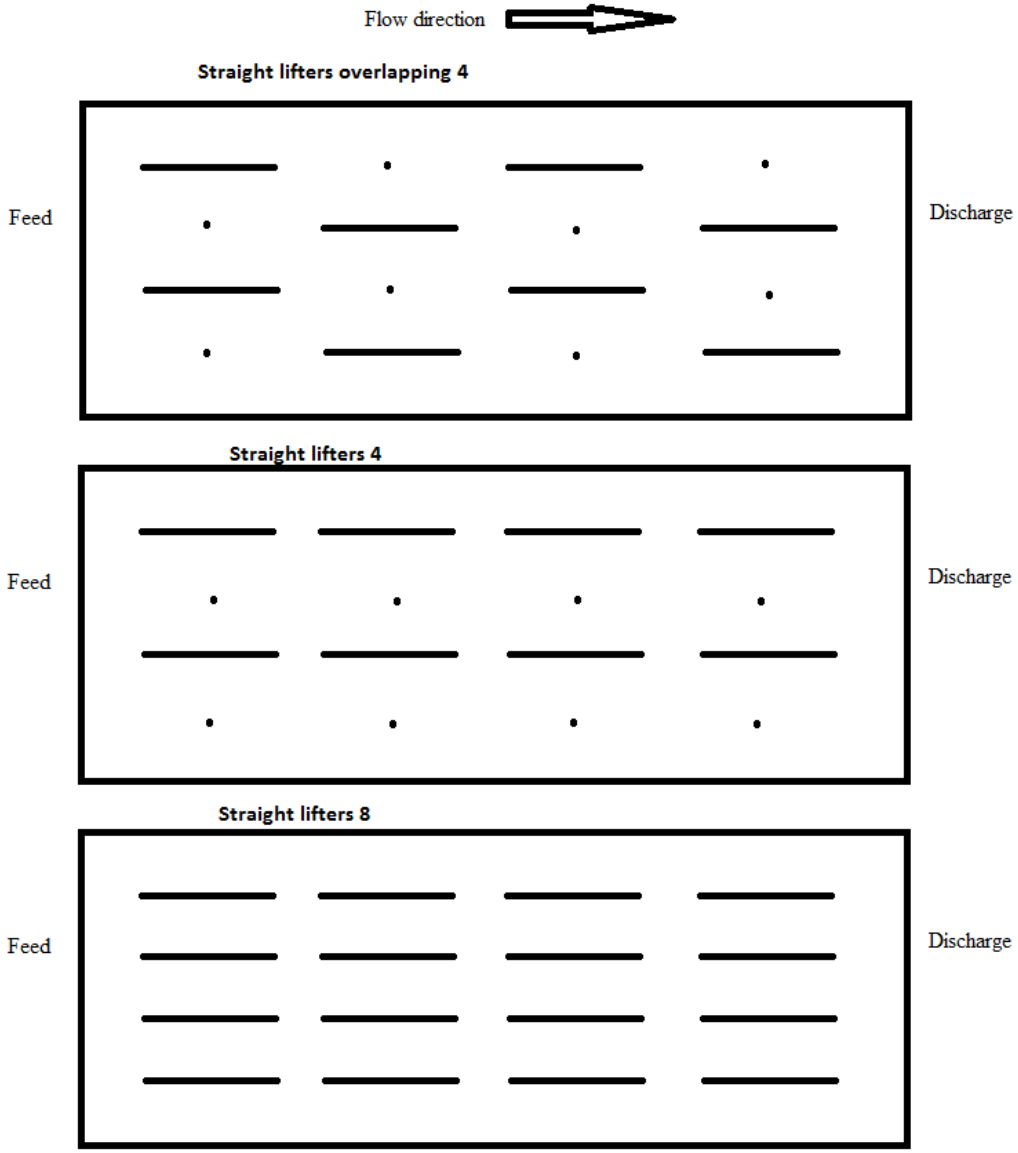
Flow direction
Straight lifters overlapping 4
Feed
Discharge
Straight lifters 4
Feed
Discharge
Straight lifters 8
Feed
Discharge